Abrupt climate change and high to low latitude teleconnections as simulated in climate models

Cvijanovic, Ivana

Publication date:
2012

Document version
Early version, also known as pre-print

FACULTY OF SCIENCE
UNIVERSITY OF COPENHAGEN

PhD thesis
Ivana Cvijanovic

Abrupt climate change and high to low latitude teleconnections as simulated in climate models

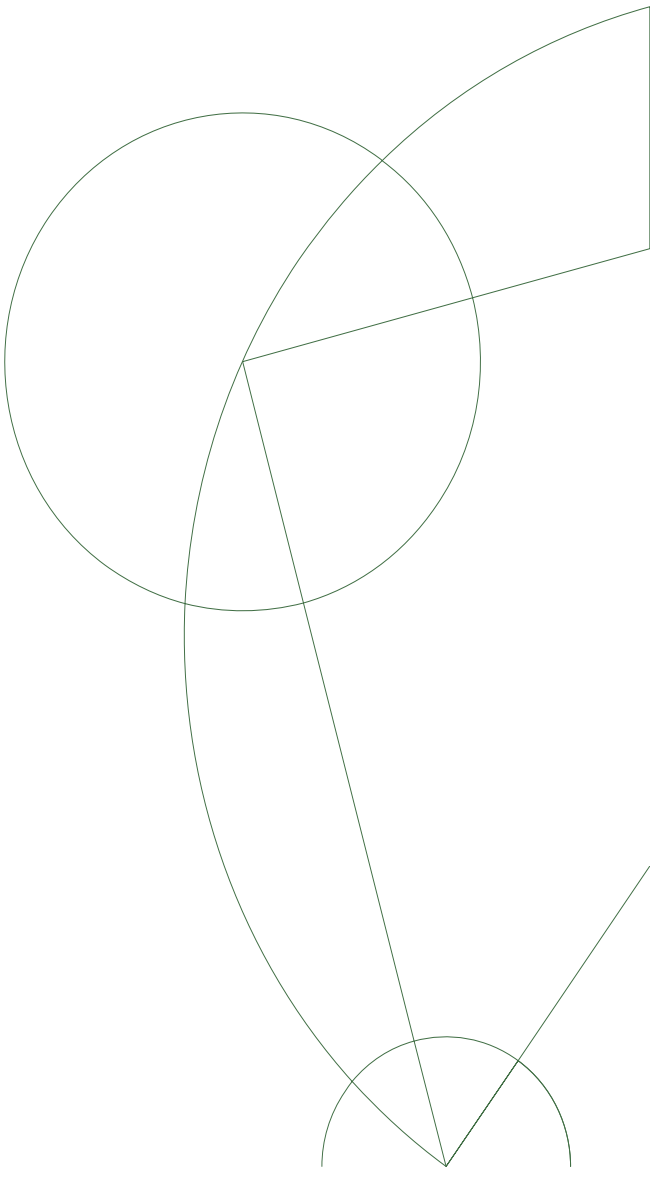

Academic advisors:

Eigil Kaas

Peter L. Langen

Centre for Ice and Climate
Niels Bohr Institute
University of Copenhagen

Submitted: March 14th, 2012

Little snail, inch by inch, climb Mount Fuji!

The Haiku of Kobayashi Issa (1763-1827)

Abstract

High to low latitude atmospheric teleconnections have been a topic of increasing scientific interest since it was shown that high latitude extratropical forcing can induce tropical precipitation shifts through atmosphere-surface ocean interactions. In this thesis, several aspects of high to low latitude atmospheric teleconnections have been considered.

The atmospheric energy transport response during Northern Hemisphere cooling and warming from present day and Last Glacial Maximum (LGM) conditions is investigated using sea surface temperature (SST) anomalies derived from a freshwater hosing experiment. The results showed the enhanced sensitivity of the present day atmospheric mid-latitude energy transport compared to that of the LGM, suggesting its ability to reorganize more easily and thereby dampen high latitude temperature anomalies that could arise from changes in the oceanic transport.

The following question was if the atmosphere-surface ocean interactions would, if enabled, affect these findings. This lead to a further re-examination of the role of tropical SSTs in the tropical precipitation shifts. An atmospheric general circulation model coupled to a slab ocean was used to investigate the relative roles of tropical SST and energy flux changes in the Intertropical Convergence Zone (ITCZ) response to the North Atlantic cooling. The results revealed a partial (local) energy compensation in the high latitudes, arising chiefly from the negative temperature feedback. The main energy compensation was shown to come from the southern tropics, with the energy gain originating from the cloud radiative feedbacks, temperature and longwave water vapor feedbacks. Regarding the role of tropical SST changes to ITCZ shifts, using the set of idealized simulations with the fixed tropical sea surface temperatures, it was shown that the ITCZ shifts are not possible without the tropical SST changes.

The work was further extended by considering all other scenarios that can induce the southward ITCZ shifts, namely the Northern Hemisphere cooling, Southern Hemisphere warming and a bipolar seesaw like forcing that encompasses both. In respect to the overall energy budget, these shifts were followed with entirely different energy flux changes that, in the first scenario, provided the global energy surplus; in the second, provided a global energy loss; and in the third, kept the global energy budget changes close to zero. These simulations have provided an insight into two key areas over which the convection strongly reorganizes in order to provide the energy flux changes required by the system. The two areas are the East Tropical Pacific and the Northern Tropical Atlantic with positive and negative top-of-the-atmosphere energy flux anomalies, respectively. Furthermore, Southern Hemisphere warming simulations have not only caused the ITCZ shift, but have also affected the high northern latitudes, as seen from the surface temperature and wind strength changes. These results may have important paleo implications to the Dansgaard-Oeschger type of events.

Resumé

Der er blevet vist øget videnskabelig interesse for atmosfæriske langdistanceforbindelser mellem høj -og lavbreddegrader, siden det blev vist at højbreddegrad extratropisk forcering kan foresage ændringer i tropisk nedbør alene gennem interaktion mellem atmosfæren og havoverfladen. I denne afhandling er flere aspekter af langdistanceforbindelser mellem høj -og lavbreddegrader taget under behandling. Ændringen i den atmosfæriske energitransport ved afkøling og opvarming af den nordlige halvkugle mellem nutidige betingelser og betingelser under Sidste Istids Maximum (SIM) bliver undersøgt ved brug af havoverflade temperatur anomalier udledt gennem et ferskvands pertubations eksperiment. Resultaterne viser en øget følsomhed af den nutidige atmosfæriske energitransport ved mellembreddegradder sammenlignet med følsomheden under SIM, hvilket peger mod det nutidige klimas evne til lettere at tilpasse sig og derved at dæmpe temperaturanomalier ved høje breddegrader, der kunne skabes gennem ændringer i transporten i havet.

Der af følger spørgsmålet om en aktiv atmosfære-havoverflade interaktionen ændrer på disse resultater. Dette leder til en videre undersøgelse af de tropiske havoverflade- temperatures rolle i ændringer af den tropiske nedbør. En atmosfærisk generel cirkulation model koblet til en overflade oceanmodel bruges til at undersøge den relative rolle af tropiske havoverflade- temperature og energi flux ændringer i reaktionen af den Intertropiske Konvergens Zone (ITKZ) på afkølingen af Nordatlanten. Resultaterne afslører en delvis (lokal) energi kompensation i de høje breddegradder, først og fremmest på grund af en negativ temperatur-feedback. Hovedkilden for energikompensationen vises at stamme fra de sydlige tropiske egne, med energitilvæksten foresaget af sky-stråling-feedbacks. Med hensyn til de tropiske havoverflade- temperatures rolle i skift i placeringen af ITKZ vises det, ved hjælp af en række idealiserede simuleringer med faste tropiske havoverflade- temperature, at det ikke er muligt at ændre placeringen af ITKZ uden ændringer i tropiske havoverflade- temperature.

Arbejdet videreføres ved at tage alle andre scenarier i betragtning, der kan føre til skift i ITKZ mod syd, hvilket indbefatter afkøling af den nordlige halvkugle, opvarmning af den sydlige halvkugle, og en bipolær vippe lignene forcering der indbefatter begge. Disse simuleringer giver indsigt omkring to nøgleområder, hvor konvektionen gennemgår kraftig omorganisering for at levere den energi flux krævet af systemet. Disse to områder er det østlige tropiske Stillehav og det nordlige tropiske Atlanten, med henholdsvis positive og negative energi-flux anomalier ved toppen af atmosfæren. Udover dette foresager opvarming af den sydlige halvkugle ikke bare skift i placeringen af ITKZ, men påvirker også de høje nordlige breddegradder, hvilket ses af ændinger i havoverflade- temperaturen og vindhastigheden. Disse resultater kan have betydning for forståelsen af klimaskift af Dansgaard-Oeschger typen under istiden.

Acknowledgments

Some years ago I came across a book called "Frozen Annals" by Willy Dansgaard. It described the highlights of the Greenland ice cap research and showed photos of Sigfus Johansen, Henrik Clausen, Dorthe Dahl-Jensen and Jorgen Peder Steffensen nonchalantly steping into the history of the ice core research. It made a great impression on me. Thus, it is impossible to describe my excitement over starting a PhD at the Centre for Ice and Climate in September 2008. It indeed proved to be the place that gathered some amazing people and I feel greatly indebted to *everybody* from CIC on the influence they had on me over the past years.

My most sincere gratitude goes to my advisors, Eigil Kaas and Peter L. Langen. I was very lucky for having such brilliant scientists providing me with their guidance throughout the course of my PhD. Thank you for this amazing opportunity to learn from you and for believing in me.

Although not my advisor, Peter Ditlevsen always found the time for a question or two that would then turn into an hours-long discussion. These talks were not only essential for my project, but also for my personal scientific development and I will always be immensely grateful to him.

Of course, it was not always easy. And during those times, I learned that I had great friends to rely on. Thank you: Mai, Myriam, Mauro and Corentin, Copenhagen will always remind me of you; Asbjørn, for being the nicest officemate in the world; Astrid, Marie and Anne-Katrine, for sharing our trouble of writing up; Michelle, Hans Christian and Mads, for your enthusiasm and for being my "silver lining"; Lone, for reminding me what is really important in life; Jakob and Christo, for making fun of everything; and finally, *thank you* Jesper, for saving the day at least million times (per day). The time spent in Copenhagen lead also to meeting two amazing people: first Jelena and afterwards Carl. I am so grateful for having you around!

My biggest scientific transformation happened during my stay in Berkeley. My deepest gratitude for this goes to John Chiang who pointed towards a light at the end of the tunnel, which turned out not to be a train. Time spent at his Climate Dynamics group in Berkeley stays in wonderful memory and I feel that my life has been greatly enriched by knowing Andrew, Ching-Yee, Juli, Shih-Yu, Yuwei and of course, John. I am so grateful to you all for making me feel at home when I was so far away from my own.

Another huge thank you to Sophia and Ching-Yee for allowing me to use Sophia's drawing in this thesis.

The stay in Berkeley and the life in general would not have been the same without James Begg (aka MMMB). Thank you MMMB, for our bike trips, road trips, shark saving actions; for your support, love, funny emails, article corrections and making me smile. I will take you to Guca someday.

Speaking of Serbia, my old friends remained being my friends throughout the years I have spent in Germany, Denmark and California. I am so grateful to Milanka and Nenad, Marina and Lela, Olja and Marko, Micko and Natalia for making our bonds last.

Finally, I am so grateful to my family, who were a true support throughout these years and without whom I would not have made it. Tremendous thanks to my mother Sonja, who always kept a smile on in order to keep me brave; to Marica who unselfishly took care of so many things and to my father Milan, who was always there for me.

My greatest gratitude of all goes to my sister. Thank you, Bojana, for your patience and love.

Copenhagen, March 12th, 2012.

Contents

Chapter 1

Introduction

1.1 Motivation

Abrupt climate change represents one of the major concerns for modern societal development. The ability to predict the climate shifts provides an opportunity for the adaptation of socioeconomic and environmental systems that, in turn, can decrease the magnitude of the impact. As a result, significant scientific efforts have been focused on the topic of future climate change. However, it is imperative to also consider past climate change, as the past provides a test for our current understanding, and, more importantly, represents a tool for constraining and verifying some of the possible future scenarios.

The demise of a number of past civilizations (Akkadian (4.2 kyr BP), Mochica (1.500 kyr B.P.) and Classic Maya (1.200 kyr B.P.)) has been linked to sudden and persistent change in climate conditions (De Menocal 2001). This has often been related to enhanced aridity - as in the case of the Mayan society, where rainfall decline and abrupt droughts were associated with the southward Intertropical Convergence Zone (ITCZ) shift (Haug et al. 2003). According to this study, in addition to the limited adaptation capabilities, another factor that contributed to the enhanced sensitivity to climate change was reaching the limits of the environmental carrying capacity. It remains uncertain whether this historical lesson has been embraced by modern society and for how long the projected global population of 10 billion will continue to, with an increasing pace, exploit the available resources (UNEP report, 2011).

In the context of abrupt climate change, much effort has been made to identify the "tipping points" in the climate system. In that sense, the stability of the ice sheets (and their effect on the sea level rise), the state of the Atlantic Meridional Overturning Circulation and the possible shifts in the location of the Intertropical Convergence Zone (ITCZ) represent some of the major uncertainties and concerns. Mentioned elements of the climate system are not only significant because of their ability to shift into different equilibrium

states but also because their changes have a global impact through oceanic and atmospheric teleconnections.

This thesis addresses the global atmospheric responses caused by changes in oceanic circulation with the major focus being the atmospheric teleconnections due to the high latitude forcing. In particular, this includes the analysis of the tropical response to the North Atlantic, Southern Ocean and a bipolar seesaw like forcing; study of the atmospheric teleconnections between the high latitudes of the opposite hemispheres; and consideration of the atmospheric heat transport sensitivities under glacial and interglacial conditions. Although the main aim of the thesis is to address the mechanisms of high to low latitude communication, the possible implications to the actual paleoclimate events have been broadly discussed. In that sense, of main interest are the two abrupt events occurring towards the end of the last glacial period, namely the Younger Dryas and Bølling-Allerød.

1.2 Abrupt climate change recorded in paleo data

The last glacial period was intercepted by a number of very fast abrupt warming events, referred to as Dansgaard-Oeschger (D/O) events, that were followed by more gradual cooling over a longer time period (Dansgaard et al. 1984). Their amplitudes have been estimated to range between 9°C and 16°C (Lang et al. 1999, Severinghaus and Brook 1999). The most recent of these abrupt warming events, the Bølling-Allerød, occurred towards the end of the last deglaciation and was followed by the abrupt Younger Dryas cooling in which the temperature almost returned to glacial conditions (Steffensen et al. 2008).

The most detailed records of the D/O and Younger Dryas climate shifts originate from Greenland ice cores (Dansgaard et al. 1984 and 1993, NGRIP members, Steffensen et al. 2008). However, the signature of these events has been found across the globe implying a global scale changes. Some of the best known records are the Asian Hulu cave stalagmites (Wang et al. 2001 and 2007), Arabian sea deposits (Banakar et al. 2010), tropical Atlantic ocean sediment cores (Peterson et al. 2000, Haug et al., 2001, Lea et al., 2003, Peterson and Haug, 2006), tropical Pacific ocean sediment cores (Lea et al. 2006, Kienast et al. 2006, Koutavas and Sachs 2008, Dubois et al. 2011) and the Antarctic ice cores (EPICA members 2004).

Signals of the Younger Dryas and D/O events documented in Bermuda Rise records by Sachs and Lehman (1999) and Keigwin and Boyle (1999) suggest about 4K SST change across the climate transitions. A similar number was estimated by Lea et al. (2003) for the Cariaco Basin, which showed SST changes of about 3°C at the start of the Bølling and during the Younger Dryas. Cariaco basin records also reveal changes in the precipitation amount (Peterson et al. 2000, Peterson and Haug 2006), considered to be a consequence of changes in ITCZ location. Precipitation decrease coincident with high northern latitude cooling has also been observed in speleothem records across the Asia (Fleitmann et al. 2003, Wang et al. 2001, Yuan et al. 2004, Kelly et al. 2006) suggesting a more southward ITCZ position during these cold periods.

Within dating uncertainty, tropical changes are found to be in phase with Greenland temperature shifts (Peterson et al. 2000, Kienast et al. 2001, Wang et al. 2001, Peterson and Haug 2006, Koutavas and Sachs 2008). Antarctic temperatures, on the other hand, reveal a complex relationship with their northern counterparts, with changes that are smaller and less abrupt compared to those observed in Greenland ice cores (Jouzel et al. 1987, Blunier et al. 1998, Grootes et al. 2001). For example, Antarctic Dome C and EDC record show a maximum amplitude of about 3°C during D/O events (Jouzel et al. 2007). Consideration of Antarctic and Greenland ice core record temporal characteristics and their relation, has (amongst others), lead to the bipolar seesaw theory which argues for the antiphase relationship between the two (Broecker 1998, Stocker 1998). However, a shortcoming of this classic bipolar seesaw theory was the assumption of zero lag time between the changes observed in Greenland and Antarctica. A study by Stocker and Johnsen (2003) suggests a thermal bipolar seesaw model according to which the abrupt climate signals from the North Atlantic are dampened and integrated into the southern heat reservoir (mainly represented by the Southern Ocean). This proposed relationship is in agreement with the coupled model studies (Vellinga and Wood 2002, Stouffer et al. 2006) while the suggested time scale for thermal damping requires an additional heat reservoir in addition to the Southern Ocean.

High resolution NGRIP ice core data (Steffensen et al. 2008) shown in Figure 1.1 offers the most comprehensive existing evidence for the abrupt climate shifts at the end of the last deglaciation. The time period presented spans from 15.5 till 11 kyBP and includes the Bolling-Allerod warm period starting at 14.7 kyBP, cold Younger Dryas conditions at 12.9 kyBP and the start of the Holocene at 11.7 kyBP. NGRIP ice core data reveals the extreme abruptness of these transitions by showing that changes in $\delta^{18}O$ (a proxy for

air temperature at the site of deposition) changed by more than 10°C within a 3 year period at 14.7 kyBP. The transition into Holocene was somewhat slower and had lasted about 60 years. The cooling transition into Younger Dryas, on the other hand, had lasted more than two centuries. Greenland temperature changes associated with these climate shifts are about 10K (Severinghaus et al. 1999, Landais et al. 2005).

Deuterium excess *d*, shown in red in Figure 1.1, is considered to be a proxy for past ocean surface temperatures at the moisture source region. Its record reveals even more abrupt transitions compared to $\delta^{18}O$, that correspond to 2-4°C temperature changes at the source regions over periods of 1 to 3 years, during both warming and cooling transitions. Steffensen et al. (2008) argues that such fast change points to an atmospheric reorganization that happens from one year to another.

An intriguing question arises from insoluble dust and Ca^{+} records in the NGRIP ice core. These two proxies are believed to reflect the atmospheric transport and dust source conditions. For Greenland, the main dust source regions are the deserts of East and Central Asia (Svensson et al. 2000). According to NGRIP record, both dust and Ca^{+} concentrations decrease by a factor of 5 to 7 within four decades during the warming events. Furthermore, this decline precedes the changes in deuterium excess. However, during the cooling events, an increase in dust and Ca^{+} is slower and it lags behind the deuterium excess shift. This evidence led Steffensen et al. (2008) argue that during the abrupt warming events, the changes in tropics preceded the changes in the high northern latitudes. Moreover, they proposed that the trigger for this high northern latitude warming is a tropical atmospheric reorganization that lead to a northward ITCZ shift.

However, the proposed scenario requires some issues to be resolved, as there is no known mechanism that would enable the ITCZ shift to the colder hemisphere (Chiang and Cuffey 2008). In this thesis, an alternative chain of events is proposed, whereby Southern Ocean temperature changes are identified as a possible trigger for high northern latitude temperature changes. In this interpretation, Southern Ocean cooling (due to, for example, meltwater or ice discharge) could have triggered the initial tropical reorganization through the fast atmosphere-surface ocean teleconnection causing the ITCZ to shift northwards. As it will be shown, these tropical changes could, in turn, affect the high northern latitudes, through the interaction between the tropical Atlantic dipole and North Atlantic Oscillation (NAO). This leads to circulation changes over the North Atlantic area, affecting the high northern latitude wind strengths and surface temperatures.

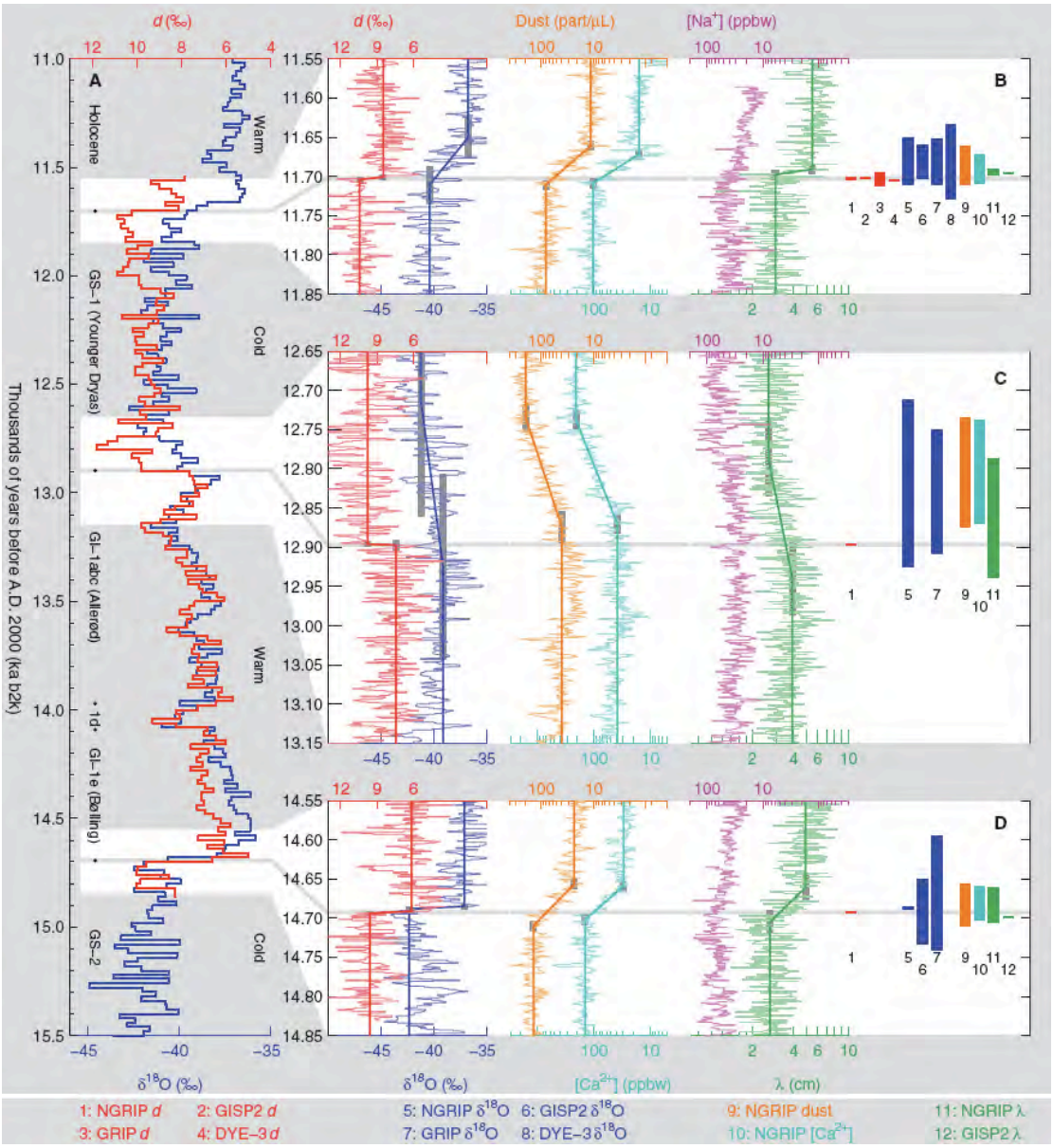

Figure 1.1: NGRIP ice core multiple-parameter records from 11.0 to 15.5 ka: (A) *d* (red) and $\delta^{18}O$ (dark blue) at 20-year resolution over the entire period and details of the transition zones: (B) from GS-1 into the Holocene at 11.7 ka, (C) from GI-1a into GS-1 at 12.9 ka, and (D) from GS-2 into GI-1e at 14.7 ka. [Left part of (B) to (D)] NGRIP records of d (red), and $\delta^{18}O$ (dark blue) and logarithmic plots of dust content (yellow), calcium concentration ($[Ca^{2+}]$, light blue), sodium concentration ($[Na^{+}]$, purple), and annual layer thickness (l, green) at annual resolution. Bold lines show the fitted ramp functions; gray vertical bars represent the 95% (2σ) confidence intervals of the ramp point locations. [Right part of (B) to (D)] Bars representing the locations of the fitted ramp functions for the NGRIP records shown to the left and for the corresponding results obtained using DYE-3, GRIP, and GISP2 data, where these are available at sufficient resolution (see list of records below the figure). From Steffensen, J. P. et al. (2008), Science 321, 680–684. Reprinted with permission from AAAS.

1.3 Abrupt climate change in modeling studies

Changes to the Atlantic Meridional Overturning Circulation (AMOC) are often regarded as a trigger of abrupt warming and cooling events (Bond et al. 1993, Alley et al. 1999). The most common scenario for such slowdown or shutdown of the AMOC involves meltwater fluxes or sea ice discharge (Manabe and Stouffer 1988, Vellinga and Wood 2002, Dong and Sutton 2002, Rahmstorf 2003, Dahl et al. 2005 and many others). While the first coupled General Circulation Model (GCM) simulations did not appear to capture the global effect of the freshwater discharge into the North Atlantic (Manabe and Stouffer 1988), later studies with the new generations of GCMs have shown pronounced tropical precipitation response to high latitude freshwater forcing (Vellinga and Wood 2002, Dahl et al. 2005, Zhang and Delworth 2005, Stouffer et al. 2006). Furthermore, a study by Cheng et al. (2006) illustrated the robustness of the tropical precipitation shift induced by the North Atlantic cooling under both present day and LGM conditions.

In parallel with the mentioned coupled ocean-atmosphere experiments, high to low latitude atmospheric teleconnections have been the subject of extensive atmospheric modeling studies, following pioneering work by Chiang et al. (2003) and Chiang and Bitz (2005). The latter study showed that an increase in the high latitude sea ice or land ice cover can induce the tropical precipitation shifts via an atmosphere-surface ocean teleconnection. The succeeding study by Broccoli et al. (2006) investigated the tropical response to the idealized bipolar seesaw like forcing in the simulations of present day climate confirming the significant shifts in the ITCZ position. In both studies, atmospheric model was coupled to a mixed layer (slab) ocean, allowing only for the atmosphere-surface ocean interactions.

Several mechanisms have been proposed to explain the link between the overall tropical precipitation changes and temperature shifts in the extratropical North Atlantic. These can be summarized as follows (following Clement and Peterson, 2008): (1) zonal linkages in the tropics (2) zonally symmetric adjustments (3) fast oceanic teleconnections and (4) thermohaline circulation impact on ENSO variability. These mechanisms will now be described briefly.

The first interpretation, which proposes the tropical zonal teleconnections, originates from the coupled GCM simulations of Dong and Sutton (2002). In this study, applied freshwater forcing in the North Atlantic shuts down the thermohaline circulation and induces the high latitude cooling. In less than a decade, tropical Atlantic response to this extratropical forcing develops,

featuring the cold sea surface temperature anomalies to the north and warm to the south of the equator. Connection with the tropical Pacific is achieved by the atmospheric Rossby wave propagation from the tropical Atlantic. This was suggested to affect the Pacific surface winds and initiate coupled feedbacks that lead to El Niño conditions. In turn, El Niño conditions cause the weakening of the rainfall over the west tropical Pacific and India due to the westward propagating Rossby waves.

The zonaly symmetric adjustment theory suggests that the signal of high latitude cooling is propagated through atmospheric interaction with the surface ocean (both in the Atlantic and Pacific basins). This theory thus implies that except for the initial trigger, no further changes in ocean dynamics are required for the tropical response to develop (Chiang and Bitz, 2005). The mechanism of this atmospheric teleconnection has been invoked throughout this thesis and a more detailed explanation will be provided towards the end of this section.

The fast global oceanic teleconnection interpretation is based on global baroclinic adjustment due to North Atlantic freshening. The signal of high latitude density perturbation is spread globally within decades (or even a few years) by coastal Kelvin and interior ocean Rossby waves propagation causing the equatorial thermocline deepening. This has been confirmed in simple ocean model simulations by Cessi et al. (2004) and Huang (2000). However, it is not clear if this adjustment, which relates the North Atlantic density changes with the Pacific thermocline and surface temperatures, is as important in more complex ocean models. For example, a study by Timmermann et al. (2005) shows smaller response of the Pacific thermocline than predicted by the simple models. This, in turn, results in only a small surface temperature response although it does imply weakening of the El Niño Southern Oscillation (ENSO) due to equatorial thermocline deepening. However, a subsequent freshwater hosing multimodel study by Timmermann et al. (2007), shows intensification of ENSO due to the AMOC shutdown in four coupled models and weakening of ENSO in one model. This study implies that ENSO weakening caused by thermocline deepening (due to purely oceanic processes) is overruled by the atmospheric circulation changes that act to shoal the thermocline through changes in Ekmann pumping, with the overall result being a strengthening of the ENSO instead.

Chiang et al. (2008) reexamined the proposed fast teleconnection mechanisms in the first decade of adjustment to North Atlantic cooling and identified the influence of both baroclinic ocean adjustment and atmospheric-surface ocean mechanisms. According to this study, an ocean-driven extratropical cooling is followed by atmosphere-surface ocean equatorward

cooling progression, which includes the evaporative cooling in the tropical North Atlantic and causes a southward ITCZ shift. The main argument of the study arises from the fact that the baroclinic ocean adjustment acting alone requires warmer tropical sea surface temperatures symmetrically distributed about the equator after AMOC slowdown. This is in contrast to the asymmetric response about the equator in coupled model simulations. The later, hemispherically asymmetric, response in the tropical Atlantic concurs with the atmospheric surface-ocean mechanism proposed by Chiang and Bitz (2005) and strengthens the argument for the dominance of the atmospheric response. Oceanic response, however, does alter the atmospheric signals, by dumping and reinforcing them depending on the region, indicating a complex relation between the two.

Even within the studies that propose the atmospheric teleconnections as underlying the tropical-extratropical communication, there are some differences in the exact interpretation of the mechanism of ITCZ shift. The main points regarding the two most common views, namely the SST and energy flux perspective, are therefore addressed in the next section.

1.4 SST and energy flux perspective of tropical precipitation shifts

The studies by Chiang and Bitz (2005) and Broccoli (2006) were the first to propose atmospheric-surface ocean interactions as a key element of high to low latitude communication. The work by Chiang and Bitz (2005) aimed to investigate the atmospheric response to anomalous Northern Hemisphere sea ice cover and LGM land ice cover in an AGCM coupled to a mixed layer ocean. Two mechanisms, the equatorward propagation (through the wind-evaporation-sst feedback) and the tropical marine ITCZ feedback, were proposed to explain the atmospheric teleconnection between the high latitudes and tropics.

In these simulations, increased NH ice cover causes weakened latent and sensible heat fluxes to the atmosphere, making the atmosphere above colder and drier. The progression of cooling is dominated by the sensible heat flux in the midlatitudes and latent heat flux in the tropics. The advection of high latitude cooling over the extratropical oceans causes an increased air-sea temperature difference increasing the sensible (and latent) heat fluxes out of the ocean. In the northern tropics, cooling affects the easterly winds due to

the increased meridional surface pressure gradient, increasing the wind speeds. As a result of surface wind strengthening, the latent heat flux out of the ocean increases and the cooling spreads equatorward. Above the cold SSTs areas, anomalies in the specific humidity develop. The observed relation between the increased wind, evaporative cooling and the spread of surface cooling resembles the wind-evaporation-SST (WES) feedback described by Xie (1999). However, later studies by Kang et al. (2009) and Mahajan et al. (2011) showed that the ITCZ shifts are possible even when the WES feedback is disabled, although the magnitude of the ITCZ response is larger in the presence of WES feedback (Mahajan et al. 2011).

According to the Chiang and Bitz (2005) study, tropical marine ITCZ feedback activates as the cold SST front arrives to the ITCZ latitudes making it shift southward. Cold SST front affects the surface pressure anomalies through hydrostatic adjustment, producing the anomalous pressure gradient across the ITCZ latitudes. This in turn causes a southward cross-equatorial flow and the ITCZ shift. The proposed interpretation on meridional SST gradient affecting the cross-equatorial flow by creating a surface pressure gradient, is based on a previous work by Lindzen and Nigam (1987) and Hastenrath and Greischar (1993). This cross-equatorial boundary layer flow changes the meridional position of maximum surface wind convergence which is equivalent to shifting ITCZ (Chiang et al. 2003). Study by Chiang et al. (2002) confirms the relationship between the meridional surface temperature and pressure gradients and the tropical convection locations, showing that the anomalous tropical Atlantic SST gradient of about 1K can shift the ITCZ by hundreds of kilometers.

The positive marine ITCZ feedback arises due to strengthened north easterlies and weakened south easterlies. As a consequence, latent heat flux is reduced to the south of the mean ITCZ position and increased to the north helping maintain the anomalous meridional SST gradient. As the ITCZ displacement occurs, the anomalous Hadley circulation causes asymmetry in the moisture content by increasing the moisture transport from the colder into the warmer hemisphere. Therefore, it is the atmospheric humidity that sustains the hemispheric SST asymmetries. Once the northern hemisphere becomes dryer it remains colder because of the greenhouse effect of the water vapor. Increased subtropical winds that caused the initial SST anomalies are only responsible for the initialization and not for the maintenance.

From the energy budget perspective, the ITCZ moves southward in order to increase the northward energy transport via the Hadley cell and to compensate for the high latitude energy loss due to the imposed sea ice. There is a partial local compensation of the imposed cooling in the high latitudes,

seen through reduced outgoing longwave radiation due to decrease in a temperature and humidity. However, this is not sufficient and the anomalous atmospheric northward heat transport is required to make up for the energy loss. Southward movement of the ITCZ affects the radiative balance in such way that more energy is absorbed due to the switch into a deeper convective regime. This energy surplus is then transported northwards.

Annual mean energy fluxes at the top-of-the-atmosphere (TOA) and the atmospheric heat transport anomalies from the study by Chiang and Bitz (2005) are shown in Figure 1.2. The anomalies represent the difference between imposed LGM land ice simulation and a present day control run. The first panel (1.2*a*), showing the TOA shortwave anomaly, indicates that an increase in albedo causes a decrease in shortwave radiation at about 60^{o}N while there is an increase in shortwave radiation in the northern tropics due to cloud cover changes related to the southward ITCZ shift. Outgoing longwave radiation (1.2*b*) is also reduced in the extratropics is not sufficient to make up for the extratropical shortwave energy loss. Overall, positive TOA longwave changes occur in the northern extratropics and southern tropics while negative changes arise in the northern tropics. Maximal total energy is absorbed in the southern tropics (1.2*c*). Northward atmospheric energy transport anomalies (1.2*d*) show a significant increase in the southern tropics while the most of transported energy is lost in the northern tropics and northern midlatitudes.

The energy flux perspective of high to low latitude atmospheric teleconnections originates from the studies by Broccoli et al. (2006) and Yoshimori and Broccoli (2008). Broccoli et al. (2006) suggest that changes in atmospheric heat exchange between the tropics and midlatitudes are the likely cause of the tropical response. Furthermore, Yoshimori and Broccoli (2008) demonstrated that the interhemispheric contrast in radiative forcing better correlates with the tropical Hadley cell response than the interhemispheric temperature contrast.

Aquaplanet modeling studies by Kang et al. (2008) and Kang et al. (2009) further expand the energy flux perspective. These studies postulate that the tropical response to extratropical thermal forcing is determined by the atmospheric heat transport response which, in turn, is governed by the extratropical eddy energy fluxes. In this view, the tropical precipitation response can be predicted from the Hadley mass response and this is further related to the atmospheric energy transport response. The magnitude of the tropical precipitation response is therefore determined by the fraction of the

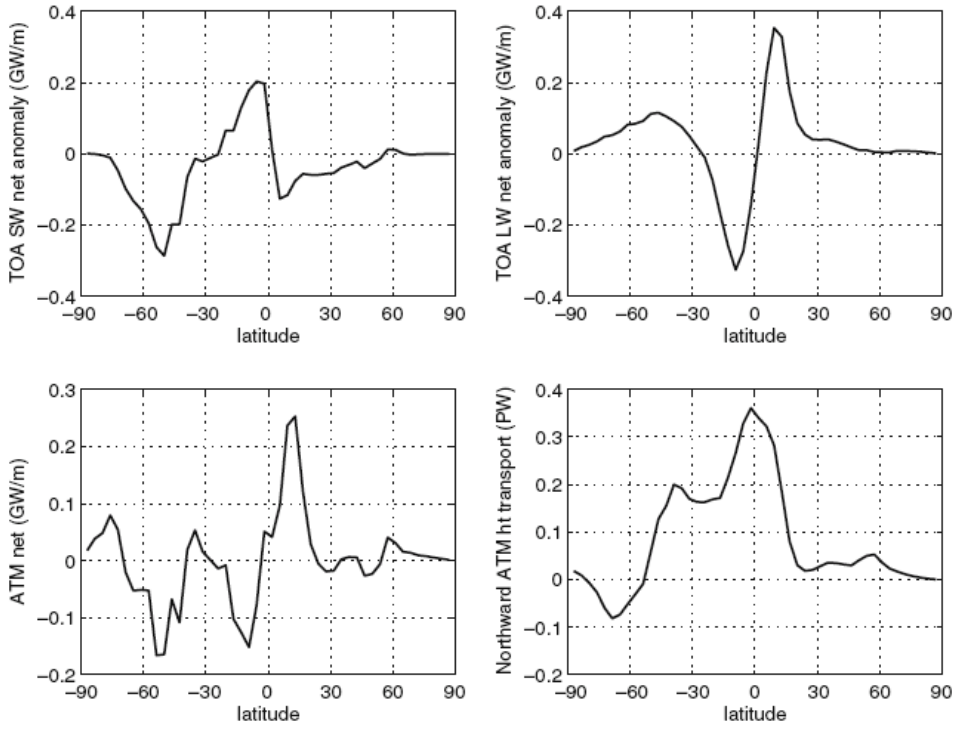

Figure 1.2: Annual mean energy flux summed over latitude bands, and zonal and annual mean atmospheric heat transport differences between the LGM land ice simulation and control. a TOA shortwave flux (GW/m, positive values are towards the surface), b TOA longwave flux (GW/m, positive values are towards the surface), c total energy absorbed in the atmospheric column (GW/m), d total northward energy transport by the atmospheric circulation (PW). From: Chiang, J. C. H. and C. M. Bitz (2005), Influence of high latitude ice cover on the marine Intertropical Convergence Zone, Climate Dynamics (10.1007/s00382-005-0040-5). Reprinted with permission from Springer.

imposed forcing that is balanced by atmospheric meridional moist static energy fluxes This is justified by the fact that while the anomalous Hadley circulation transports the energy to the cooled hemisphere (in order to compensate for the implied oceanic transport), it also increases cross-equatorial moisture transport (to the warmed hemisphere), causing an increase in the tropical precipitation response.

This perspective builds up on arguments by Held and Hou (1980) and Lindzen and Hou (1988) which imply that in the presence of the asymmetric thermal forcing about the equator, it is necessary for the rising branch of the Hadley cell to shift to the warmer hemisphere (in order to avoid large temperature gradients). This arises from the angular momentum conservation consideration which provides an upper limit for the horizontal temperature gradients allowed in the tropics. The implications of angular momentum

conservation for the tropical temperature gradients are discussed in detail in Appendix 1. Study by Neelin and Held (1987) also emphasizes the relation between the tropical circulation response and atmospheric energy budget changes.

In the aquaplanet model simulations without cloud and water vapor feedbacks, Kang et al. (2008) found that about 25% of the implied oceanic heat transport in the tropics was compensated for by atmospheric transport. By adding the cloud and water vapor feedbacks, and altering the convection scheme (in GFDL AM2 model), they showed that the compensation could increase to 115%. This increase in compensation is attributed to subtropical radiative feedbacks that act to further increase the interhemispheric gradient in radiative imbalance. This study therefore also indicates the strong dependence of the tropical response on the model convection scheme used, a factor which may be of importance when comparing the tropical response obtained by different models.

Succeeding work by Kang and Held (2011) suggests that the atmospheric energy budget, controlled primarily by the surface energy budget, is more fundamental in controlling the tropical precipitation shifts than the SSTs. In this sense, the SST response is viewed as a result of the surface energy budget and not as a driver of the precipitation response. This is to some extent in contrast with the SST perspective in which SST changes are considered to be the cause (and not the consequence) of the atmospheric heat transport and precipitation response.

Chapter 2 of this thesis describes an attempt to reconcile these two views and provides some further constraints on the role of tropical SSTs in ITCZ shifts.

1.5 Employed models and experimental setups

The simulations presented in this thesis were obtained using two atmospheric general circulation models, namely the National Center for Atmospheric Research Community Climate Model version 3.6 (CCM3) and Community Atmosphere Model version 3 (CAM3). The characteristics of both are briefly summarized in this section together with the description of the experimental configurations.

The CCM3 model has been described by Kiehl et al. (1998). It is a global spectral model with a physics package that includes radiation, convection, boundary layer processes as well as a diagnostic treatment of clouds and

prescribed sea ice. It contains a Land Surface Model (LSM) (Bonan et al. 1998) that allows detailed treatment of land surface processes. Its standard horizontal resolution is T42 (approximately 2.8° × 2.8° transform grid) with 18 levels in the vertical and a model top at 2.9 mb. The corresponding model time step for this resolution is 20 minutes. Radiative fluxes are calculated every hour and between hourly calculations, the radiative fluxes are held fixed. In its default setup (which was also applied in our simulations) it is run in the data ocean mode, meaning that it uses prescribed sea surface temperatures.

Dynamical simulations of the CCM3 model were analyzed by Hurrell et al. (1998), who found the simulated pressure field patterns to be reproduced very well. Over the subtropics, the reproduced surface pressure is larger than that observed as a consequence of the bias in the simulated trade winds and the corresponding surface wind stress. The amplitude and location of the main upper tropospheric circulations were very well captured. However, simulated 200 hPa westerlies were stronger than observed between 40^{o} and 50^{o} in the Northern and Southern Hemisphere. Improvements to the tropical hydrologic cycle and Walker circulation resulted in a significant decrease of the westerly bias in the equatorial upper troposphere compared to a previous model version. The same study also found that the main storm tracks and transient eddy flux fields are reasonably well simulated. Discrepancies related to the simulated transient eddy heat flux maximum are present in the winter over the North Pacific, while the transient kinetic energy is somewhat underestimated by the model. Meridional heat transport in the CCM3 compares well with that obtained by Trenberth and Caron (2001) from the reanalysis data, both in terms of peak value and the latitude of maximum transport (Magnusdottir and Saravanan, 1999).

The results described in Chapter 2 were obtained by applying the freshwater forcing SST anomalies from the intermediate complexity model ECbilt-CLIO (Goosse and Fichefet, 1999, Opsteegh et al. 1998) into the CCM3 simulations of both the present day and the Last Glacial Climate. Freshwater simulations have been described by Wang et al. (2009) and they correspond to freshwater pulse of 1.5 Sv applied to the North Atlantic over the period of 20 years.

Detailed description of the Community Atmosphere Model (CAM3) and its simulations is given in Collins et al. (2004) and Collins et al. (2006). This model version has been used in the studies described in Chapter 3 and Chapter 4 of the thesis. CAM3 dynamic formulation includes options for Eulerian spectral, semi-Lagrangian, and finite-volume formulations. In our simulations we applied T42 spectral resolution with 26 levels in the vertical.

The model includes the land surface model CLM3 (the Community Land Model version 3; Bonnan et al. 2002, Oleson et al. 2004), a slab ocean model and a thermodynamic sea ice model. The slab ocean model formulation is optional to CAM3 and the simulations can either be performed in the data ocean mode (prescribed sea surface temperatures) or the slab ocean mode (prescribed Q-flux field). The net heat removal rate out of the slab ocean (Q-flux) is specified for each ocean grid point and month in order to maintain the climatological observed annual cycle of sea surface temperatures. Q-flux field is computed as the residual from the surface heat budget using the corresponding data ocean model simulations. Mean ocean mixed-layer depths are derived from a data set of the observed vertical profiles of ocean salinity (Levitus, 1982). For illustration, mixed layer depths in the tropics are between 10 and 30 m.

Compared to the previous versions, major improvements to the parameterizations of cloud and precipitation processes, radiative processes, and aerosols have lead to more realistic simulations of tropical tropopause temperatures, boreal winter land surface temperatures, surface insolation, and clear-sky surface radiation in polar regions. In addition, better agreement with the satellite observations of cloud radiative forcing variation during ENSO events is achieved. The main biases are related to an underestimation of tropical variability, oceanic surface flux values in the tropics, an underestimated implied ocean heat transport in the Southern Hemisphere as well as the offsets in the 500-mb height field and the Aleutian low.

Three types of CAM3 simulations have been performed: a default slab ocean mode simulation; a combined data and slab ocean mode simulation (prescribed sea surface temperatures in the tropics and slab ocean in the extratropics); and an aquaplanet slab ocean mode simulation.

The simulations described in Chapter 3 include the standard slab ocean model but also a formulation in which the sea surface temperatures are fixed over the tropical parts of the ocean and the slab ocean boundary condition is applied north and south of this area. Later setup was applied in order to investigate the role of tropical sea surface temperatures in tropical precipitation shifts. Changes to the model code were introduced in order to include both DOM and SOM sea surface temperatures in the same simulation. In order to avoid large gradients in sea surface temperature fields when switching from one formulation to another, a “border” area was introduced in which the SST values were interpolated between the prescribed DOM values and calculated SOM values. The idealized control simulation was found to compare reasonably well with the standard slab ocean simulation.

The results presented in Chapter 4 were obtained in the slab ocean mode with changes introduced in the treatment of Q-flux adjustment terms. In this setup, Q-flux correction factors were excluded from sea surface temperature calculations over the warm (temperatures larger than zero) ocean points.

As described by Collins et al. (2004), in the CAM3 slab ocean model there are two types of Q-flux adjustments which serve to: (1) reduce the loss of heat from the mixed layer to zero - in situations when its temperature approaches the freezing point; and (2) ensure that the sea ice distribution is bounded against unrealistic growth or loss. These adjustments are applied to the background Q-flux field and the mixed layer sea surface temperatures are updated accordingly. In the next step, the global energy conservation is checked in order to ensure that the global average of the adjusted and original Q-flux field is the same. If this is not the case, the difference between the two is redistributed over the warm ocean points around the globe (by once more altering their Q-flux values), in order to ensure energy conservation. This Q-flux difference term is then also used to update the temperatures over the warm ocean points. It is this step that has been disabled in the model runs described in Chapter 4.

The problem of high to low latitude atmospheric communication was the major motivation for applying this decoupling. In order to study the atmosphere–surface ocean teleconnections only, it was necessary to make sure that Q-flux adjustments are not affecting the surface temperatures in areas away from the sea ice. However, in order to avoid unrealistic sea ice growth or loss, Q-flux adjustments were kept over the sea ice area. The (small) amount of energy that was not used to update the temperatures over the warm ocean points is thus considered to be exchanged with the deeper ocean (transmitted below the mixed layer). This may well be a more realistic scenario compared to the option of the energy being instantly redistributed around the globe over non-ice covered ocean points.

During the investigation of the southward ITCZ shifts in Chapter 4, aquaplanet slab ocean simulations were also employed in order to eliminate the possible effects of asymmetries in land-ocean distribution between the two hemispheres as well as the sea ice effects. In these simulations, the effect of sea ice is excluded by uniformly fixing the surface albedo to 0.15, meaning that the points in which the temperature drops below the freezing are still treated as open ocean points. Mixed layer ocean heat flux (Q-flux), aerosols and ozone forcing have been symmetrized and zonaly averaged around the equator. Other simulation details were kept the same as those in the corresponding slab ocean experiments with the exception of eccentricity which was set to zero.

1.6 Overview and the thesis outline

High to low latitude atmospheric teleconnections during abrupt cooling and warming events are the major focus of this thesis. The work encompasses a study of the sensitivity of atmospheric heat transport under glacial and interglacial conditions, followed by an investigation of global energy flux changes to North Atlantic cooling and the role of tropical sea surface temperatures in ITCZ shifts. In the final study, possible triggers of southward ITCZ shifts are considered and a unique comparison of the fast atmospheric teleconnections during different phases of the slower oceanic response is provided.

Presented work has several paleo implications. Firstly, it illustrates a two step atmospheric forcing on tropical ITCZ, due to the initial high northern latitude ocean cooling and due to the subsequent high southern latitude ocean warming caused by the oceanic bipolar seesaw mechanism. Secondly, it demonstrates the existence of an atmospheric teleconnection between the high latitudes of the two hemispheres and therefore points towards an atmospheric bipolar seesaw mechanism which acts on top of the oceanic one. Despite the idealized forcing applied in model simulations, mechanistic implications described in this study could be applied to the Younger Dryas or Heinrich type of events.

Chapter 2 details work performed with Peter L. Langen and Eigil Kaas and appears in Cvijanovic et al. (2011). The chapter contains a sensitivity investigation into atmospheric transport feedbacks to imposed oceanic cooling and warming. An introduction and experimental configuration are given in Sections 2.1 and 2.2, respectively. The sensitivities of the total atmospheric heat transport and its components, dry static energy transport and latent heat transport are considered in Section 2.3.1, while the meridional structures of the transport responses are addressed in Section 2.3.2. In order to better understand the mid and low latitude transport changes in the two climates, mid-latitude transient and stationary eddy heat flux anomalies are first compared. This is followed by a consideration of the location of tropical ITCZ. The overall conclusion of the study points to a larger negative atmospheric heat transport feedback to imposed temperature gradients under present day conditions compared to the Last Glacial Maximum. The prescribed sea surface temperature setup used to study the atmospheric heat transport feedbacks, have influenced the results by not allowing for the atmosphere surface-ocean interactions. This was a major motivation for

employing an AGCM coupled to a mixed layer ocean model in the subsequent analyses.

Chapter 3 provides an investigation into the role of tropical sea surface temperatures in the tropical response to high latitude cooling. This was accompanied by an investigation of global top of the atmosphere (TOA) energy budget changes in response to high latitude cooling. The general characteristics of the equilibrium response are described in Section 3.3.1. In order to decompose the TOA flux changes into individual feedback effects, the radiative kernel technique of Soden et al. (2008) was applied. An overview of this technique is given in Section 3.3.2 along with its application to the energy balance decomposition in performed slab ocean simulations (Section 3.3.3). Proposed interpretation based on the comparison to the idealized experiments with fixed tropical sea surface temperatures is given in Section 3.3.4. At the end of this chapter the results of transient simulations are examined by considering the establishment of anomalous atmospheric northward heat transport. This study shows that the main energy flux compensation for high latitude cooling comes from the southern tropics due to the southward ITCZ shift and the corresponding longwave cloud and water vapor feedbacks. It also demonstrates that the ITCZ shifts are not possible without the sea surface temperature changes. The results presented in Chapter 3 are joint work with John C. H. Chiang, and this chapter is the basis for a manuscript currently under revision (Cvijanovic and Chiang, 2012).

In Chapter 4 several triggers of southward ITCZ shifts are compared with respect to the tropical precipitation response and global energy flux changes. Following the introduction and model setup (Sections 4.1 and 4.2), three southward ITCZ shifts are considered: due to the Northern Hemisphere cooling, Southern Hemisphere warming and due to a bipolar seesaw forcing (which encompasses both Northern Hemisphere cooling and Southern Hemisphere Warming). The results of corresponding aquaplanet simulations are also considered in this chapter, confirming the larger cross-equatorial heat transport response due to high latitude southern warming compared to the northern cooling (Section 4.3.2). The main tropical radiative feedback effects following the three ITCZ shifts are discussed in Section 4.3.3. Furthermore, the possibility of atmospheric bipolar seesaw (atmosphere-surface ocean teleconnection from the Southern Ocean to North Atlantic) is discussed in Section 4.4 along with an overview of the paleo-data implications in Section 4.5.

Conclusions (including a thesis summary) are given in Chapter 5 followed by an Epilogue. Appendix 1 describes in more detail the upper tropospheric implications of angular momentum conservation in the tropics.

Chapter 2

Weakened atmospheric energy transport feedback in cold glacial climates

In this chapter, the response of atmospheric energy transport during northern hemisphere cooling and warming from present day (PD) and Last Glacial Maximum (LGM) conditions is investigated using sea surface temperature anomalies derived from a freshwater hosing experiment.

The present day climate shows enhanced sensitivity of the atmospheric mid-latitude energy transport compared to that of the LGM suggesting its ability to reorganize more easily and thereby dampen high latitude temperature anomalies that may arise from changes in the oceanic transport.

This effect is found to be a result of both the atmospheric and surface flux response. The increased PD transport sensitivity relative to that of the LGM is linked to a stronger dry static energy transport response which, in turn, is mainly driven by larger changes in the transient eddy heat flux. In comparison, changes in mid-latitude latent heat transport play a minor role in the overall transport sensitivity.

2.1 Introduction

Proxy climate data from around the world show enhanced variability, such as the presence of Dansgaard-Oeschger events, during glacial periods compared to the interglacials (Greenland ice cores (NGRIP Members, 2004), Antarctic ice cores (EPICA Members, 2006), Cariaco Basin sediment cores (Peterson et al., 2000), Asian cave stalagmites (Wang et al., 2001) and Arabian Sea sediment cores (Banakar et al., 2010)). Changes in the oceanic circulation and halocline stability (due to, e.g., ice discharge or meltwater events) are considered a potential driver of these events as inferred from the ocean sediment data and modeling studies (Keigwin et al. 1994, Broecker et al. 1994, Dahl et al. 2005). Although the role of the atmosphere is often considered

secondary in this regard, various atmospheric and surface feedbacks, such as clouds, albedo, atmospheric energy transport, can enhance or weaken the initial anomaly in the oceanic state. The focus of this study is on a presumably negative feedback, namely the atmospheric heat transport and its response to high northern latitude temperature anomalies under warm interglacial and cold glacial conditions.

Numerous modeling studies have addressed communication between high and low latitudes, showing that changes in ice cover, Atlantic Meridional Overturning Circulation (AMOC) or generally antisymmetric interhemispheric heating in the high latitudes can induce a displacement of the Intertropical Convergence Zone (ITCZ) (Zhang and Delworth 2005, Chiang and Bitz 2005, Broccoli et al. 2006, Chiang et al. 2008). Trenberth and Caron (2001) and Wunsch (2005) have demonstrated a dominance of atmospheric over oceanic transport in the extratropics. Nevertheless, possible changes in the sea ice extent due to oceanic transport variations, and their further influence on the atmospheric circulation leave the ocean a relevant trigger for abrupt climate shifts despite the small high latitude ocean heat transport.

The sensitivity of the atmospheric energy transport to global mean temperature and meridional temperature gradients was previously studied by Caballero and Langen (2005) in a series of aquaplanet simulations. They found atmospheric heat transport independent of global mean temperature in cases when the global mean temperature was high and meridional temperature gradient low. These climate states were also the ones in which sensitivity to temperature gradient was largest. Cheng et al. (2007) focused on the atmospheric and oceanic heat transport responses due to AMOC slowdown under LGM and PD conditions. They found the oceanic heat transport largely compensated by the atmospheric heat transport with midlatitude transient eddy transport playing an important role for the overall atmospheric response in both climates. Hwang and Frierson (2010) investigated the atmospheric poleward energy transport under global warming and found the change in atmospheric moisture content and latent heat transport to be the main cause for the total atmospheric transport increase with the dry static energy transport playing a smaller, compensating role.

This study investigates the sensitivity of the atmospheric energy transport to meridional temperature gradients under glacial and interglacial climates. In contrast to the previous studies that compared the transport response in the two climates, we address its actual sensitivity and its ability to feed back negatively on the imposed changes. Variations in temperature gradients were

imposed by changes in sea surface temperatures (SST) and sea ice lines, reflecting the sea surface response to oceanic heat transport variations. A weakened atmospheric transport sensitivity, i.e. a less negative atmospheric feedback, would imply a climate state with the atmosphere less capable of damping high latitude temperature anomalies arising from changes in the oceanic transport. In this case, the climate is thus likely to be influenced more strongly by excursions in the oceanic circulation. In an atmospheric general circulation model (AGCM), high latitude SST anomalies are applied mainly in the North Atlantic mimicking the effect of changing AMOC strength. The sensitivity of the atmospheric response to different sea ice extents and SSTs is then tested with the anomalies applied in two background climates, PD and LGM.

2.2 Experimental configuration

The atmospheric transport sensitivity is tested using the National Center for Atmospheric Research's CCM3 (Kiehl et al., 1998), employing T42 horizontal resolution with 18 levels in the vertical. This AGCM was run in prescribed SST mode with both PD SSTs (Shea et al., 1992) and LGM SSTs (CLIMAP, 1994) in order to obtain the two control simulations. LGM topography and land mask is taken from the ICE-5G reconstruction of Peltier (2004). Experiments have been run for 30 years and averages over the last 20 years are used in the analysis. The main parameters describing the experiments are given in Table 2.1.

experiment	GHG (CO_2, N_2O, CH_4)	orbital forcing (obliq., lve, eccen.)	SST
PD_ctrl	280 ppm, 270 ppb, 760 ppb	23.446 °, 102.04 °, 0.016724	Shea et al.
PD_px PD_mx	as in PD_ctrl	as in PD_ctrl	PD_ctrl + x*ANO PD_ctrl - x*ANO
LGM_ctrl	200 ppm, 190 ppb, 350 ppb	22.949 °, 114.42 °, 0.018994	CLIMAP
LGM_px LGM_mx	as in LGM_ctrl	as in LGM_ctrl	LGM_ctrl +x*ANO LGM_ctrl - x*ANO

Table 2.1: Resulting Northern Hemisphere meridional temperature difference (NHTD) from the various experiments.

The performance of the model dynamics was analyzed by Hurrell et al. (1998) and it was found that CCM3 reasonably well depicts the main storm tracks and transient eddy flux fields. Differences occur in the winter over the North Pacific, where the simulated transient eddy heat flux maximum is too strong and displaced to the north. The simulated transient kinetic energy is somewhat underestimated, especially over the summer hemispheres. Magnusdottir and Saravanan (1999) analyzed the meridional heat transport in CCM3. Both in terms of peak value and the latitude of maximum atmospheric transport their results compare well with those obtained by Trenberth and Caron (2001) based on reanalysis data.

SST anomalies are derived from a freshwater hosing experiment in the intermediate complexity model ECBilt-CLIO (Goosse and Fichefet 1999, Opsteegh et al. 1998). The ECBilt-CLIO was spun up for 1500 years using present day orbital forcing and pre-industrial GHG levels and this state was used as a starting point for the freshwater hosing experiments. In a manner similar to that of Renssen et al. (2002), a freshwater forcing of 1.5 Sv was applied to the ECBilt-CLIO for 20 years in the North Atlantic and SST anomalies are calculated from the difference between the resulting on-state after recovery and the off-state of the AMOC (details are given by Wang (2009)). These annually varying SST anomaly fields are multiplied by a series of different strength factors and added to the two background control fields, representing the present day and Last Glacial Maximum, in the CCM3 (Figure 2.1*a*). A total of 18 experiments were performed: two control runs (PD and LGM) and 8 sets of perturbations starting from each. Experiments are named after the strength factor used to multiply the anomaly: prefix *p* refers to positive anomalies (NH warming) and *m* to negative anomalies (NH cooling), with strengths ranging from -2 to 2 in steps of 0.5. The same SST anomalies are applied in both sets of experiments. We limit this study, by construction, to the mechanism of the fast atmospheric response under the two climates and do not consider potential differences in the slower oceanic response between PD and LGM.

In the simulations, a sea surface temperature of -1.8^{o}C (freezing point) is used as the criterion to distinguish between the open ocean points and sea ice, with a fixed thickness of 2 m. Therefore, when preparing the perturbation input fields, surface temperature (T_s) fields from the control experiments were employed at the ocean points to allow for temperatures below -1.8^{o}C in the presence of sea ice. During summer, however, sea ice T_s may attain values between -1.8 ℃ and 0 ℃, which would imply that a sea ice point is mistaken for an ocean point. To avoid this, we subtracted 1.8^{o}C from the sea ice points with temperatures above the freezing point of sea water. The SST anomaly

fields were then added to these control T_s fields and Figure 2.1 (*b* and *c*) demonstrates the resulting sea ice lines. Note that summer (JJA) is shown here as it is the season with the highest sea ice decline due to the anomalies imposed.

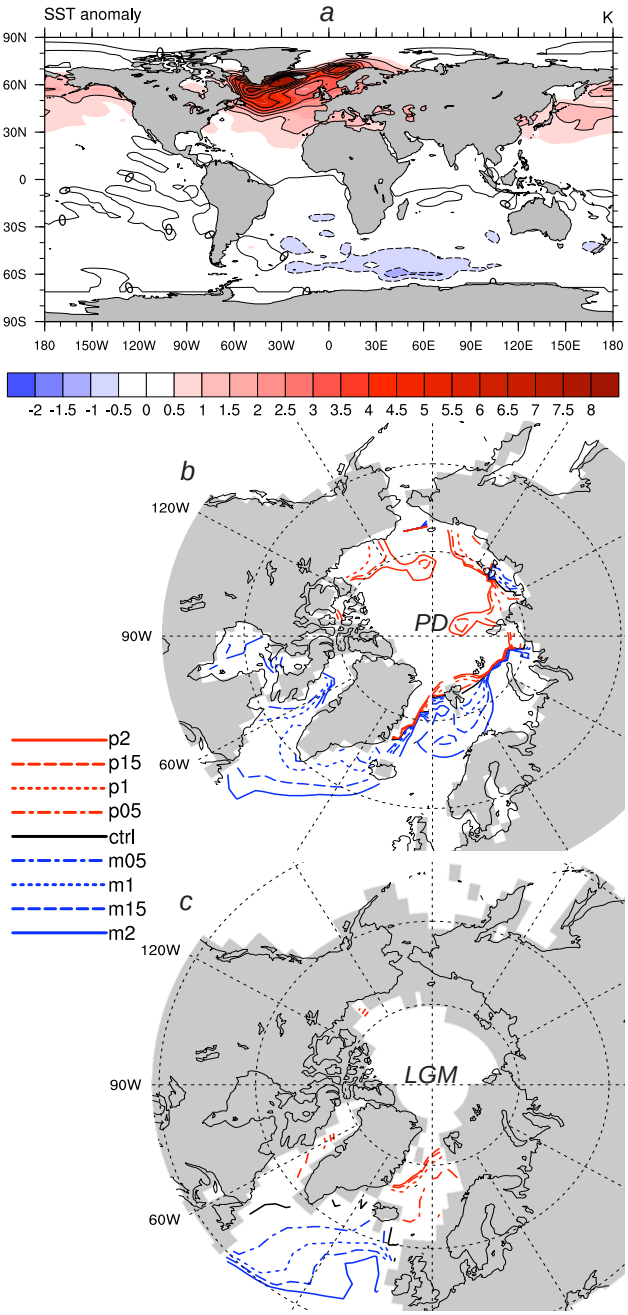

Figure 2.1: (*a*) Annual sea surface temperature anomalies from ECBilt-CLIO experiments. Negative anomalies: dashed (0.5K intervals), positive anomalies: solid (1K intervals). Panels (*b*) and (*c*): NH summer (JJA) sea ice lines (-1.8°C SST isotherms) for PD and LGM simulations, respectively.

Although we do impose perturbations that tend to realistically represent the effects of changes in the oceanic heat transport, the important point, however, is not the exact SST and sea ice line geometries, which will depend on model and background climate, but the general alteration of the large scale Northern Hemisphere meridional temperature difference (NHTD) obtained in this way. Here we define NHTD as the difference of the average surface temperatures over the areas 0^{o}-30^{o}N and 30^{o}-90^{o}N including both land and ocean points. Using the NHTD as a metric enables a comparison between the two climates that significantly differ from each other in their surface conditions.

We consider the NHTD and not the alteration of the implied ocean heat transport in the following sensitivity analysis. This is due to the fact that the SSTs are prescribed in the simulations and there is no possibility of ocean transport feedback. Thus, given a surface temperature perturbation, which in this case is measured by the meridional temperature difference, we investigate the resulting atmospheric heat transport response. The normalization is performed using the surface temperatures as the primary cause of change and not the surface fluxes or, equivalently, the implied ocean heat transport. Of course, the surface fluxes influence the atmospheric state and the atmospheric heat transport, and are in turn influenced by the latter two. Hence, it is important to evaluate how the SST change is communicated to the atmosphere by the surface fluxes and so we complete our analysis by also considering the surface budget imbalance per NHTD.

The SST anomalies applied in the PD and LGM simulations are identical, but the resulting NHTD anomalies are not, because the large LGM sea ice extent with low surface temperatures requires much larger anomalies for open ocean points to emerge. Therefore, the resulting range of the imposed NHTD changes is around 3K for LGM simulations and 5K for PD. In order to obtain a LGM NHTD anomaly with a value similar to that in the maximum PD warming case (PD_p2) we have included in our analysis an additional experiment in which three times the initial anomaly was added to the LGM background climate (LM_p3). NHTD values for each experiment are summarized in Table 2.2. Due to the strength of the coupling between surface and surface air temperature, all conclusions in the following remain unchanged if the surface air temperature or lower tropospheric temperature was used instead of surface temperature in the definition of NHTD.

experiment	NHTD [K]
PD_m2	*22.6*
PD_m1.5	*22.1*
PD_m1	*21.4*
PD_m0.5	*20.06*
PD_ctrl	*20.1*
PD_p0.5	*19.6*
PD_p1	*18.9*
PD_p1.5	*18.4*
PD_p2	*17.8*
LGM_m2	*28.85*
LGM_m1.5	*28.5*
LGM_m1	*28.13*
LGM_m0.5	*27.85*
LGM_ctrl	*27.5*
LGM_p0.5	*27.1*
LGM _p1	*26.7*
LGM _p1.5	*26.5*
LGM _p2	*26.1*

Table 2.2: Resulting Northern Hemisphere meridional temperature difference (NHTD) from the various experiments.

2.3 Results

2.3.1 Atmospheric transport sensitivities

Total northward atmospheric and latent energy transports are calculated from the atmospheric energy and fresh water budgets, respectively. Such implied transport calculations assume a steady state with constant (long term) energy and moisture content in the column, which is the case for the multi-year averages used in these calculations. In these calculations, monthly mean surface and top-of-atmosphere (TOA) fluxes and precipitation values are used. Whilst the total atmospheric transport is obtained by integrating the atmospheric net energy budget over the latitudes (from the south pole to the given latitude), latent energy transport is calculated considering the fresh water budget obtained as surface evaporation minus precipitation. Northward dry static energy transport (DSE) is obtained as the residual between the total atmospheric and latent heat transports. We do not account for the very small kinetic energy transport and it remains a part of the DSE transport. These calculations have been verified by direct calculation using the individual time step values of vertical integrals of meridional advection of temperature, water vapor and geopotential (vT, vq and $v\phi$), but as these fields were not obtained for all experiments we use the approach described above.

Total transport anomalies at the equator and 30°N are plotted as a function of NHTD anomalies in Figure 2.2. Imposed NH warming (negative NHTD anomalies) causes a decreased total atmospheric transport, while NH cooling causes an increased transport. Panels *a*, *b* and *c* show total, dry static energy and latent cross-equatorial heat transport for PD (solid circles) and LGM (open circles) warming and cooling simulations. Panels *d*, *e* and *f* show the same for the transports across 30°N.

Linear regression coefficients *rc* (and the corresponding r^2 values) of transport versus NHTD anomalies provide a measure of the sensitivity of the atmospheric transport. Statistical significance of the results was confirmed by Monte Carlo sampling, giving frequency distributions of regression coefficients differences between the two climates based on yearly samples. The LGM simulations indicate an enhanced total transport sensitivity at the equator and decreased sensitivity at 30°N relative to PD (Figure 2.2*a* and *d*). The PD simulations show weaker response at the equator with sensitivity increasing northward and peaking in the mid-latitudes, as it can be seen from Figure 2.3*a* and *d* showing the meridional transport anomalies.

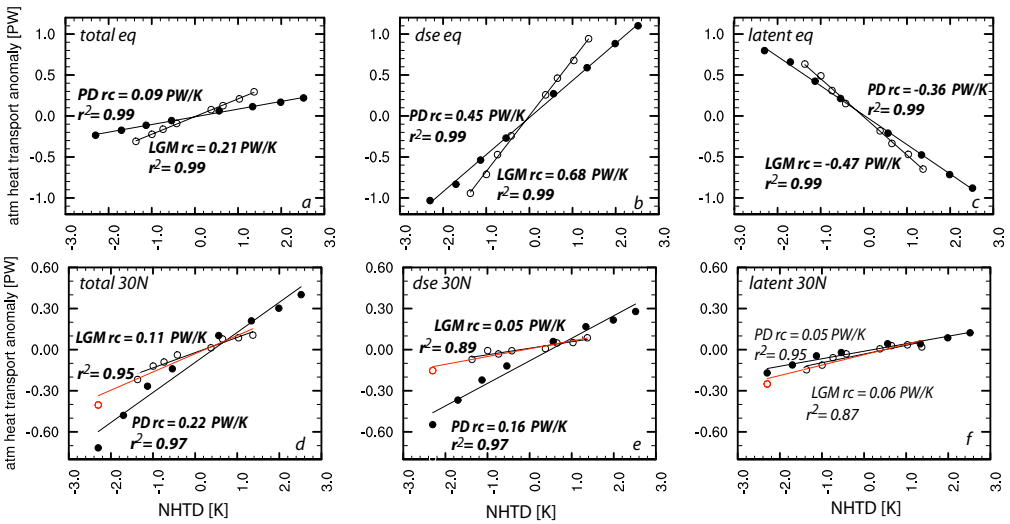

Figure 2.2: Atmospheric transport anomalies (PW) at the equator (*a*, *b*, *c*) and 30°N (*d*, *e*, *f*) for PD (full circles) and LGM (open circles) simulations as a function of NHTD anomaly (K). Positive/negative NHTD anomalies refer to NH cooling/warming. Linear regression coefficients and r^2 values of the fit are indicated. Bold font indicates that the difference between PD and LGM slopes is statistically significant at the 95% level. Red open circle represents the LGM_p3 experiment.

Separation of the total transport into DSE (2.2*b*) and latent heat (Figure 2.2*c*) components reveals the canceling effect of the two at the equator with DSE giving the sign of the total response in both climates. Slopes for DSE are 0.45 PW/K and 0.68 PW/K compared to -0.36 PW/K and -0.47 PW/K for latent transport, for the PD and LGM cases, respectively. Both components show stronger cross equatorial response in the LGM climate compared to the PD.

At 30°N the PD total response is double that of the LGM with the DSE component being the main cause of the difference (Figure 2.2*d* and 2.2*e*). Compared to the LGM, the PD DSE response is almost three times larger with slopes 0.16 PW/K and 0.05 PW/K for PD and LGM. Latent energy transport (Figure 2.2*f*) shows lower sensitivity compared to DSE (Figure 2.2*e*) in PD simulations. In contrast to this, in LGM simulations DSE and latent heat transport sensitivities are approximately the same.

An additional experiment, in which three times the initial anomaly was added to the LGM background climate (LM_p3), was performed in order to obtain a NHTD anomaly with a value similar to that in the maximum NH PD warming case (PD_p2). This additional experiment also allows for a comparison between the two climates under similar sea ice extents. This is

illustrated in Figure 2.2 (in red open circles). The overall slope of the midlatitude LGM response is still much smaller than the PD even when including such an extreme perturbation.

We also tested whether the above findings are valid for the monthly transport anomalies due to the seasonal changes in NHTD (not shown). In comparison with our original experiments with high- to mid-latitude perturbations, the NHTD has much larger variations throughout the course of the year with amplitude close to 30K. The weakened LGM mid-latitude transport sensitivity to NHTD perturbations remains valid for the monthly values: the response is higher in the PD than in the LGM simulation and this becomes even more pronounced in the higher mid-latitudes. DSE transport remains the main contributor to the total transport sensitivity with enhanced influence over latent heat transport.

2.3.2 Meridional structure

To further investigate the atmospheric transport response to the imposed perturbations, we consider the meridional structure of the anomalies (Figure 2.3). PD total transport anomalies (Figure 2.3*a*) peak around 35°N with larger amplitude than the LGM anomalies (Figure 2.3*d*) whose peak is located close to the equator. Separating the total transport into its two components, we find that the larger anomalies are seen in DSE, both in PD and LGM climates. An interesting feature is the tail in the PD DSE transport anomaly (Figure 2.3*b*) that reaches up to 60°N. Here DSE and latent heat transport anomalies have the same sign and this is thus the main cause of the extratropical peak in the PD net transport anomaly (Figure 2.3*a*). Northward of 60°N we see a negative DSE anomaly as a consequence of decreased temperature gradient between 60°N and the area poleward of it. Such features are not present in the LGM and the peak in total atmospheric LGM transport (Figure 2.3*d*) comes from a weaker cancellation between equatorial DSE and latent heat transport changes.

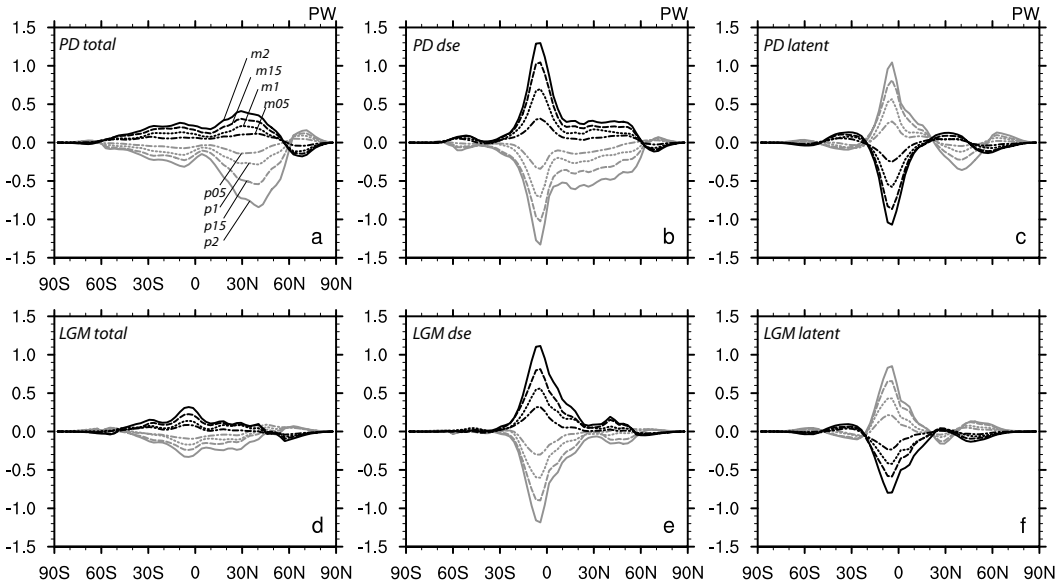

Figure 2.3: Atmospheric transport anomalies: total (*a* and *d*), DSE (*b* and *e*), latent heat (*c* and *f*) for PD (upper plots) and LGM (lower plots) simulations. Black curves: NH cooling simulations (*m2*, *m1.5*, *m1* and *m0.5*), grey curves: NH warming simulations (*p2*, *p1.5*, *p1* and *p0.5*).

In order to evaluate how the alterations to the atmospheric heat transport (AHT) compare to model-observation biases, we have plotted in Figure 2.4 total atmospheric heat transport from our PD control run, together with NCEP and ECMWF (ERA15) data (based on years 1985-89). Re-analysis based transport data are derived by Trenberth and Caron (2000). Atmospheric heat transport from the PD_ctrl run is quite close to the atmospheric heat transports from the re-analyses. The anomalies to the re-analysis plots have the same order of magnitude as the anomalies in our perturbed experiments but the locations where they appear to be the strongest are far from the locations of the maximum anomalies in the perturbed experiments. Our perturbations to AHT are small, and in this aspect, they do not force the model to unphysical conditions. The fact that the transport anomalies are much smaller than the model climatologic transports, confirms that a simple linear perturbation study is suitable approach.

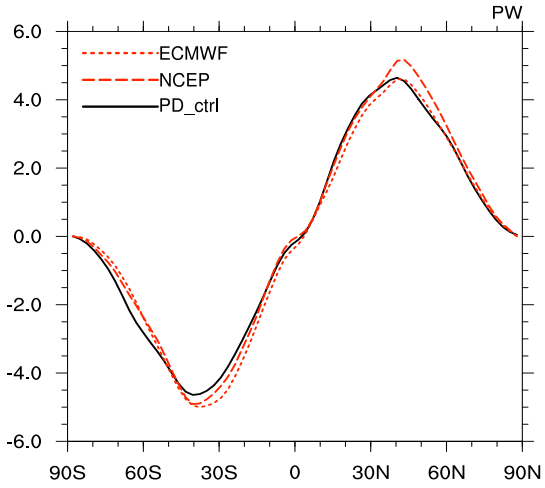

Figure 2.4: Atmospheric heat transport for PD_ctrl, ECMWF ERA15 and NCEP data (reanalysis data: Feb 1985 - Apr 1989 annual mean, from Trenberth and Caron (2001) and Trenberth et al. (2000)).

2.3.2 *a* Mid-latitude response

Through direct transport calculations using vertical integrals of meridional advection of temperature and geopotential, dry static energy transport anomalies have been decomposed into their sensible and potential components (not shown). This revealed the canceling effect that the two have, with the sensible heat transport anomaly yielding the sign of the mid-latitude PD DSE response. In contrast, in the LGM simulations both components have much smaller anomalies with the sensible heat transport determining the overall DSE anomaly in lower mid-latitudes and potential energy transport in the higher mid-latitudes. Given that the atmospheric heat transport in mid-latitudes is mainly done by eddies, the different responses of the sensible heat transport in the two climates can be explained by considering the stationary and transient eddy heat flux components. Figures 2.5 and 2.6 show stationary $\left[\overline{v^*}\,\overline{T^*}\right]$ (upper panels) and transient eddy $\left[\overline{v'T'}\right]$ (lower panels) meridional heat flux anomalies for PD and LGM simulations, respectively. Square brackets denote zonal means and overbars time means, primes and stars denote deviations from the time and zonal mean, respectively. Eddy momentum diagnostics presented here are obtained from the monthly model output, using the decomposition of the total flux into a mean meridional circulation term and stationary and transient eddy flux terms (Peixoto and Oort, 1992). In this manner, total flux and mean meridional circulation terms are obtained directly from the model output, the stationary eddy flux is

calculated by subtracting the zonal means while the transient eddy flux is given as the difference between the total flux and the other two terms. We have verified this approach by calculating the transient eddy flux from the daily data (by subtracting the 8 day means from the daily values, but using a smaller sample of years) and arrived at the same conclusions.

We find the glacial control climate to have enhanced stationary eddy heat fluxes compared to the PD control and weaker transient eddy heat fluxes (not shown). A similar result was found by Murakami et al. (2008) who saw increased mid-latitude dry static energy transport during LGM due to increased stationary wave activity. Increased stationary wave activity in LGM has been shown to be caused by the LGM orography (Cook and Held, 1988). Despite the increased stationary eddy heat flux in the glacial control, it is the transient eddy heat flux anomalies that determine the overall eddy heat flux response to the added surface perturbations in both climates (Figures 2.5 and 2.6). With NH cooling, the transient eddy heat flux increases with the equator to pole temperature gradient and conversely, it decreases with NH warming, but in the LGM simulations this response is weaker than in PD and displaced towards lower mid-latitudes. Figure 2.7, showing the vertically integrated transient and stationary eddy heat transport anomalies, confirms this picture of significantly larger transient transport anomalies (left plot) compared to the stationary transport anomalies (right plot) and the enhanced PD response (black lines) compared to the LGM (grey lines).

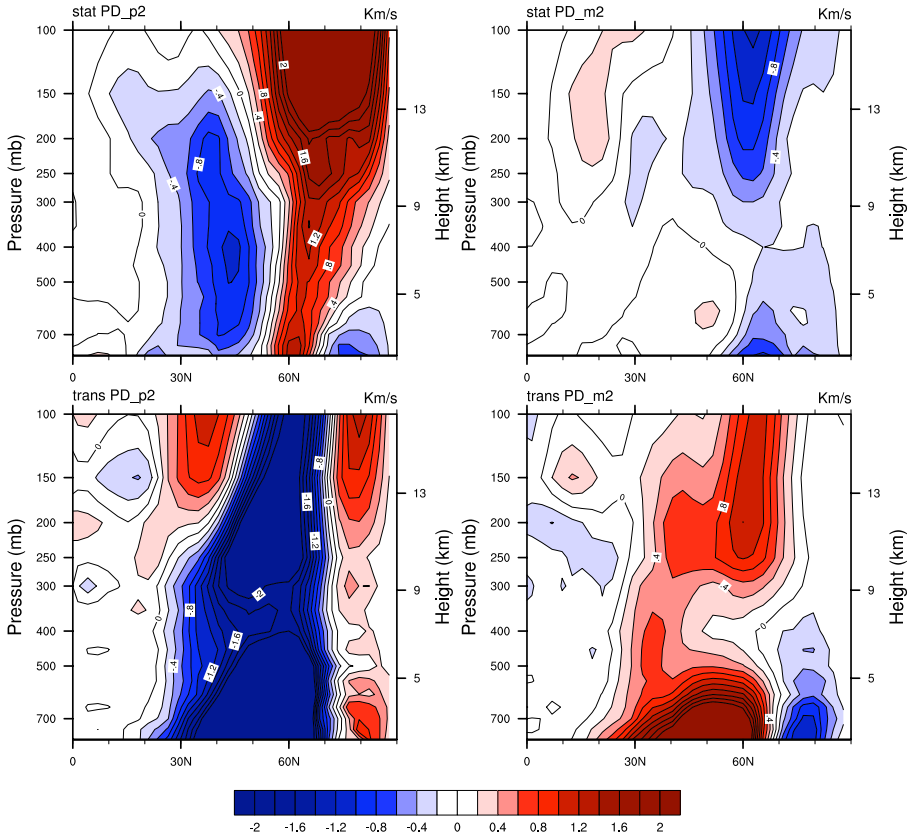

Figure 2.5: Stationary (upper plots) and transient eddy (lower plots) annual meridional heat flux anomalies for PD_m2 and PD_p2 simulations.

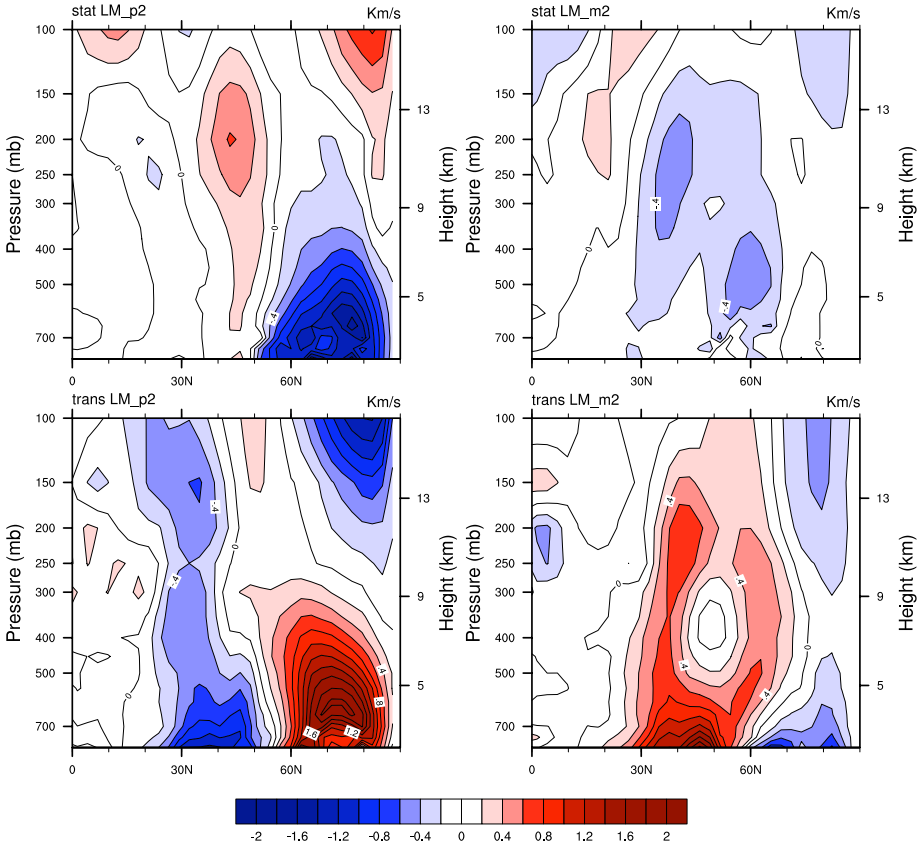

Figure 2.6: Stationary (upper plots) and transient eddy (lower plots) annual heat flux anomalies for LGM_m2 and LGM_p2 simulations.

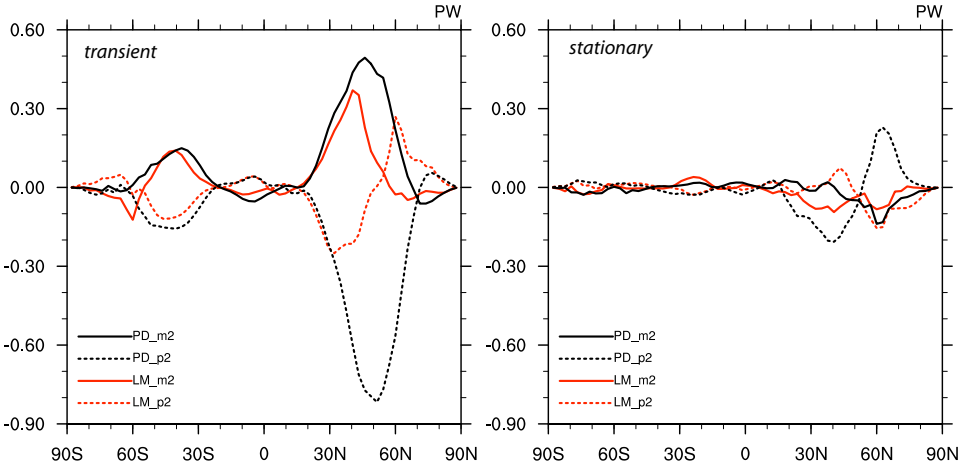

Figure 2.7: Vertically integrated transient (left plot) and stationary (right plot) annual eddy heat transport anomalies for PD (black) and LGM (red) simulations.

In conclusion, the cause of the decreased mid-latitude dry static energy transport sensitivity in cold glacial climates is the decreased sensible heat transport sensitivity, which, in turn, is a consequence of the weakened transient eddy heat flux response. In our LGM simulations we see an enhanced and narrower polar jet (Figure 2.8*c*) and decreased eddy kinetic energy (Figure 2.8*d*) in the North Atlantic compared to the PD simulations (Figure 2.8*a* and *b*).

Other studies (Li and Battisti, 2008, Donohoe and Battisti, 2009) have noted reduced storminess under glacial conditions despite the stronger Atlantic jet, which is in line with our findings. The dominance of mid-latitude DSE response in AMOC slowdown experiments was also found by Cheng et al. (2007) who also attributed it to increased transient eddy activity. It is important to note the difference to the global warming experiments of Hwang and Frierson (2010), where latent heat transport dominates the overall response.

Caution should be taken given that CCM3 overestimates the winter maximum in transient eddy heat flux over the North Pacific (Hurrell et al. 1998). Nevertheless, our analysis focuses on relative changes (compared to the base state) and is in line with existing studies (Cheng et al. 2007, Li and Battisti, 2008, Donohoe and Battisti, 2009) suggesting that the found response is robust.

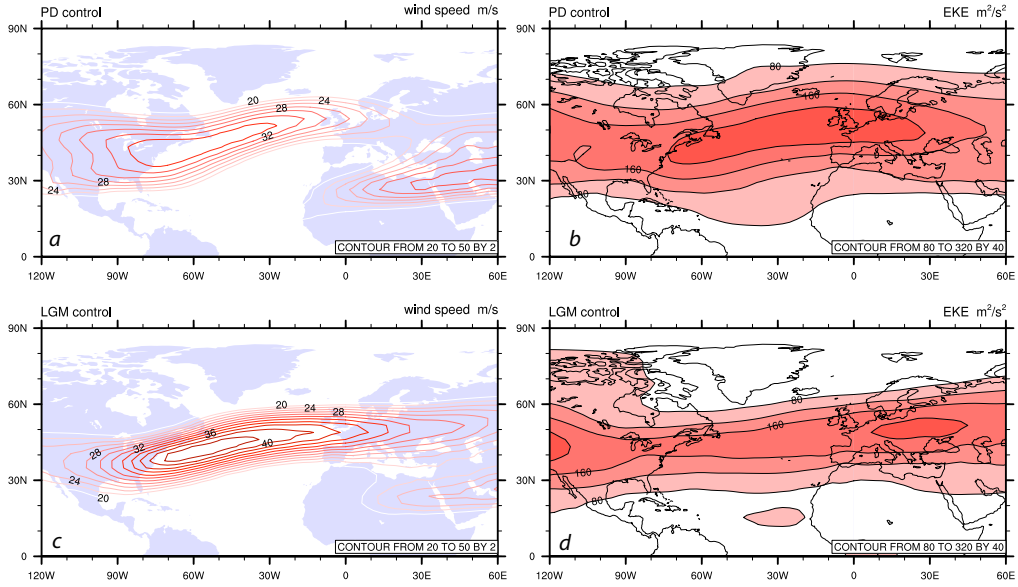

Figure 2.8: Annual 200 hPa wind speed (*a* and *c*) and eddy kinetic energy (*b* and *d*) for PD and LGM control climates.

2.3.2 *b* Low-latitude effects

Changes in cross-equatorial energy transports are related to changes in the Hadley cell dynamics and ITCZ shifts. A more northward ITCZ location results in more energy transported to the Southern Hemisphere and vice versa. Dry static energy transport increases towards the cooled hemisphere and latent heat transport towards the warmed one. The location of the crossover between the annual latent heat and DSE transports was found by Trenberth and Stepaniak (2003) to coincide with the time mean location of the ITCZ, and we will exploit that here and use it as a proxy. This is shown in Figure 2.9 for the PD and LGM simulations as the intersection of lines with the same dash pattern and color. In PD simulations the crossover is located in the Northern Hemisphere for all of the perturbations. The position is at 5°N in the control, and with increasing perturbation strength it gets displaced northward (6°N in PD_p2) or southward (3°N in PD_m2), while staying in the NH. In contrast, the LGM time mean ITCZ location is closer to the equator and more sensitive to the imposed perturbations such that it shifts all the way to 6°S in the cooling simulation (LM_m2) and to 6°N in the warming simulation (LM_p2). In comparison to the Trenberth and Stepaniak (2003), (Figure 1 in their study, top panel), we see that the DSE and latent heat transport crossover is located at approximately 5°N which fits very well with the location of the crossover in our PD control simulation.

The fact that the crossover between the two transports co-locates with the present day ITCZ does not necessarily carry over to LGM conditions and this may therefore not be a suitable mean ITCZ location proxy in the cold glacial climates. Nevertheless, consideration of the crossovers reveals that the energy transport partitioning under glacial and interglacial conditions is essentially different.

The Hadley cell's efficiency in transporting energy poleward can be inferred from the total gross moist static stability, by considering the ratio between the total energy and mass transports as done in the study by Kang et al. (2009). In our experiments, the Hadley cells are not necessarily located over the same areas in the different simulations. Similarly to the described ITCZ shifts, the meeting points of the northern and southern Hadley cell move more in LGM than in PD simulations, and locations of the Hadley cell maxima can be at different heights or latitudes in different simulations. Such is the case for the annual PD and LGM northern Hadley cells maxima that are located close to 15°N but at 700 hPa and 500 hPa, respectively. Therefore, instead of specifying a certain latitude and height, we simply consider the

point of the maximum of the mass stream function. We then calculate the ratio of the northward energy transport at this latitude and the stream function maximum itself. In this manner we obtain a measure of the northern Hadley cell efficiency in transporting energy to the mid-latitudes, which is directly comparable for PD and LGM conditions. Such analysis shows that the drier low-level LGM atmosphere increases the total gross moist static stability ($2.6 \cdot 10^4$ J/kg compared to $2.0 \cdot 10^4$ J/kg in PD), weakens the canceling effect that the latent heat transport has on the DSE transport and yields a larger LGM total northward transport in the low latitudes compared to the present day. We speculate that this larger efficiency permits the LGM energy transport at low latitudes to respond more readily to the circulation changes imposed by the meridional temperature gradients. Further details behind the different Hadley cell responses in the two climates are beyond the scope of the study.

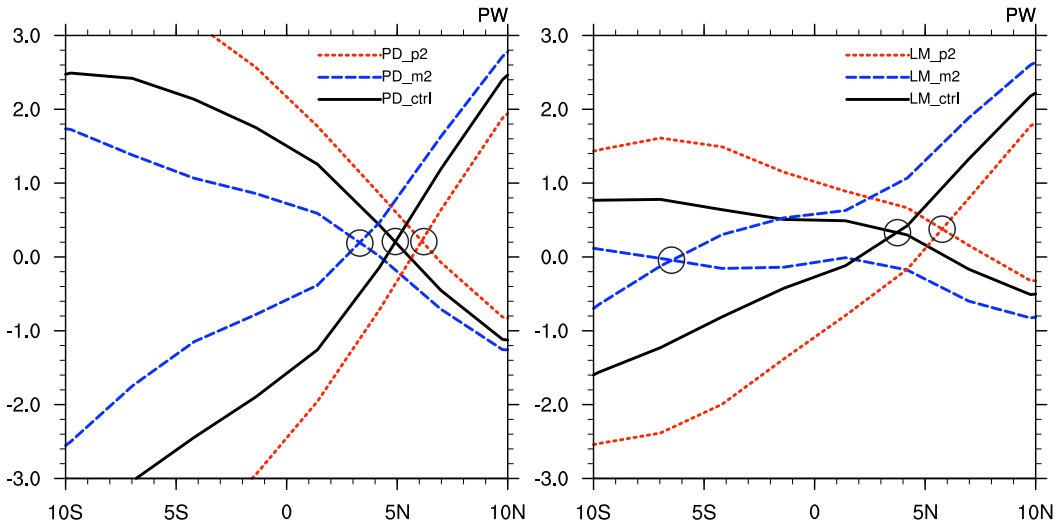

Figure 2.9: Locations of annual DSE and latent heat transport crossovers in PD (left plot) and LGM (right plot) simulations.

2.3.3 Integrated surface budget response

The atmospheric heat transport calculated above as the residual between the TOA and surface fluxes is the actual heat transported by the atmosphere since each atmospheric column must be in long-term energetic equilibrium. An implied ocean heat transport calculated analogously from the surface fluxes, on the other hand, represents the transport that would be necessary to uphold the SST field given the set of surface fluxes resulting from the experiment. One is thus implicitly assuming the SST field to be one of equilibrium, but given that the climate was perturbed away from the reference state and that the SSTs are fixed, there is little reason to expect this to actually be the case. To avoid confusion, it will thus be designated the integrated surface budget (ISB) in the following.

In our experiments, AHT responses occur because a high-latitude cooling, for instance, leads to a drop in the surface-to-atmosphere energy flux. Unless the TOA flux responds in concert with the surface, this leads to a cooling of the atmospheric column, which continues until a new equilibrium has been attained between the decreased surface flux, increased atmospheric heat transport and decreased TOA flux. As it turns out in the following, this atmospheric equilibrium tends to be one where the AHT responds much more strongly than the TOA flux, an effect which is manifested as Bjerknes compensation. The atmospheric heat transport response is thus a result of the combined surface flux and atmospheric changes per NHTD. The sensitivity of the surface fluxes to the imposed SST forcing may not be the same in the two climates and it is instructive to consider the integrated surface budget response per unit change in the NHTD.

At the equator (Figure 2.10*a*), the ratio of the LGM and PD integrated surface budget slope equals 1.5, while for the atmospheric heat transport (Figure 2.2*a*) this ratio is 2.33, showing that in part the difference between the LGM and PD AHT response is due to the different atmosphere-surface flux interactions. This is even more pronounced at 30 °N (Figure 2.10*b*) where the integrated surface budget and atmospheric heat transport ratios of the LGM and PD slopes are the same (they equal 0.5) and it suggests that the doubled PD AHT response at 30 °N is linked to the doubled PD ISB response. This is equivalent to saying that the atmosphere and surface flux changes yield the same degree of Bjerknes compensation in the two climates, the conclusion that can also be inferred by comparing the ISB to AHT sensitivities: the atmospheric heat transport compensates integrated surface budget changes by 0.22/0.28 = 0.79 in LGM and 0.11/0.14 = 0.79 in PD. As discussed above, both

the surface flux and AHT changes result from a two-way atmosphere-surface interaction following the imposed SST changes. We find here that the magnitudes of these changes are such that there is a stronger stabilizing feedback by the combined response in PD than in LGM.

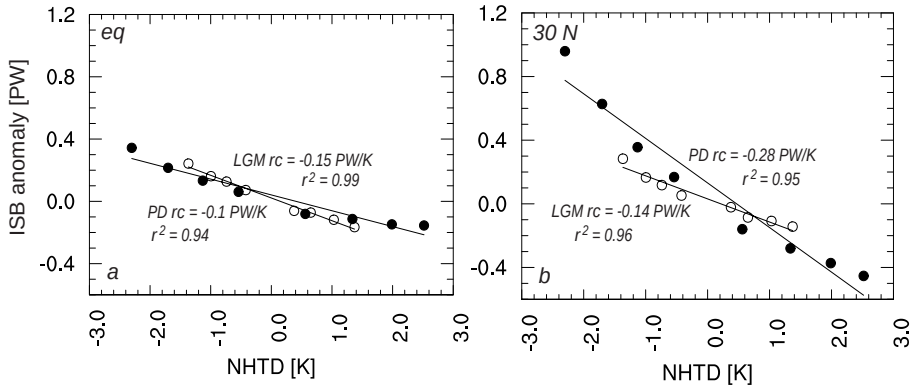

Figure 2.10: Integrated surface budget anomalies (ISB), in PW, at the equator (*a*) and 30°N (*b*) for PD (full circles) and LGM (open circles) simulations as a function of NHTD anomaly (K). As in the Figure 2.2, positive NHTD anomalies indicate NH cooling and vice versa. Linear regression coefficients and r^2 values of the fit are indicated.

2.4 Discussion and conclusions

This study demonstrates enhanced mid-latitude atmospheric heat transport sensitivity to the imposed high latitude surface temperature perturbations under warm (interglacial) compared to cold (glacial) conditions. This is shown to be a feature of both annual mean transports (in the experiments with added SST perturbations) and of monthly transports (in the control runs, due to seasonal variations of NHTD). The weakened glacial transport sensitivity is linked to a reduced transient eddy heat flux response. In comparison to the PD climate, the glacial climate is found to have stronger overall stationary eddy heat fluxes, weaker transient eddy heat fluxes, a stronger and narrower polar jet and decreased eddy kinetic energy in the North Atlantic. The transient eddy heat flux responses dominate over those of the stationary eddy heat fluxes, an effect which is larger in PD than in LGM simulations.

Consideration of the integrated surface flux budget reveals a significant role of the surface response in the upward propagation of the imposed SST forcing between the two climates, especially in the high latitudes where the TOA changes are small. Therefore, the effect found is a consequence of the combined surface-atmosphere interaction in which the final equilibrium surface and AHT response per NHTD is smaller in LGM than in PD. The atmosphere and surface fluxes react in a manner that provides a smaller negative feedback in the LGM per NHTD change.

Consequently, the PD climate appears more capable of damping high latitude anomalies due to the strong mid-latitude response while much less change is seen in the tropics. In contrast, the LGM simulations display the major response in the tropics where the cancellation between dry static energy and latent heat transports is weaker and energy is transported more efficiently away from the tropics. From Figure 2.2 it is possible to estimate the sensitivity of transport convergence into the area 0°-30°N for the PD and LGM experiments. When the NHTD increases by 1K (as a result of the added surface perturbations), the PD equator sees an increased import of energy from the southern hemisphere of 0.09 PW and at 30°N an increased poleward transport of 0.22 PW is found. The area 0°-30°N thus encounters a net loss of 0.13 PW. In the LGM experiments, the resulting import of energy from the southern hemisphere is considerably larger (0.21 PW) and the poleward transport at 30°N is considerably smaller (0.11 PW) and the area 0°-30°N encounters a net *gain* of 0.10 PW. The two effects of the prime LGM response being in the tropics and the prime PD response being in the mid-latitudes thus combine to yield opposite tendencies on the 0°-30°N energy budget with a gain in LGM and a loss in PD. The net contribution to the 30°-90°N budgets from the energy transport are just equal to the 30°N sensitivities, i.e., 0.22 PW for PD and 0.11 PW for LGM. From these quantities we can calculate the energy transport contribution to the tendency on NHTD as the net for the low latitude area less that of the high latitude area. For the PD experiments we find -0.13 PW - 0.22 PW = -0.35 PW, and for the LGM we find 0.10 PW - 0.11 PW = -0.01 PW. The contribution of the meridional energy transport to the negative tendency on the NHTD is thus much larger for the PD than for the LGM. In the PD, there is thus a much larger negative feedback on the imposed temperature gradients as a consequence of the enhanced atmospheric transport response.

Although the atmospheric circulation changes are not considered to be the primary cause of decreased interglacial variability, these results give an important indication of a varying ability of the surface and atmosphere to feed back negatively on imposed oceanic changes in different climates.

Surface boundary conditions as seen by the atmosphere, i.e., topography, sea ice and SST, are quite different in PD and LGM, and the decreased LGM response we find is therefore a combination of all these factors. In order to qualitatively constrain the importance of the sea ice geometry, an additional experiment with three times the initial anomaly added to the LGM background climate was performed. This simulation had much less summer sea ice and a NHTD anomaly similar to that of the PD_p2 case. The overall slope of the LGM response was not affected significantly by the inclusion of this point, although if one considers only the warming LGM simulations (including the LM_p3 experiment), then the slopes in the two climates are more similar. Since these are all cases with less sea ice, the large sea ice extent in LGM simulations is possibly an important component in the decreased glacial energy transport feedback. This is, however, not necessarily the only reason given that according to, for instance, Cook and Held (1988), it is the LGM orography that causes a change in the stationary eddies and thus forces a different partitioning of the transient and stationary components between the two climates.

In conclusion, the sensitivity of the atmospheric transport to NHTD changes, which depend on the background surface conditions described above, shows less negative transport feedback during Last Glacial Maximum as compared to present day. Choosing the prescribed SST configuration in our experiments enabled the study of the atmosphere only response to the applied perturbation, but did not allow for surface ocean feedbacks. Further work is required to evaluate the complete long term response when interactions with the ocean surface are allowed. Presumably such interactions could tend to reduce the effect of the meridional transport feedback discussed here.

Chapter 3

Global energy budget changes to high latitude North Atlantic cooling and the tropical ITCZ response

This study investigates the nature of global energy flux changes in response to North Atlantic high latitude cooling applied in an atmospheric general circulation model coupled to a slab ocean. We focus on key local and remote feedbacks that collectively act to alter the energy budget and atmospheric energy transport. We also investigate the relative roles of tropical SST and energy flux changes in the ITCZ response to North Atlantic cooling.

Using a radiative kernel technique, we quantify the effects of key feedbacks temperature, cloud and water vapor, to the top-of-the-atmosphere radiative flux changes. The results show partial local energy flux compensation to the initial perturbation in the high latitudes from the negative temperature feedback. However, shortwave albedo and longwave water vapor act as strong positive feedbacks, and as a consequence drive a significant increase in the atmospheric energy transport to the Northern extratropics. The additional energy flux providing this increase comes from the southern tropics, where the majority of feedbacks are negative and act to warm the area, with the energy gain originating from the cloud radiative feedbacks, temperature and longwave water vapor feedbacks.

It has been previously argued that the role of tropical SST changes was secondary to the role played by the atmospheric energy flux requirements in controlling the ITCZ shifts, proposing that the SST response is a result of the surface energy budget and not a driver of the precipitation response. Our study attempts to further constrain the proposed role of tropical SST changes. In our idealized simulations with the fixed tropical SSTs, we show that the ITCZ shifts are not possible without the tropical SST changes and demonstrate the atmospheric preference for getting the energy from the northern tropical surface flux changes over the tropical atmospheric reorganization. The ITCZ shift is influenced mainly by the local (tropical) SST forcing, apparently independent of the actual high latitude energy demand.

3.1 Introduction

High latitude temperature perturbations simulated in atmospheric or coupled models have been shown to shift the meridional position of the Intertropical Convergence Zone (ITCZ) to the anomalously warmer hemisphere (Chiang and Bitz 2005, Broccoli et al. 2006, Chiang et al. 2008, Mahajan et al. 2011). The shift in the ITCZ implies a meridional displacement of the rising branch of the Hadley circulation. Viewed in terms of the angular momentum conservation, the circulation shifts towards the warmer hemisphere in order to avoid the high temperature gradients in the upper part of the Hadley cell (due to asymmetric cooling/heating in the subtropics) (Lindzen and Hou 1988).

Chiang and Bitz (2005) proposed a mechanism for the communication of the high latitude Northern Hemisphere cooling to the tropics through the progression of the surface cooling by the equatorward advection of cold air in the midlatitudes, and a wind-evaporation-sea surface temperature (WES) feedback in the subtropics. Their focus on sea surface temperature (SST) followed a longstanding argument that the ITCZ shifts in response to cross-equatorial SST gradients. As the cooling reaches the tropical latitudes, anomalous cooling in the Northern subtropics creates the anomalous meridional pressure gradient that drives an anomalous southerly cross-equatorial flow and causes the ITCZ displacement (Chiang and Bitz 2005). Hereafter, we will refer to this view as the 'SST' perspective of ITCZ shifts. This interpretation is based on an argument by Lindzen and Nigam (1987) that tropical surface pressure gradients are tied to SST gradients through the effect that the latter have on temperatures in the boundary layer. They showed that the cross-equatorial flow is very sensitive to near-equatorial pressure gradients, similar to the conclusion derived in other studies (e.g Chang et al. 2000, Chiang et al. 2002). Later studies also noted significant positive feedbacks that act to augment the existing meridional SST gradient and cross-equatorial wind anomalies, including a 'near-equatorial' WES effect and low cloud feedbacks (Xie and Carton 2004).

From the energy budget perspective, cooling in the high northern latitudes cannot be locally compensated and an increased northward atmospheric heat transport is required to close the extratropical energy budget (Chiang and Bitz, 2005). The additional energy is provided by the tropics, from increased radiative flux absorption resulting from the ITCZ shift to the anomalously warmer hemisphere. This energy surplus is then transported from the tropics into the high and mid latitudes of the cooled hemisphere (Chiang and Bitz

2005, Cheng et al. 2007). ITCZ shifts appear to be a robust response to high latitude cooling, independent of the background climate (Cheng et al. 2007), although the sensitivity of the atmospheric transport response varies between the interglacial and glacial conditions (Cvijanovic et al. 2011).

The global energy budget response to extratropical thermal forcing has also been investigated by Kang et al. (2008, 2009) in a set of idealized aquaplanet experiments. Forcing applied in these two studies resembles the "bipolar seesaw" pattern, with cooling in one and warming in the other hemisphere, with the global average forcing equal to zero. They find a close connection between the ITCZ shifts and cross-hemispheric energy transports, and interpret this link as follows. Their applied forcing implies an anomalous cross-hemispheric oceanic heat transport, which is compensated to a degree by the anomalous cross-hemispheric atmospheric heat transport resulting from the atmospheric response to the imposed forcing. Given the level of compensation and the ambient tropical gross moist stability, the change in the cross-equatorial mass flux (and hence tropical precipitation response) can be predicted. They argue for a dynamically-determined level of compensation (presumably through altered eddy fluxes) of around 25%, based on aquaplanet-model calculations with no cloud and water vapor feedbacks. The addition of cloud and water vapor feedbacks, however, brings up the level of compensation up dramatically, up to around 115% in the atmospheric general circulation model used in their study. These studies thus also illustrate the sensitivity of the tropical response to model convection scheme and cloud feedbacks.

Kang and Held (2011) showed that ITCZ shifts to extratropical thermal forcing are also possible without the WES feedback. In a series of idealized experiments with WES feedback suppressed, they demonstrated that the ITCZ precipitation still responds as before to extratropical thermal forcing, even though the simulated tropical surface temperature gradient changes are smaller. According to the study, atmospheric energy budget and the moist static stability determine the precipitation response in the model. They interpret this result as supporting the energy flux perspective of ITCZ shifts, and further argue that the SST response is caused by the surface energy budget changes and it is not a driver of the precipitation response. This perspective is in accord with previous studies (e.g. Neelin and Held (1987), Lindzen and Hou (1988)) that emphasize the atmospheric energy budget in understanding tropical circulation changes.

Reconciling the SST and energy flux perspective is not a trivial task, but could immensely help the current understanding of tropical precipitation shifts. There is a significant overlap between the two views in sense that in

both the ITCZ shifts to the warmer hemisphere in order to allow for the increased energy transport to the cooled hemisphere. Thus, in both perspectives the ITCZ shift is associated with the change in AHT. Also, both perspectives agree that the meridional SST gradients play a role in the tropical adjustment. However it is the mechanism of the shifts that still needs to be reconciled. While Kang and Held (2011) showed that the energy flux perspective was more predictive of the tropical precipitation response, the causality of the events leading to precipitation shifts were still open to question. They have suggested that the SST changes result from the surface flux changes in response to the AHT requirements that determine the precipitation response. Chiang and Bitz (2005) SST perspective however assumes that the SST changes are the trigger to tropical precipitation shifts.

Our study examines the response to high-latitude North Atlantic cooling in an atmospheric general circulation model (AGCM) coupled to a slab ocean model. In comparison to the previous studies like Kang et al. (2009) and Kang and Held (2011), our simulations are not performed in the aquaplanet mode, but use realistic surface boundary conditions. Another point is that the imposed cooling is applied only in the high-latitude North Atlantic and it is not 'compensated' in the southern hemisphere. This scenario is based on abrupt climate change events during the last glacial that are thought to be driven by North Atlantic cooling. As the atmospheric response timescales are much shorter than oceanic, our approach reflects the global atmospheric adjustment after the high latitude cooling has been imposed.

We focus on two specific aspects: (i) motivated by the energy flux viewpoint, we examine the response to high-latitude North Atlantic cooling in a relatively realistic model configuration (an AGCM coupled to a slab ocean model), specifically considering the origins of the zonal mean energy budget changes; and (ii) we further investigate the relative roles of the atmospheric energy budget and SSTs in causing the ITCZ shift, following Kang and Held (2011).

The global top-of-the-atmosphere (TOA) energy budget changes to high latitude cooling are examined by considering the extratropical, northern and southern tropical energy budget anomalies and decomposing their corresponding TOA flux changes into individual feedback effects. In particular, the radiative kernel technique of Soden et al. (2008) is used to quantify individual shortwave and longwave feedbacks arising from the temperature, cloud, water vapor and albedo changes. The radiative kernel approach was previously used by Shell et al. (2008) and Zelinka and Hartmann (2011) to assess the role of different feedbacks in global warming experiments. Another study by Yoshimori and Broccoli (2009) used a 'partial

radiative perturbation' method to assess the radiative feedbacks in AGCM-slab ocean simulations with reduced solar irradiance in the northern extratropics. They found the energy budget changes to be chiefly influenced by the water vapor and lapse rate feedbacks, with cloud feedbacks playing the role in cooling the northern tropics and midlatitudes. Our study, on the other hand, provides the quantitative radiative feedback analysis for simulations with the imposed high latitude North Atlantic surface cooling. We focus on the atmospheric reorganization that provides the energy compensation for the high latitude energy loss, and identify the main radiative feedbacks and the locations responsible for the energy gain.

We also examine the relative roles of SST versus the atmospheric energy flux changes in the ITCZ shift, in a series of idealized experiments that allow us to separate the influence of the remote (high latitude) and local SST forcing on tropical circulations. Our results emphasize the constraints that tropical SST changes impose on the ITCZ, and in doing so, show that while the energy flux perspective does represent a useful diagnostic tool for predicting the tropical precipitation shifts, the actual mechanism of the shift requires the SST perspective. The manuscript is organized as follows: in Section 3.2 we introduce the model and the experiments. Results are presented in Section 3.3 by first considering the global energy budget changes in the slab ocean experiments. In Section 3.4, we describe the hypothesis on the importance of tropical SSTs in the final energy compensation. This hypothesis is then tested in series of idealized experiments with fixed tropical SSTs in Sections 3.4.1 and 3.4.2, while in Section 3.4.3 the results of transient experiments are briefly discussed. Section 3.5 summarizes the conclusions and discusses the possible implications.

3.2 Model setup and simulation design

We use the NCAR's Community Atmosphere Model version 3 (CAM3) in the slab ocean mode, with T42 resolution and 26 vertical levels. The physics and dynamics of the CAM3 model are described by Collins et al. (2004) and Collins et al. (2006). The model includes the Community Land Model (CLM) version 3.0 (Bonan et al. 2002, Oleson et al. 2004). Spatially varying annual mixed layer depths for the slab ocean are derived from the Levitus data (1982), and a monthly-varying ocean heat flux convergence (aka the Q-flux) is applied to keep the simulated SST close to present-day. Present day land surface conditions, orbital and greenhouse forcing are applied. High-latitude North Atlantic cooling is imposed by altering the Q-flux field in the manner as shown in Figure 3.1.

We undertake two sets of simulations, one where the slab ocean is applied globally, and the other set where there are mixed surface ocean boundary conditions – fixed SSTs in the tropics, and slab ocean elsewhere. We start by running the control (hereafter labeled 'CTRL') and the North Atlantic cooling ('SOM1') cases in the CAM3 coupled to the slab ocean (a summary of all the simulations done is listed in Table 3.1). For the SOM1 simulation, the magnitude of maximal cooling equals 15 W/m^2 and it is applied as shown in Figure 3.1. In these slab ocean simulations, the model was run for 40 years with the first 10 years of output discarded as spin up.

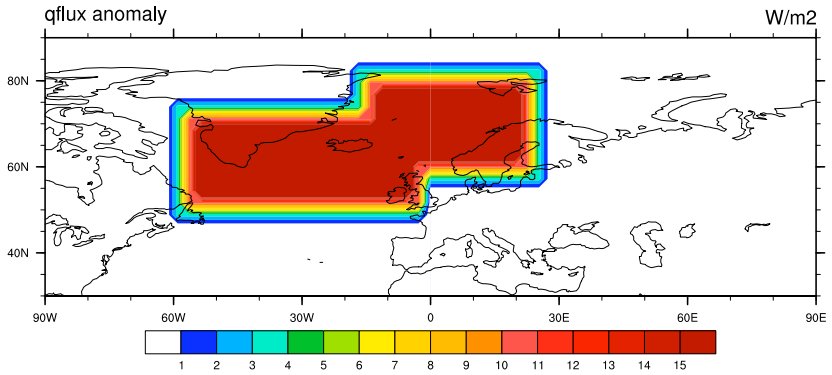

Figure 3.1: Geometry of the Q-flux anomaly applied over the North Atlantic sector

To assess the role that tropical SST changes played in determining the ITCZ response, we take the SSTs generated by these two simulations, and impose them in the CAM3 model simulations as a tropical fixed SST boundary condition (see next paragraph for specifics). The fixed SSTs are applied over the global tropics from 26.5°S - 26.5° N. South and north of 32.1°S and 32.1°N respectively, a slab ocean is applied. In the transition regions (26.5° to 32.1° in either hemisphere), the SST values are nudged between the fixed and slab ocean (calculated) values. More precisely, the surface temperature values over the ocean surface points in the transition regions, are obtained as a weighted average of the fixed and calculated SST values with the weights of the calculated SSTs increasing linearly from 0 at 26.5° till 1 at 32.1° and the opposite for the fixed SST weights.

In total, there are four idealized experiments with the SSTs fixed in the tropics (and slab ocean elsewhere): 1. FCTRL - unperturbed tropical SSTs corresponding to the ones from the control slab ocean experiment, and no North Atlantic cooling applied to the slab ocean; 2. HL – fixed climatological tropical SSTs as in FCTRL, plus the North Atlantic high latitude cooling; 3. TROP - fixed tropical SSTs corresponding to those simulated by the slab ocean experiment with North Atlantic cooling, but with no North Atlantic high latitude cooling applied to the slab ocean and 4. HL+TROP – fixed tropical SSTs as in TROP, plus the North Atlantic high latitude cooling applied to the slab ocean. In these idealized experiments, the model was run for 60 years, with output of the first ten discarded as spin up.

In addition to this, we have performed a set of transient simulations that have enabled to follow the adjustment period in more detail and test the conclusions derived from the idealized experiments. Presented climatologies for the transient simulations represent the mean of 20 ensemble members, obtained by branching from the initial control run each 5 years and applying the North Atlantic cooling.

experiment	fixed tropical SSTs	NA qflux
CTRL	no	no
SOM1	no	yes, 15 W/m^2
FCTRL	yes, as in CTRL	no
HL	yes, as in CTRL	yes, 15 W/m^2
TROP	yes, as in SOM1	no
HL+TROP	yes, as in SOM1	yes, 15 W/m^2

Table 3.1: Experiment summary

3.3 High latitude and tropical response to North Atlantic cooling

3.3.1 General characteristics of the equilibrium response

Annual surface temperature anomalies due to imposed high latitude cooling are shown in the Figure 3.2 (upper panel) for SOM1 experiment. Similar to Chiang and Bitz (2005) and Mahajan et al. (2011) we find that the high latitude cooling has spread into the northern tropics, forming a dipole with colder northern and warmer southern tropics. This is especially pronounced over the Pacific sector. Maximal (annual) cooling is about 8^{o}C in the high latitudes and 0.5^{o}C in the northern tropics while the southern tropics became warmer by about 0.5^{o}C.

Precipitation anomalies (Figure 3.2, lower panel) show a southward shift of the maximal precipitation zone over all ocean basins, with ~2mm/day increase over the southern tropics and a similar decrease over the northern tropics, indicating a southward shift in the ITCZ. Precipitation also decreases by ~1.5mm/day in the North Atlantic, where the cooling was imposed. The mean meridional stream function anomaly (Figure 3.3, left panel) indicates a southward displacement of the uplift region, leading to a strengthening of the northern Hadley cell and weakening of the southern cell. Surface wind anomalies (3.3, right panel) reveal an increase in the north-easterly trades and a decrease in the south-easterly winds.

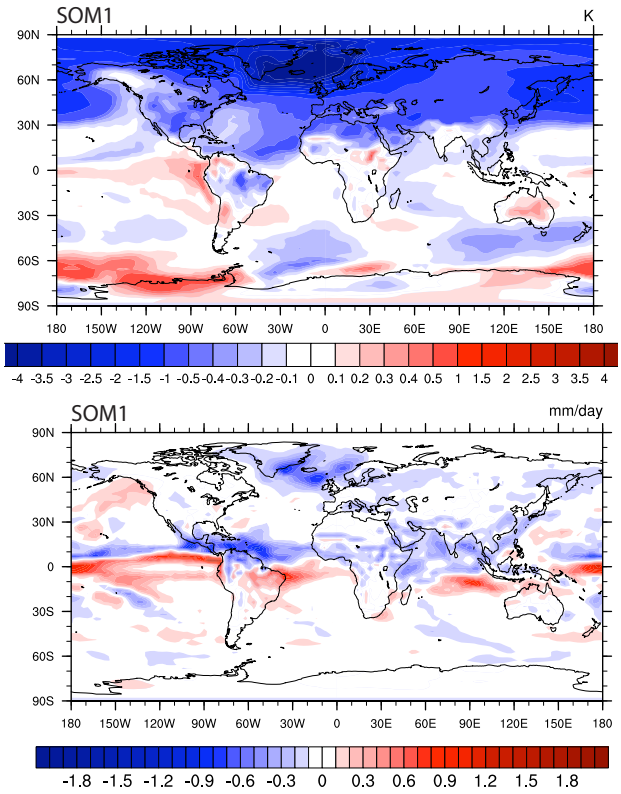

Figure 3.2: Annual mean temperature and precipitation anomalies in the SOM1 experiment

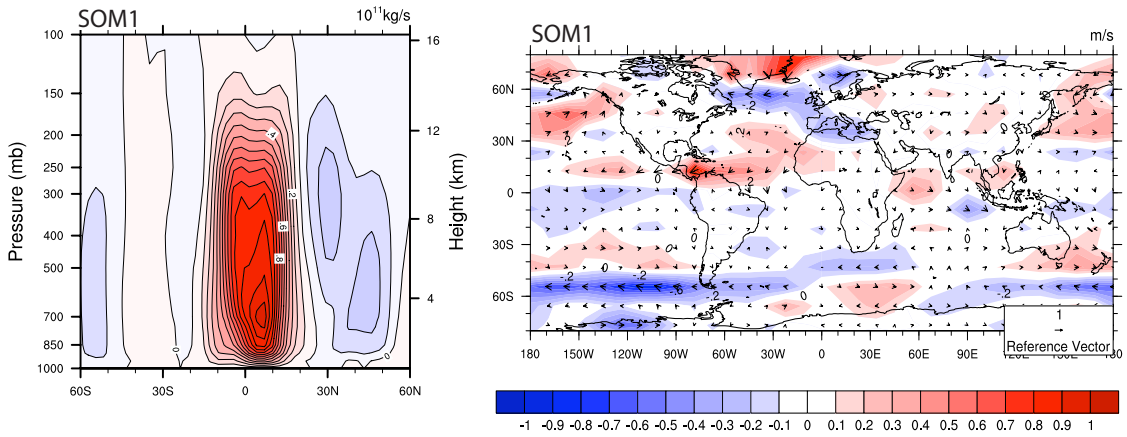

Figure 3.3 (left plot): Annual meridional stream function anomaly [kg/s], contour lines are shown every 10^{11} kg/s (positive – red shading, negative – blue shading) and (right plot): annual surface wind speed anomalies [m/s] for the SOM1 experiment.

We now examine the energy budget and poleward energy transport changes (Figure 3.4). The surface energy budget (black dashed line) is altered essentially only over the latitudes of imposed cooling. The top-of-the-atmosphere (TOA) energy budget (solid black line), on the other hand, shows change across all the latitudes, with a maximal anomaly of 0.06 GW/m in the southern tropics. The northward atmospheric heat transport anomalies (Figure 3.9) show increased transport from the southern tropics to the northern mid and high latitudes. The additional energy deposited in the northern mid and high latitudes originates from increased TOA energy flux in the southern tropics. If we increase the magnitude of the high latitude forcing, we find the same qualitative response in rainfall and energy fluxes, but with increased magnitude (not shown).

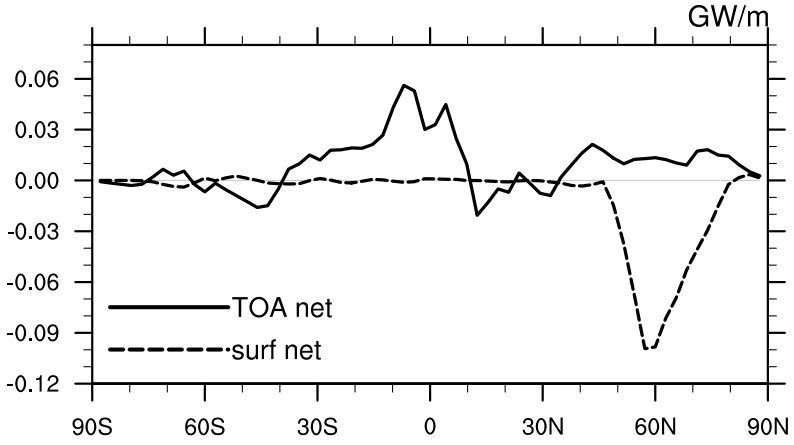

Figure 3.4: Top-of-the-atmosphere (solid) and surface (dashed) annual zonal net energy budget anomalies

Similar features of the tropical response due to the North Atlantic cooling were found in study by Chiang and Bitz (2005), in simulations where increased land ice or sea ice cover were applied in the Northern hemisphere. It has also been noted previously, in this and other studies (Chiang et al. 2003, Mahajan et al. 2011) that the southern tropics tend to be the location where increased TOA energy flux arises providing the additional energy flux to the northern high latitudes. Our aim is to broaden these conclusions by addressing the exact feedback mechanisms that act to provide the TOA energy surplus locally and remotely and offer an explanation why the southern tropics are favorable area instead of, for example, northern tropics. We continue our analysis by investigating how the high latitude energy demand propagates to the tropics and what would be the requirement for the energy compensation to occur somewhere else.

3.3.2 Global energy budget and radiative feedbacks response

3.3.2 *a* Radiative kernel technique

We apply the radiative kernel technique developed by Soden et al. (2008) and implemented for the CAM3 by Shell et al. (2008) which allows us to decompose the TOA changes into various climate feedbacks. The technique separates the individual climate feedbacks into two parts: the radiative kernel term $\frac{\partial R}{\partial X}$ and the climate response of the feedback variable $\frac{\partial X}{\partial T_s}$. Here ∂R refers to the total change at the TOA, X is the considered climate variable and ∂T_s is the change in the global mean surface temperature (in a steady state). Defined as such, the radiative kernel quantifies the change in TOA flux due to small perturbations in the corresponding climate variable. Given the climate response (from the model output) we can combine the two and calculate the individual feedback parameters, while the total feedback parameter γ is considered a sum of the individual feedbacks and a small residual *Re*:

$$\gamma = \sum_{i=1}^{n} \frac{\partial R}{\partial X_i} \frac{dX_i}{dT_s} + \mathrm{Re} \qquad (1)$$

The total change in the top of the atmosphere energy budget can then be approximated as:

$$\Delta R = \gamma \Delta T_s = (\gamma_T + \gamma_q + \gamma_{alb} + \gamma_c)\Delta T_s \qquad (2)$$

where γ_T , γ_q , γ_{alb} and γ_c are the temperature, water vapor, surface albedo and cloud radiative feedbacks. Shortwave and longwave radiative kernels are provided for most of the climate variables except for the clouds. Due to the non-linearities associated with the cloud feedbacks, the later are calculated by applying the corrections to calculated cloud radiative forcing (CRF). For details on the feedback calculations, we refer the reader to Soden et al. (2008) and Shell et al. (2008).

Given that the radiative kernels are calculated around a predetermined present-day base state climate that may differ in details from our simulations and that their application was mainly tested in the CO_2 doubling experiments, we first evaluate the technique by considering only the clear sky feedbacks (Figure 3.5*a* and *b*). Figure 3.5*a* shows that there is an excellent agreement between the TOA longwave energy flux changes (solid red line) and the sum of longwave feedback effects (dashed red line) comprising of those for

temperature, surface temperature and water vapor. Shortwave feedbacks (dashed red line, 3.5*b*) do not show as good agreement with the total TOA shortwave energy budget changes (solid red line, 3.5*b*). This difference mainly occurs in the high latitudes, suggesting that the cause of disagreement is the shortwave surface albedo feedback by sea ice. Shell et al. (2008) discusses the uncertainties related to the radiative kernel technique and its limitations in surface albedo feedback calculations. They noted that this parameter tends to behave more nonlinearly compared to the other feedbacks, with the effect being especially pronounced at the edges of sea ice cover.

All-sky feedbacks, shown in Figures 3.5*c* and *d*, behave in similar manner with a very good agreement between TOA longwave changes and the sum of the longwave feedback effects but with lesser, but still reasonable, agreement between the shortwave feedback effects and TOA shortwave changes in the high latitudes. For this reason, we are cautious in interpreting high and midlatitude shortwave feedbacks. Despite of that, the comparison of the zonal TOA energy budget anomalies and the overall feedback effects in Figure 3.5 suggest that the disagreement between the two is much smaller than the actual anomalies and therefore is not likely to significantly alter our findings.

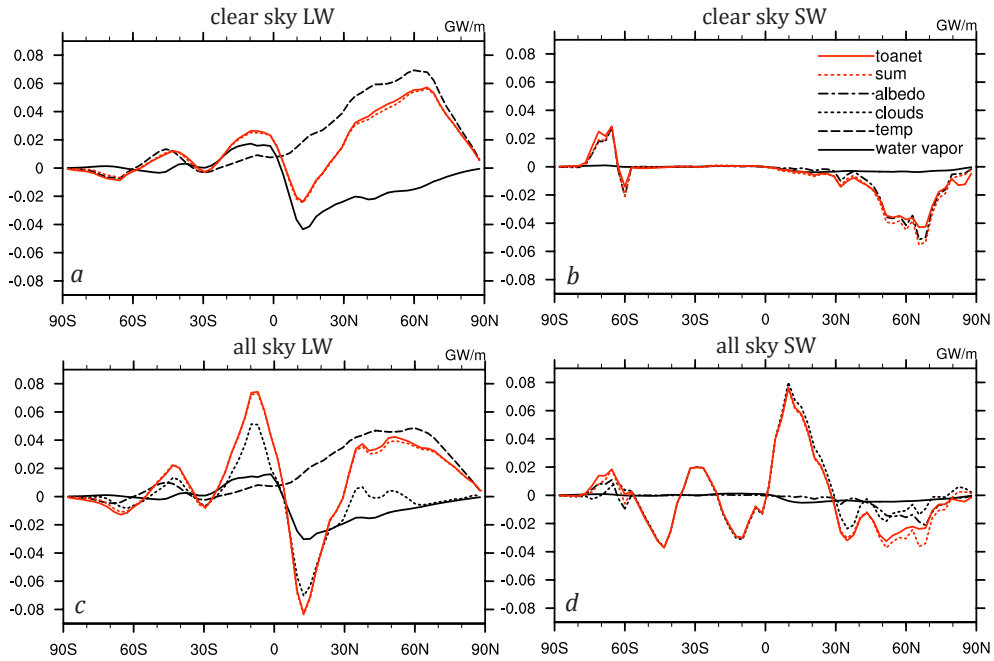

Figure 3.5: Clear-sky (a and b) and all-sky (c and d) longwave (a and c) and shortwave (b and d) feedback effects and TOA energy budget anomalies in SOM1 experiment. Black lines: shortwave feedback effects (water vapor (solid), albedo (dot dashed) and cloud (dotted)) and longwave feedback effects (temperature - surface and air (dashed), water vapor (solid) and cloud (dotted)). Red lines - sum of corresponding feedback effects (dashed) and the respective TOA energy budget anomalies (solid).

3.3.2 *b* Energy balance decomposition

The principal high latitude effect originates from the temperature longwave feedback (Figure 3.5*c* and *d*). It consists of both the surface and air temperature feedbacks, and it is a negative feedback as it acts to damp the initial cooling. In the tropics, the majority of TOA energy budget changes are due to the longwave and shortwave cloud and longwave water vapor feedbacks. Longwave cloud feedbacks act to warm the southern and cool the northern tropics, while the shortwave cloud feedback has an opposite effect.

In order to summarize the essential features of the energy flux changes and the role of radiative feedbacks, we simplify the considered regions into three distinct latitude bands: 90°N till 30°N (northern extratropics), 30°N till 10°N (northern tropics) and 10°N till 40°S (southern tropics). These bands were chosen based on an assessment of regions that exhibit similar behavior,

specifically using the sign of the zonal TOA net energy budget anomaly. The analysis is shown in Figure 3.6*a* where all the fluxes are being defined positive into the box.

Applied North Atlantic cooling causes a surface energy imbalance of -0.191 PW over the northern extratropical box (90°N - 30°N). We use the anomalous surface energy budget from this box to normalize the energy flux and transport changes in this and other regions, making the surface loss in the northern extratropical box equal -1 (-100%). It is important to mention that this surface energy loss encompasses both the applied cooling and the surface feedbacks. The Figure 3.6*a* further shows that 36% of this initial loss is compensated by the TOA energy budget changes over the same region (0.069 PW). The TOA response results from a complex mix of negative and positive feedbacks. The longwave temperature feedback has the strongest effect, and with 0.256 PW (134%) is more than the amount lost to the surface. Countering this are the positive feedbacks that act to cool the area, with the biggest contributions coming from water vapor longwave -33% (-0.064 PW), cloud shortwave -26% (-0.049 PW) and albedo -29% (-0.036 PW) feedback effects. The overall energy flux between TOA and the surface in the northern extratropical box is negative, and to maintain energy balance the atmosphere needs to import energy from the lower latitudes at a rate of 0.121 PW (64%) across 30°N. In summary, because of the large cancellation between the negative and positive radiative feedbacks, the majority of the surface cooling has to be balanced by northward atmospheric transport.

We now consider the northern tropical box (10°N - 30°N). The surface flux changes are essentially zero (less than a percent), as it has to be because of the slab ocean constraint. The TOA net radiative flux shows a small loss of 3%, which is in agreement with the coupled atmosphere-ocean experiments by Cheng et al. (2007) who also noted small negative TOA anomalies over the northern tropics. Main changes in the TOA energy budget in this box originate from the cloud feedbacks due to the southward ITCZ shift and longwave water vapor feedbacks due to the cooling and drying of the northern tropics. Negative TOA flux anomaly arising from the cloud and water vapor longwave feedback effect is larger than the positive anomaly due to the shortwave cloud and temperature feedbacks. Overall, the TOA flux changes are small, but negative, and the northward energy transport of 0.121 PW out of the northern tropics is compensated for by somewhat larger atmospheric transport from the southern tropics of 0.128 PW (67%).

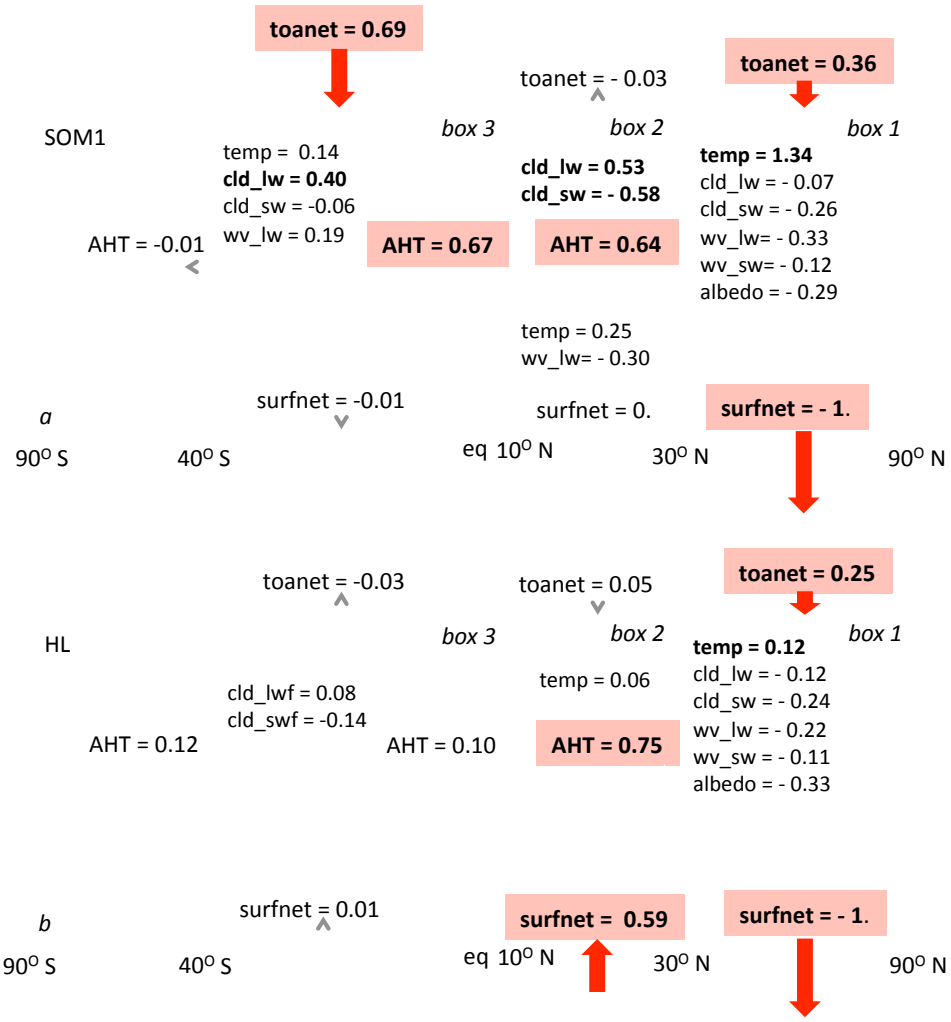

Figure 3.6: Schematic box energy budget - TOA and surface net energy budget anomalies are given at the top and bottom of each box (respectively), anomalous atmospheric heat transports are shown at the borders between the boxes and the main feedback effects are listed within the each box. All values are normalized by the surface energy budget anomaly from box 1, fluxes are defined positive into the box. (a): SOM1 experiment, (b): HL experiment. Legend: temp – temperature (including surface temperature), wv_lw - water vapor longwave, wv_sw - water vapor shortwave, crf_sw - cloud shortwave, crf_lw - cloud longwave feedback effects; toanet – TOA net energy flux, surfnet – surface net energy flux

In the southern tropical box (40° S - 10°N), the northward flux across its southern boundary is essentially zero, meaning that the energy required to supply the energy flux out of the northern edge has to come from TOA flux changes within the box. This positive TOA energy budget anomalies result from the longwave feedback effects arising from clouds 40% (0.076 PW), water vapor 19% (0.037 PW) and temperature 14% (0.027 PW). The total effect of the shortwave cloud radiative feedbacks over this area is small and negative (-6%).

We summarize the global energy budget response as following: the initial northern high latitude surface cooling is first compensated by the local TOA changes (about one third) while the rest of the energy is transported from the lower latitudes. The northern tropics do not provide required energy to close the energy budget, this is because despite the fact that there are sizable changes in TOA longwave and shortwave fluxes, they essentially cancel each other out. Rather, it is the southern tropics that provide the energy required, which is transmitted by atmospheric energy transports across the northern tropics to mid and high latitudes.

Tropical top-of-the-atmosphere energy flux changes result from the three main feedback effects, originating from clouds, water vapor and temperature. Temperature and water vapor feedbacks have opposing effects: over the colder and consequently drier areas, temperature feedback provides positive and water vapor negative TOA energy flux changes. In the high northern latitudes, the temperature feedback is stronger, so the overall sign of the TOA anomaly is determined by the temperature feedback. In the tropics on the other hand, the strongest feedback effect comes from the clouds due to the ITCZ shift and it exerts two opposing effects. The longwave cloud feedback induces positive TOA energy budget anomalies in the southern hemisphere and negative in the northern hemisphere, while the shortwave cloud feedback has the opposite effect, but smaller, making the overall TOA anomalies in the tropics follow the sign of the longwave cloud feedback effect. Overall, the colder and drier northern tropics are not capable of providing significant positive TOA energy flux changes (as shown earlier they are actually negative) due to the cancelation between longwave and shortwave feedback effects. In contrast, warmer and wetter southern tropics with the southward-displaced ITCZ, represent the perfect location to gain the energy required due to the high latitude energy loss.

Our results are in contrast to those by Kang et al. (2009), as in their aquaplanet simulations shortwave cloud feedback dominates over the longwave cloud feedback in the tropics. Consequently, the overall cloud feedback effect induces positive TOA flux anomalies in the northern tropics

and negative in the southern tropics, an outcome which is attributed to the increased low cloud cover in the northern tropics. In the next chapter we provide a possible explanations for this discrepancy, and clarify the relationship between the tropical SST anomalies and the precipitation shifts.

3.4 Proposed interpretation

Despite the fact that the southward ITCZ shift is causing a small amount of energy loss in the northern tropics due to the cloud feedbacks, it appears advantageous for the atmosphere to move the ITCZ south, because of the large energy gain accomplished by the convection reorganization there. The question we ask is: why the southern tropics and not somewhere else? Inspection of the tropical TOA anomalies (Figure 3.7, top panel - contours) shows, more accurately, that the areas of maximal (positive) TOA budget changes are located in the east tropical Pacific, encompassing the Pacific cold tongue area.

Tropical convection is known to be "tippy" as there is a threshold for deep convection, such that small changes in temperature (and consequently, moisture) at the margins of deep convective regions (so called 'convective margins') can initiate (or halt) deep convection. Locations with large zonal and meridional temperature gradients neighboring deep convection regions are such convective margins. During El Nino, warmer SSTs over the cold tongue leads to SST regions neighboring the Pacific warm pool to become sufficiently warm to exceed the threshold for deep convection.

In our case, however, convection is initiated over the marginal regions as a result of both the warmer SSTs in the tropical east Pacific region and colder mid-troposphere above it that lowers the threshold for convection. As previously noted by Chiang and Bitz (2005), weakened easterlies over the south-east tropical Pacific give rise to the initial SST warming while the SST dipole is maintained due to the higher moisture content in the warmed hemisphere. Although the observed warming is smaller than during the El Nino events, combined with lowered convection threshold it is sufficient in triggering the convection over the marginal regions. This additional deep convection provides the necessary increase in the TOA energy flux that makes up for the high latitude energy loss. Observed changes in global TOA absorption (Wong et al. 2009) shows that the convective reorganizations

related to ENSO events are indeed capable of affecting the global energy budget.

In comparison with the experiments by Kang et al. (2009), there are several differences to our setup that may have attributed to different conclusions, mainly the use aquaplanet model with the zonaly uniform SSTs and the differences in cloud parameterizations. Our experiments point out the importance of tropical meridional and zonal temperature gradients in creating the convective margins, an effect that can't be studied in the aquaplanet experiments. In addition, the model applied in our study responds by increasing the high cloud cover, in contrast to the predominant low cloud changes in Kang et al. (2009). Since our proposed interpretation favors the SST perspective, we further focus on the significance of tropical SST changes in ITCZ shifts in series of idealized experiments.

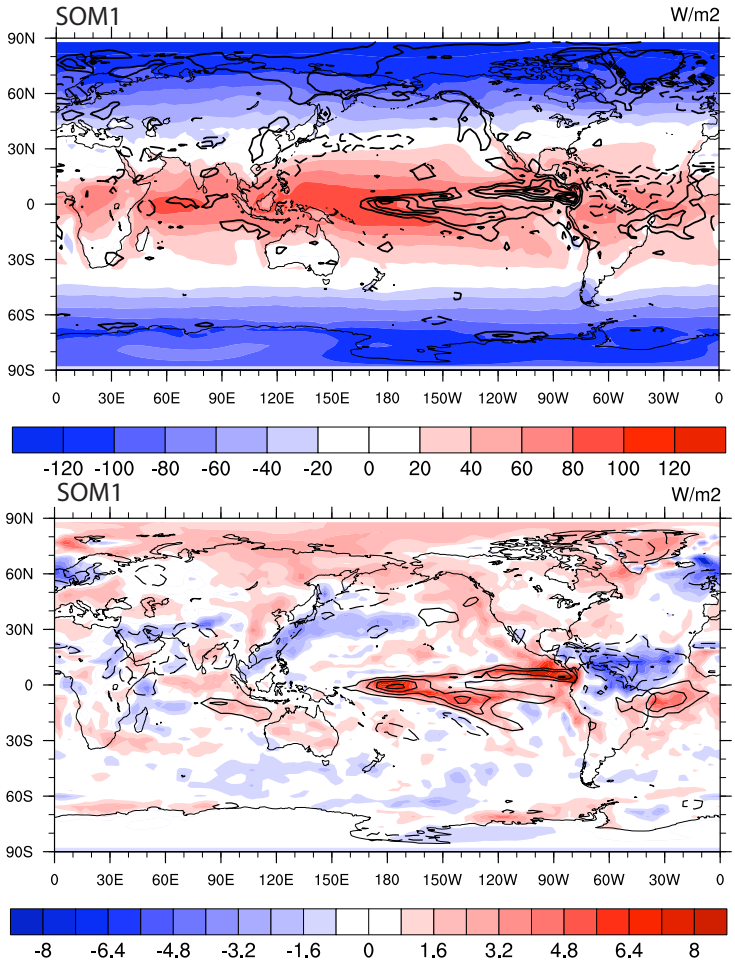

Figure 3.7 (upper plot): TOA flux climatology (colors) and its anomalies (contours) in SOM1 experiment, (lower plot): tropical TOA flux anomalies (colors) overlayed with high cloud cover anomalies in the SOM1 experiment. Contours: full lines - positive anomalies, dashed - negative anomalies, contour interval equals 0.02 for the high cloud anomalies and 2 W/m^2 for the TOA energy budget anomalies, zero contour ommited

3.4.1 Tropical SST anomalies as fundamental to ITCZ shifts

In order to investigate the role of tropical SSTs in ITCZ shifts, we perform idealized simulations in which the tropical SSTs are fixed to specified values, while keeping the slab ocean lower boundary condition in the extratropics (see Section 3.2 for details). In the control experiment (FCTRL), the tropical SSTs are fixed to climatology, and no high latitude North Atlantic cooling is applied. In the forced experiment (HL), high latitude North Atlantic cooling is applied in the same way as in the full slab ocean experiment, but tropical SSTs are not allowed to respond to these changes.

Surface temperature anomalies from HL experiment are shown in the upper panel of Figure 3.8. The cooling is limited to northern high and mid latitudes except for the small progression of cold anomalies into the tropics over land. Compared to the full slab ocean case, there is less cooling over the north-east Asia while the cooling pattern over the north-west America is reversed and the south-east remains warm. Annual precipitation anomalies are shown in the lower panel of Figure 3.8. The high latitude precipitation response features decreased values over the North Atlantic (where the cooling was imposed), similar to SOM1 case. In contrast, tropical precipitation changes are essentially not present, and show no southward ITCZ shift. This confirms that SST changes are necessary for the ITCZ shifts.

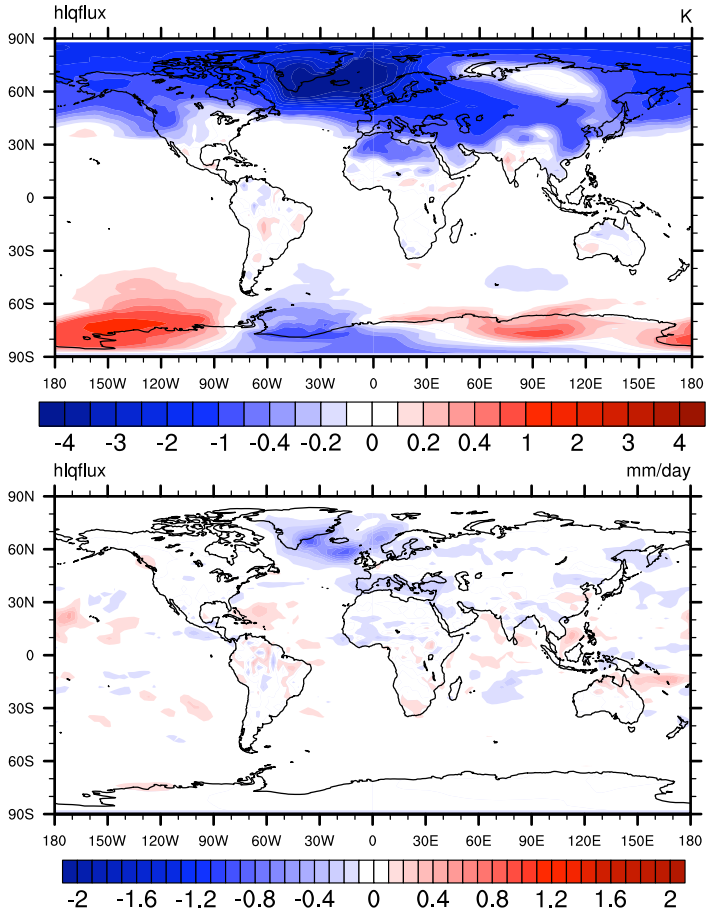

Figure 3.8: Annual mean surface temperature (upper plot) and precipitation (lower plot) anomalies in idealized experiment HL (tropical SSTs fixed to unperturbed values).

Northward heat transport anomalies, shown in Figure 3.9, reveal that the energy is transported from the *northern* tropics into the high latitudes, making the northern tropics the source of the additional energy. In the cases with fixed tropical SST, tropical surface energy budget anomalies are at least as important as the TOA changes for the energy absorbed in the column, and the northward energy transport is clearly affected by this.

Figure 3.6*b*, showing the box model, summarizes the way in which the energy flux changes come about in the HL experiment. In the northern extratropical box, there is a loss of -0.15 PW to the surface, due to the imposed cooling. As in the previous case, this will be used as a normalization factor, so that the total loss of energy to the surface in this box equals -1. Local TOA energy budget changes balance 25% of this initial energy loss to the surface. As in the full slab ocean case, temperature acts as the strong negative feedback, while the other feedbacks act to increase the initial cooling. The energy budget in the northern extratropical box is balanced by a

northward energy transport of 0.11 PW (75%) from the northern tropics. Most of the energy required for this anomalous northward heat transport comes from the northern tropical box itself, and mainly from the surface (59%), while the most of the remainder is supplied from the southern tropics (10%). Small amount is also acquired through positive TOA anomalies due to longwave feedbacks (5%). The southern tropics, in turn, gain most of the energy through northward transport across 40^{o}S.

The fixed tropical SSTs (set at climatology) provide an infinite heat source. As the cold air from the high and mid latitudes advects southwards into the northern tropics, the air-sea temperature difference over the northern tropics increase, resulting in increased surface fluxes into the atmosphere, in this case providing the bulk of the energy required by the northern extratropics. The increased surface fluxes arise largely from increased evaporation. In this idealized experiment, the crucial difference (from the full-slab setup) is that the surface is mainly providing the necessary energy to supply the northern extratropics; whereas in the full slab ocean experiment this energy can only come from the TOA flux changes (chiefly due to the cloud radiative feedbacks over the east tropical Pacific).

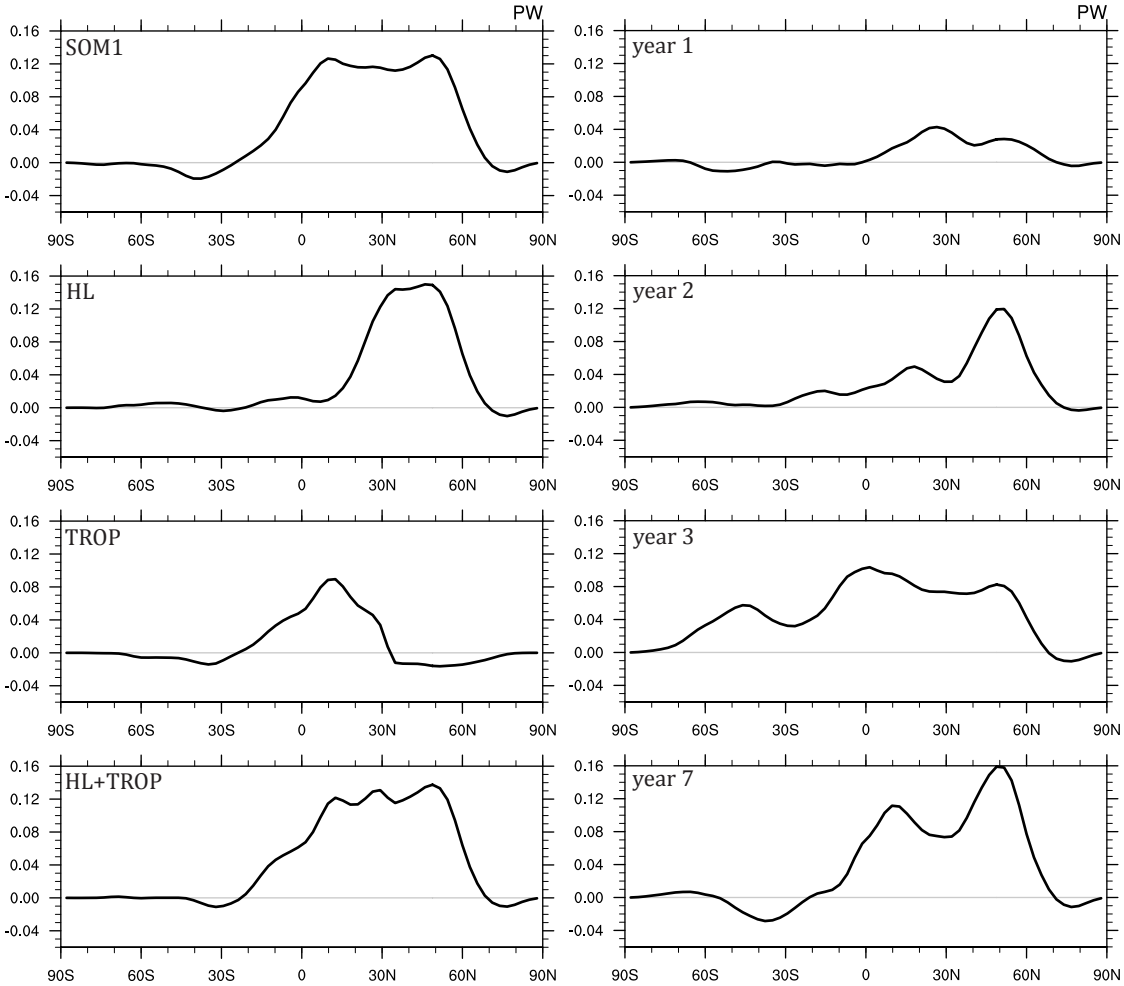

Figure 3.9: Northward atmospheric heat transport anomalies (PW): first column - SOM1 and the idealized experiments HL, TROP and HL+TROP, second column - transient experiments (years 1, 2, 3 and 7).

The main conclusion to be drawn from this idealized experiment is that tropical SST anomalies are crucial in order for the ITCZ to shift. From the energy viewpoint, the first place where the atmosphere tries to obtain the increased energy supply from is the northern tropics, specifically from the surface fluxes. In the fixed SST experiment, this supply can be maintained because it is an infinite source. In the slab ocean (and presumably the real world), this source is finite, and the subsequent northern tropical SST cooling leads to the southward ITCZ shift and relocation of tropical convection that leads to the southern tropical TOA energy gain. In both the fixed-SST and slab ocean cases, TOA fluxes in the northern tropics do not provide the needed energy. In the fixed SST scenario, the northern tropical climate does not change much and so the temperature, water vapor and cloud feedbacks are much smaller. As such, the northern tropical TOA energy budget changes are again not the main contributor to the energy gain.

Both SST and energy flux perspectives agree that without the ITCZ shift there will be no equatorial AHT response. In agreement with this, the cross-equatorial anomalous AHT in HL experiment is close to zero (Figure 3.9). However, this does not necessarily carry over onto the mechanism of the shift and into the conclusion that the ITCZ did not shift because there was no AHT response. Although the energy flux perspective shows that precipitation shifts can be predicted from the AHT response, there is no proof that they are triggered by the later. In HL experiment the tropical SST are not allowed to respond but there is no direct constraint on the development of the AHT response or atmospheric fluxes. The only limitation to AHT and atmospheric flux response comes from the fact that the SSTs are fixed. The results illustrate that the atmosphere rather gets the energy from the northern tropical surface fluxes than from the tropical atmospheric reorganization. In this idealized experiments, SSTs have completely determined the response.

3.4.2 Locally driven ITCZ shifts

The previous experiment showed that the tropical SSTs are required to change in order for the ITCZ to shift. We now ask whether the tropical SST changes are sufficient for the ITCZ to shift, regardless of whether high latitude North Atlantic cooling is imposed. To examine this, we expand our analysis with two new experiments. In both experiments, tropical SSTs are fixed and set to values corresponding to those in the full-slab ocean simulation with imposed cooling. However, in the extratropical slab ocean, one has no high-latitude North Atlantic cooling (hereafter the TROP experiment), while the other does (hereafter the HL+TROP experiment). We compare these simulations to the same control run as before (FCTRL).

The annual mean temperature and precipitation anomalies for the two experiments are shown in Figure 3.10. Temperature changes in HL+TROP case resemble the full slab ocean case, while TROP case exhibits cooling over the North Atlantic and warming over the northern Euro-Asia and northern Pacific area. In both simulations, however, the tropical precipitation anomalies closely resemble that for the full-slab ocean (SOM1) case, both in terms of structure and magnitude. We compared the annual and zonal mean precipitation anomalies for cases TROP, HL+TROP and SOM1 in Figure 3.11*a*. Compared to the fixed SST cases, SOM1 has slightly smaller precipitation anomalies around the equator, but more pronounced second precipitation peak and a wider zone of positive precipitation anomalies.

TROP and HL+TROP show very similar equatorial precipitation responses, suggesting the same ITCZ shifts in the two simulations.

The northward atmospheric heat transport anomalies in the HL+TROP case (Figure 3.9) resemble that for the full-slab ocean (SOM1) case: an atmospheric energy gain from the southern tropics is transported to the northern extratropics, with comparable magnitudes of the poleward flux anomalies. Zonal TOA energy budget changes for HL+TROP are also in very good agreement with the ones from the SOM1 experiment (Figure 3.11*b*). This is not surprising as the climate conditions are essentially the same between the two runs.

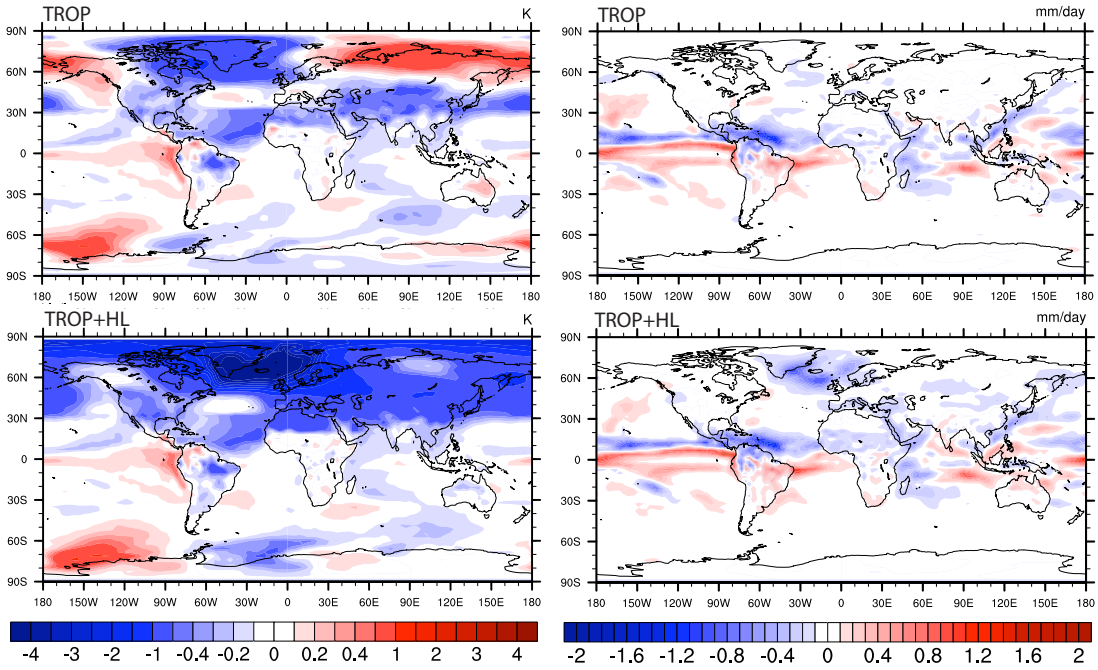

Figure 3.10: Annual mean surface temperature (upper plots) and precipitation (lower plots) anomalies in TROP and HL+TROP experiments.

The TROP simulation shows a significantly different character in the northward energy transport change – while atmospheric energy is gained in the southern tropics as in the HL+TROP case, this energy is essentially transported to, and mainly 'lost' in, the northern tropics. Relatively small anomalous northward heat transport exists from the tropics to the high and mid latitudes and it is a consequence of the overall energy surplus in the area 10°N - 30°N. On the other hand, zonal profiles of the tropical TOA energy budget anomalies displayed in Figure 3.11*b*, show almost identical changes in TROP and HL+TROP idealized cases. The two not only have the same tropical SST patterns, but also very similar precipitation and TOA energy

budget response in the tropics (as seen from Figure 3.11*a* and *b*). Thus, TROP simulation suggests that the tropical SST changes alone are sufficient to shift the ITCZ southwards and provide the same energy surplus, independently of the actual high latitude energy demand.

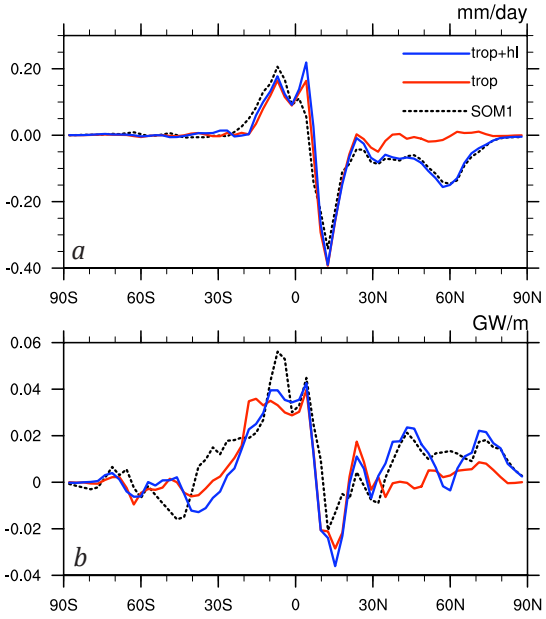

Figure 3.11: Annual mean zonal precipitation (a) and TOA flux (b) anomalies in SOM1, TROP and TROP+HL experiments.

At the equator, the same SST and AHT changes (Figure 3.9) are associated with the same precipitation changes (Figure 3.11*a*) in TROP and HL+TROP experiment. In this sense, neither SST or energy flux perspective can be disregarded.

Away from the equator, but still in the tropics, the AHT anomalies differ more in the two experiments. As the tropical TOA flux changes are the same, this indicates that different AHT responses in the two experiments are due to the difference in surface fluxes. The important point is that the tropical TOA anomalies are the same (Figure 3.11*b*) despite the different AHTs, meaning that they are controlled locally, by the SSTs, and not by AHT or high latitude energy requirements.

Our results thus agree with the energy flux perspective in sense that the same atmospheric cross-equatorial heat transport responses in TROP and HL+TROP experiments are consistent with the same precipitation responses. However, we find that this diagnostic is not sufficient to explain the mechanism of the shifts as it does not hold throughout the tropics. Our interpretation is that in these experiments, the tropical SSTs determine the

southward shift of the ITCZ and the TOA energy surplus, while the northward transport and atmospheric and surface fluxes adjust to redistribute this energy wherever needed (HL+TROP) or possible (TROP). Therefore, it is the SST and not the atmospheric energy budget changes that trigger the precipitation and TOA flux response.

The southern tropical energy gain is hence a consequence of the SST anomalies that force the tropical convection reorganization and it is independent of the global energy requirements. Of course, in an experiment where SSTs are not fixed, the SSTs itself would not be independent from the global energy requirements, what the idealized experiments are implying is that the "coupling" comes via SSTs which are fundamental for ITCZ shifts.

3.4.3 Establishment of the anomalous northward heat transport

We now analyze the transient adjustment to the high-latitude North Atlantic cooling to support our interpretation of how the tropical energy gain and northward atmospheric heat transport changes come about. The first 3 years (establishment) and the year 7 (developed response) in the transient adjustment of the anomalous northward atmospheric heat transport to high latitude cooling are shown in Figure 3.9. During the first two years, most of the additional energy transported northward comes from the mid-latitudes and northern tropics. This is especially pronounced during the first year and arises mainly from shortwave cloud feedback that causes positive TOA budget anomalies in the northern tropics (Figure 3.12*b*). As the simulation approaches equilibrium however, a longwave cloud feedback response develops that counters the shortwave cloud feedback, leading to the familiar shape of the TOA energy budget anomaly with positive values in the southern and negative in the northern tropics (year 5, Figure 3.12*d*). The strong high latitude temperature feedback characteristic of the equilibrium response is not as pronounced during the first year of adjustment (Figure 3.12*b*).

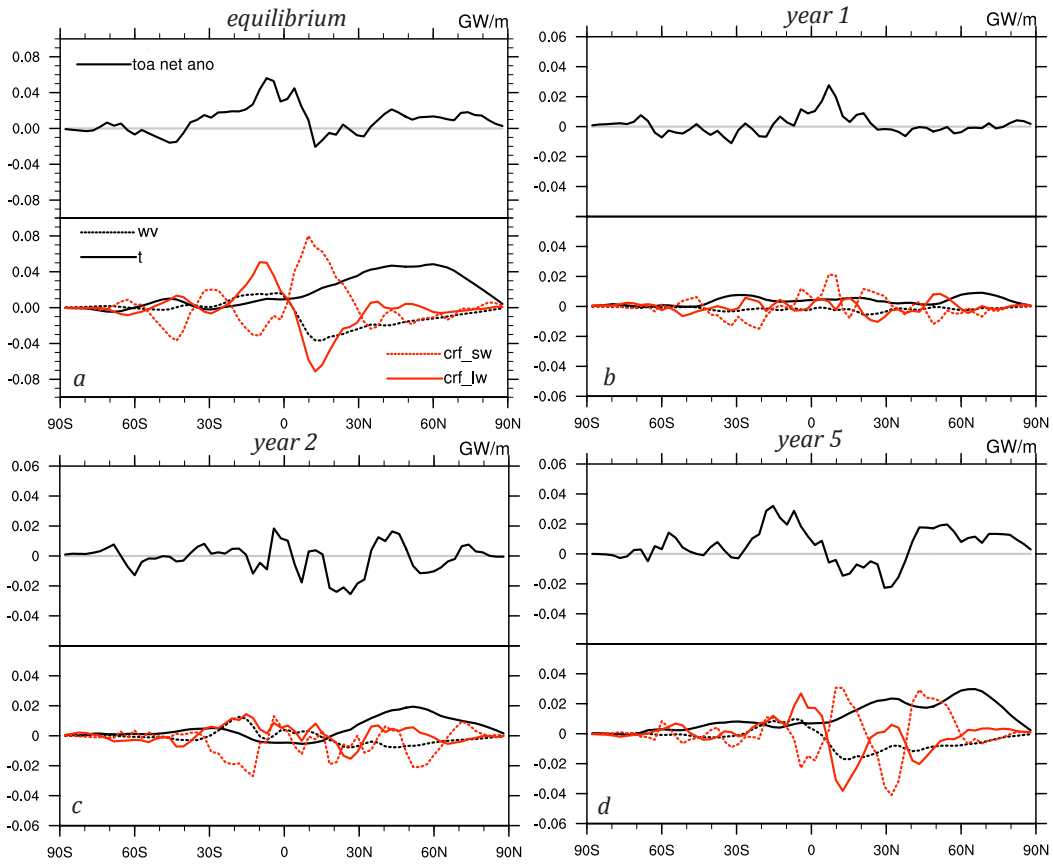

Figure 3.12: TOA flux anomalies (upper panels) and selected TOA feedback effects (lower panels) for the SOM1 experiment, in equilibrium (a) and in the transient period (b, c and d). Lower panels legend: t - temperature (including surface temperature), wv -water vapor, crf_sw - cloud shortwave and crf_lw - cloud longwave feedback effect.

A noticeable anomalous northward mid-latitude transport establishes from year 2 (Figure 3.9*b*) due to the combined effect of the temperature and cloud feedbacks (Figure 3.12*c*) (that cause positive midlatitude TOA budget anomalies) and due to the fully developed high latitude surface forcing. A small energy surplus arises in the southern tropics too, as a result of warming due to the longwave cloud feedbacks. During the year 3, positive TOA energy flux anomalies in the southern tropics increase as the cloud and temperature feedbacks develop (not shown).

Figure 3.13, showing the tropical surface temperature and precipitation changes during the adjustment period (years 1, 2, 3 and 7), reveals a development of the northern hemispheric cooling and southern tropical warming and a southward precipitation shift (especially pronounced over the Indian Ocean during the year 3). In the eastern Pacific, this signal is lost during the year 4 and recovered again in year 5, when the major energy gain

comes from the southern tropics (not shown). In the following years, stronger surface temperature dipole and more striking southward precipitation shifts develop and the southern tropics remain the area of significant energy gain. The structure of dominant feedbacks starts to resemble the equilibrium response from year 5, with the positive TOA anomalies in the southern tropics due to the cloud, water vapor and temperature feedbacks (3.12*d*). Evolution of temperature, shortwave and longwave cloud radiative feedback effects discussed above is shown in Figure 3.12 for years 1, 2 and 5.

With regards to the role that SST plays in the precipitation response, the transient experiments shows essentially simultaneous changes in the surface temperatures and precipitation. As such, it is not possible to infer which comes first (precipitation or SST change). Nevertheless, these experiments are not in disagreement with our interpretation of the idealized experiments in Section 3.4.2, as there is no indication of the precipitation shift without the tropical SST anomalies present.

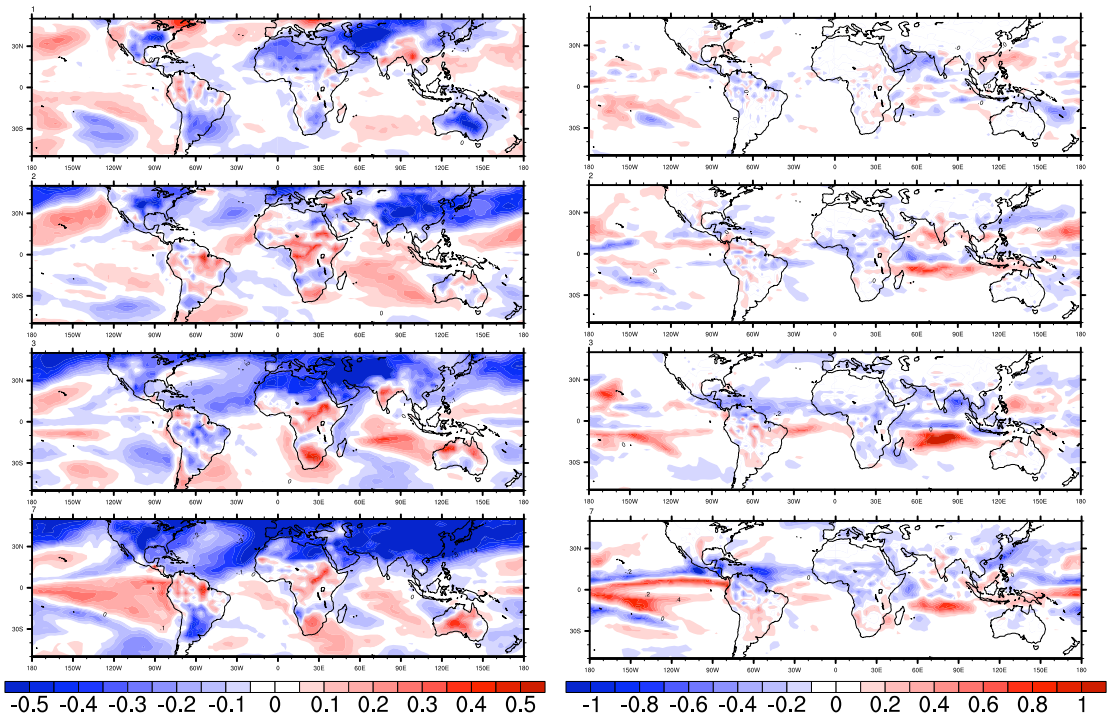

Figure 3.13 (left column): tropical surface temperature anomalies (K) and (right column): tropical precipitation anomalies (mm/day) in the transient period (years 1, 2, 3 and 7)

3.5 Summary and discussion

In this study, we examined in detail the global energy budget changes to high latitude North Atlantic cooling and the southward ITCZ shift in an atmospheric general circulation model coupled to a slab ocean. Our energy budget approach follows from previous studies that suggest the utility of this approach, in particular Kang et al. (2009). First, we have evaluated the energy budget changes in extratropics, northern and southern tropics, and quantified the individual feedbacks responsible for them using a radiative kernel technique. Second, we examined the interplay between energy fluxes and SSTs in determining the ITCZ response to high latitude North Atlantic cooling, specifically contrasting the two existing perspectives – the role of SSTs, and the role of energy fluxes in interpreting our simulations.

We found that 35% of the initial high latitude North Atlantic surface cooling is compensated by TOA changes in the northern extratropics, and mainly due to the longwave temperature feedback, while the rest of the energy required to balance the energy flux is provided from the southern tropics, mainly due to the longwave cloud feedback. The northern tropics essentially did not contribute to the net energy fluxes, because of a cancellation between longwave and shortwave feedbacks.

We also carried out idealized simulations, by fixing SSTs in the tropics while keeping the slab ocean boundary condition in the extratropics, in order to examine the role of SST anomalies in the tropical ITCZ response. Our results suggest that the tropical SST changes directly control the ITCZ response, whereas there is no direct link to the extratropical energy demand. Only as the cooling anomalies reach the tropics (due to progression of the surface temperature anomalies), does the convection reorganize; this reorganization then leads to TOA energy flux changes from cloud, water vapor and temperature feedbacks. Our result thus suggests that the SST anomalies propagating into the tropics are both necessary and sufficient for the ITCZ to shift, in accordance with the 'SST perspective' on ITCZ shifts.

Kang et al. (2008) study reports that the overall cloud effect is negative in the southern tropics and positive in the northern tropics with the shortwave component being dominant over the longwave. This result differs from our experiments, which show that longwave cloud feedback is at least as important as the shortwave cloud component (Figure 3.12 *a*). Furthermore, in our experiments the longwave cloud feedbacks together with the temperature and water vapor feedbacks determine the sign of TOA anomalies over most of the tropics. In general, total (shortwave and longwave) cloud radiative effect is

positive over the southern tropics. This discrepancy is likely to be caused by the differences in the convective and cloud parameterizations between our model and the ones used in Kang et al. (2009) study.

The applied extratropical forcing in the Kang et al. (2008) aquaplanet study was cooling in one hemisphere, and an equal but opposite warming in the other hemisphere. On the other hand, our simulation (that uses a realistic Earth boundary condition) has an imposed high-latitude North Atlantic cooling that is not 'compensated' in the southern hemisphere. Given that the time scale of the atmospheric response is much shorter than for the ocean, this analysis does make sense in the initial adjustment period. However, also during the initial period this picture may be modified by the fast oceanic teleconnections. Given that in our study we use a simple thermodynamic ocean, it was not possible to assess how the oceanic response could have modified the picture. Coupled modeling studies do agree with our results finding the similar tropical temperature and precipitation responses to high latitude cooling. In addition, study by Timmerman et al. (2007) shows that the AMOC weakening affects the northeastern tropical Pacific through changes in evaporation, mixing and Ekman forcing and further leads to ENSO intensification. Wu et al. (2007) attempt to distinguish between ocean and atmosphere driven changes, showing that the development of tropical Atlantic dipole is a consequence of the ocean dynamics while the tropical Pacific response comes from the atmosphere-surface ocean interactions.

We did not consider the role of extratropical eddy momentum fluxes that may be an important factor in determining how extratropical cooling alters the tropical Hadley circulation. Extratropical eddies have been shown to determine a sizable fraction of the Hadley cell mass flux over the areas where the Rossby number is small (Kim and Lee (2001), Walker and Schneider (2006)). Observational data also suggest that the interannual variability in Hadley cell strength is strongly correlated to the eddy stress fluctuations with the stationary eddies playing the major role in the stronger winter Hadley cell variability and transients in the weaker summer cell (Caballero, 2007, Caballero and Andersen, 2009). The role that extratropical eddy momentum fluxes play in our problem has not yet been addressed, to our knowledge, and it remains a future task. Our brief analysis of the momentum budget during the transient adjustment to imposed high latitude cooling suggests that conditions before the tropical ITCZ shift are favorable for the more significant role of the extratropical eddy momentum fluxes. Further work is required to understand the dynamics of the adjustment period and the role of eddy momentum and heat fluxes in high to low latitude communication.

Chapter 4

Southward ITCZ shifts due to interhemispherically asymmetric forcing and implications for an atmospheric bipolar seesaw

In this study, the atmospheric heat transport changes that accompany southward ITCZ shifts are considered in three different scenarios: northern hemispheric cooling, southern hemispheric warming and a bipolar seesaw-like forcing that consists of both.

We first address the dynamics of the three shifts and find different atmospheric heat transport and Hadley circulation responses regardless the same strength of the forcing imposed. These are related to different interhemispheric temperature gradients that are altered mainly by non-linearities in water vapor responses in high latitude cooling and warming experiments. In addition, we find that Southern Ocean warming does not only affect the tropics, but further has an impact on the northern extratropics as seen through mid- and high-latitude North Atlantic surface temperature and wind changes.

In the overall top-of-the-atmosphere (TOA) energy budget, the southward ITCZ shifts are associated with entirely different energy flux changes that, in the first scenario, provide a global energy surplus; in the second one, provide a global energy loss and in the third case have global TOA flux changes close to zero. Decomposition of the TOA flux anomalies into dominant atmospheric feedback effects allows for an understanding of these different global energy budget responses. In agreement with previous studies, we find a dominance of the temperature feedback in the high latitudes and water vapor and cloud feedbacks in the tropics. There are two main areas with maximum TOA flux changes due to the tropical convection reorganization, namely the East Tropical Pacific with dominant downward TOA energy flux changes and the Northern Tropical Atlantic with upward TOA energy flux changes. The two areas tend to activate depending on the global energy demand with the bipolar seesaw type of experiment showing the largest changes in both. The northward atmospheric heat transport is enhanced over the tropics in accordance with the positive TOA budget anomalies in the southern tropics and negative in the northern tropics.

4.1 Introduction

As inferred from tropical paleo-data, there is an increasing body of evidence for strong coupling between high latitude temperature changes and tropical precipitation shifts (Peterson et al. 2000, Wang et al. 2001 and 2008, Lea et al. 2003, Koutavas and Sachs 2008, Dubois 2011). However, the recorded precipitation shifts are unlikely to be exclusively influenced by northern-only or southern-only high-latitude changes. It is more likely that they reveal a complex interplay between Northern and Southern Hemisphere high-latitude climate shifts as suggested by Kanner et al. (2012). In fact, the present study argues for a two-step effect that fast atmospheric teleconnections can induce on tropical precipitation in response to the slower oceanic changes.

Due to imposed asymmetric temperature forcing around the equator, the intertropical convergence zone (ITCZ) shifts to the warmer hemisphere driven by cross equatorial flow caused by anomalous meridional tropical surface pressure gradients (Lindzen and Nigam 1987, Chiang and Bitz 2005). The same requirement for an ITCZ shift also arises from an angular momentum conservation viewpoint, as the Hadley cell rising branch shifts to the warmer hemisphere in order to avoid large horizontal temperature gradients in the upper tropical troposphere (Lindzen and Hou 1988). From an energy budget perspective, a shift to the warmer hemisphere allows for increased atmospheric heat transport to the cooled hemisphere (Chiang and Bitz 2005, Kang et al. 2009).

As the ITCZ prefers the warmer hemisphere, southward ITCZ shifts have traditionally been investigated in AGCM studies by imposing a northern high latitude cooling (Chiang and Bitz 2005, Mahajan et al. 2011, Cvijanovic and Chiang 2012) or a bipolar seesaw-like anomaly (Broccoli et al. 2006, Kang et al. 2009, Kang and Held 2011). The choice of such scenarios was based on the fact that North Atlantic Meridional Overturning Circulation (AMOC) variability is often considered the cause of abrupt climate cooling and warming events (McManus et al. 1998, McManus et al. 2004, Broecker 2000). Consequently, the atmospheric response investigated in the mentioned studies corresponded either to the situation right after the AMOC slowdown/shutdown (when the southern high latitude sea surface temperatures are not yet influenced by the ocean circulation changes) or during the advanced ocean bipolar seesaw in which one hemisphere is colder and the other warmer compared to the control state (Stocker and Johnsen 2003, Stouffer et al. 2006).

Southward ITCZ shifts can, however, also be induced by imposing warming into the Southern Hemisphere. Southern Ocean warming has predominantly been considered a consequence of AMOC changes due to freshwater hosing in the North Atlantic (Timmerman et al. 2010, Holden et al. 2010, Otto-Bliesner and Brady 2010) and the global atmospheric response to the Southern Ocean warming only scenario has therefore not been broadly investigated in AGCM simulations. With the exception of the studies by Weaver et al. (2003), Knorr and Lohmann (2003) and Stouffer et al. (2007), the Southern Ocean has generally not been considered the most likely trigger of past abrupt climate events.

Nevertheless, Southern Ocean temperature changes (in response to an AMOC slowdown or shutdown, for example) could induce additional atmospheric reorganizations that can act as a positive or negative feedback to the initial North Atlantic forcing. In that respect, the atmospheric response to Southern Ocean warming addressed in this study, enables investigation of the atmospheric teleconnection through which the southern high latitudes affect the tropics and the northern high latitudes. While the effect on the high latitudes of the opposite hemisphere may not be as substantial, southern warming or cooling will evidently influence the tropical precipitation by altering the interhemispheric temperature gradient.

This may have numerous repercussions on paleo-data interpretations. Specifically, within a decade after the North Atlantic cooling, the ITCZ shifts southward due to the atmosphere-surface ocean interaction as shown in studies by Chiang and Bitz (2005), Mahajan et al. (2011) and Cvijanovic and Chiang (2012). Assuming a lag time of decades to centuries for a full ocean response, Southern extratropical oceans will start warming *after* the ITCZ response to the North Atlantic cooling. This warming will then affect the interhemispheric temperature gradient once more and, depending on its magnitude, may cause secondary southward ITCZ shifts that will be registered in the tropical proxy data. If we take as an example the imprint of Dansgaard/Oeschger events over the northern tropics, this would mean that in addition to the monsoon weakening in phase with the Greenland cooling, there could be an additional strengthening of this signal over the following decades or centuries, in phase with the Southern Ocean. Although such examinations are possible only with very high resolution data, it is still a mechanism that needs to be considered.

Our study enables a comparison of the atmospheric response in the bipolar seesaw experiment to the northern cooling and southern warming simulations only. From an energetics viewpoint, these three southward ITCZ shifts provide entirely different energy budget responses. In addition, the

possibility of an atmospheric bipolar seesaw in which the southern high latitudes drive the northern is investigated.

Model configuration and experimental descriptions are given in 4.2, followed by discussions of the dynamics and energetics of the southward ITCZ shifts in standard slab ocean experiments (4.3.1) and in aquaplanet slab ocean experiments (4.3.2). Global energy fluxes and radiative feedback responses are further analyzed in Section 4.3.3. Effects of the Southern Ocean warming on the northern high latitudes are discussed in Section 4.4, followed by conclusions and paleo-data implications in Section 4.5.

4.2 Model setup

We employ the NCAR Community Atmosphere Model version 3 (CAM3) in slab (mixed layer) ocean mode. Under this setup, atmosphere-surface ocean interactions are enabled and the monthly-varying ocean heat flux convergence (Q-flux) is applied to the ocean mixed layer, compensating for the absence of the ocean dynamics. The experiments were performed under the present day conditions (orbital forcing and greenhouse gases), in T42 horizontal resolution with 26 levels in the vertical. A change to the experimental configuration is the exclusion of the final Q-flux correction from the sea surface temperature calculation over the warm (temperatures larger than zero) ocean points. As described by Collins et al. (2004), in the CAM3 slab ocean model, Q-flux adjustments are added in order to reduce the loss of heat from the mixed layer to zero (when the temperature approaches the freezing point) and to ensure that the sea ice distribution is bounded against unrealistic growth or loss. We have kept these adjustments, as we want to keep the changes in the sea ice geometry realistic, but we did not allow for these changes to be compensated over the global warm ocean. As our study investigates atmospheric teleconnections, we need to ensure that away from the sea ice and the areas of the imposed forcing, changes in sea surface temperatures originate solely from atmospheric processes (and not from unphysical Q-flux adjustments). The small uncompensated Q-flux difference that thus arises may be considered as energy transmitted below the mixed layer, a solution which appears more realistic than the instant global redistribution.

Cooling and warming is applied in the northern or southern high latitudes (or in the both) by adding zonal Q-flux anomalies to the background Q-flux field north and south of 46^{o} latitude. Zonal profiles of the applied Q-flux anomalies are given in the Figure 4.1*a*. Larger Q-flux anomalies in the north

compared to the south are due to the smaller ocean extent in the NH, ensuring similar total Q-flux forcing in SH warming and NH cooling experiments. However, the resulting NH and SH forcing is not exactly equal in strength (also due to the different sea ice cover in the two hemispheres) resulting in slightly stronger NH cooling than SH warming. Consequently, the bipolar seesaw experiment that consists of both the southern warming and northern cooling has an overall negative (but small) imposed global forcing.

Simulations were run for 150 years with the last 80 used in the analysis. The experiments are as follows: (1) present day control run – CTRL; (2) CTRL with imposed high northern latitude Q-flux cooling – NH_cold; (3) CTRL with imposed high southern latitude warming – SH_warm; and (4) CTRL with both northern cooling and southern warming – NS_cw.

In addition to these standard slab ocean experiments, four aquaplanet slab ocean experiments with disabled sea ice cover are performed. In this configuration, the imposed NH cooling and SH warming have equal strengths and the bipolar seesaw experiment has zero net global forcing. Since the absence of continents allows the Q-flux forcing to be imposed over a much larger area, the effect of imposed cooling or warming is much larger. For that reason, the maximum value of the applied Q-flux forcing in the aquaplanet experiments was set to about 6 W/m^2, as shown in Figure 4.1*b*. The experiments are named after the corresponding standard slab ocean simulations: aqua_CTRL, aquaNH_cold, aquaSH_warm and aquaNS_cw.

In the aquaplanet simulations, surface albedo was uniformly set to 0.15, and points with temperatures below zero were treated as an open water similar to the study by Langen et al. (2012). Model resolution, solar forcing, greenhouse gases and orbital forcing are the same as in our standard slab ocean experiments, except for the eccentricity, which is set to zero to provide symmetry between the hemispheres. Aerosol, ozone and Q-flux fields have been zonally averaged and symmetrized about the equator.

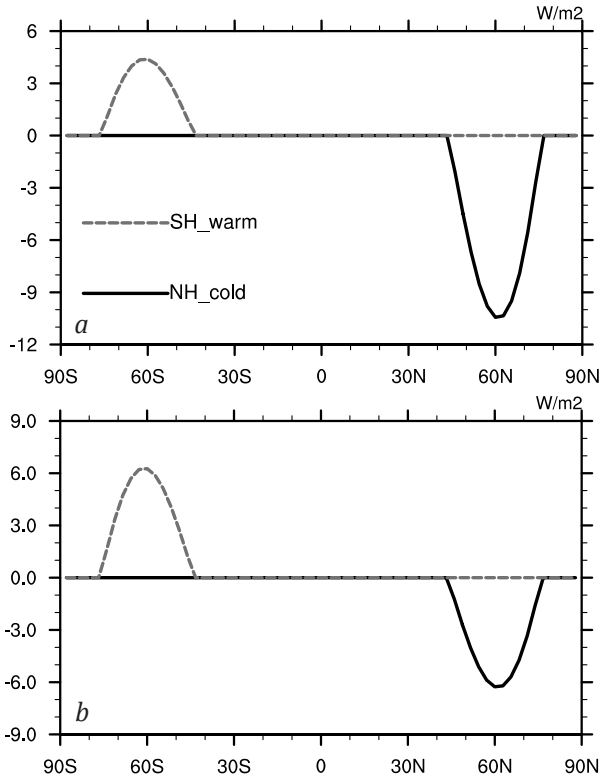

Figure 4.1: Zonal Q-flux anomalies applied in the (a) standard slab ocean experiments and (b) aquaplanet experiments. Blue full line: northern hemisphere cooling experiments NH_cold and aquaNH_cold, grey dashed line - southern hemisphere warming experiments SH_warm and aquaSH_warm. Forcing for the NS_cw and aquaNS_cw experiments is the sum of the corresponding two curves. Sign convention: positive Q-flux anomalies correspond to ocean mixed layer heating.

4.3 Results

4.3.1 Southward ITCZ shifts due to asymmetric interhemispheric forcing

Southward precipitation shifts in the NH_cold, SH_warm and NS_cw experiments are shown in the upper panels of Figure 4.2. The three shifts resemble each other over the eastern tropical Pacific, but less over the tropical Atlantic and Indian Ocean where the SH_warm and NS_cw experiments show much larger anomalies compared to NH_cold. Surface temperature anomalies, shown in the lower panels of Figure 4.2, reveal entirely different responses in the three experiments in accordance with the different forcings imposed. The largest coolings and warmings are about 3°C, located in the high northern and southern latitudes, respectively. In comparison, subantarctic sea surface temperature reconstructions by Mashiotta et al. (1999) and Shemesh et al. (2002) indicate temperature oscillations of about 2°C during the last glacial. D/O events found in Antarctic Dome C and EDC record show maximum amplitude of about 3°C (Jouzel et al. 2007). Tropical surface temperature anomalies in our simulations are around 0.5°C in magnitude, with larger surface temperature gradients over the Atlantic and Indian Ocean in the NS_cw and SH_warm cases compared to NH_cold. This is coincident with the stronger Atlantic and Indian Ocean precipitation shifts in the former two.

In terms of energetics, these experiments pose distinct energy budget requirements. In the NH_cold experiment additional energy gain is required to counteract the imposed surface cooling. In the SH_warm there is a surplus of energy due to the applied warming and a sink for this energy is required. Finally, in the NS_cw, the imposed cooling and warming almost cancel each other (with a small requirement for energy gain). It is thus compelling to investigate to what extent similar southward ITCZ shifts can provide these entirely different energy flux responses. Figure 4.3, showing top-of-the-atmosphere (TOA) energy flux changes, illustrates the main locations where energy is gained or lost. Positive, i.e. downward, TOA anomalies are mainly located over the eastern tropical Pacific, surrounding the area of the Pacific Cold Tongue (in agreement with Cvijanovic and Chiang 2012), while the highest negative values are present over the north tropical Atlantic.

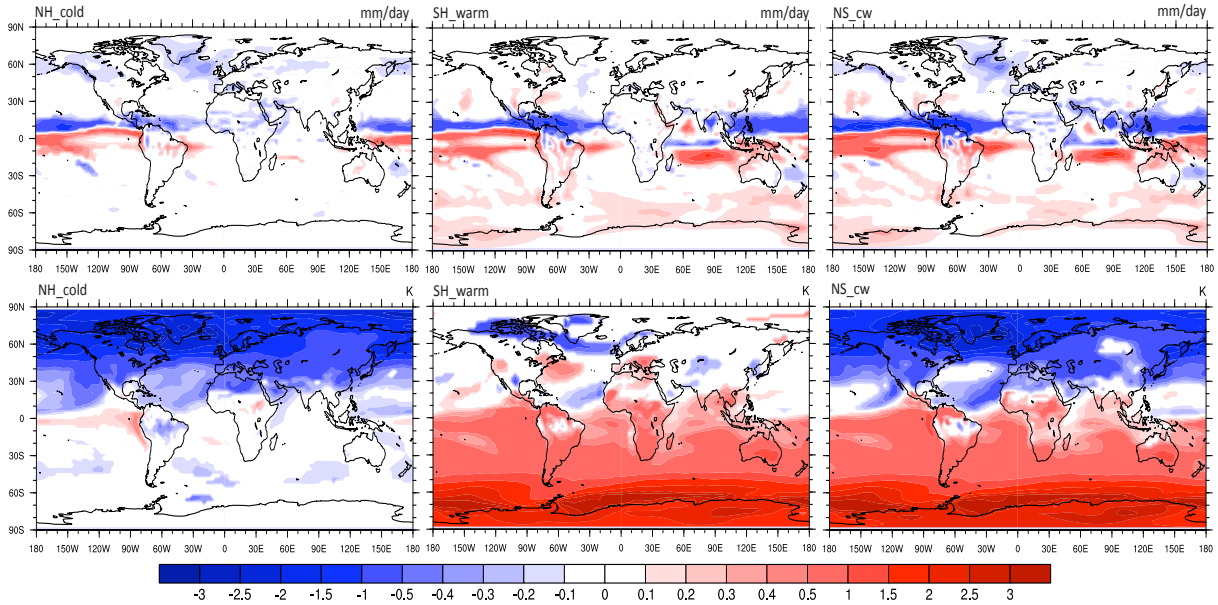

Figure 4.2: Precipitation (upper panels) and temperature (lower panels) anomalies in NH_cold, SH_warm and NS_cw slab ocean experiments. The anomalies shown are statistically significant at the 95% level using the Student's *t*-test.

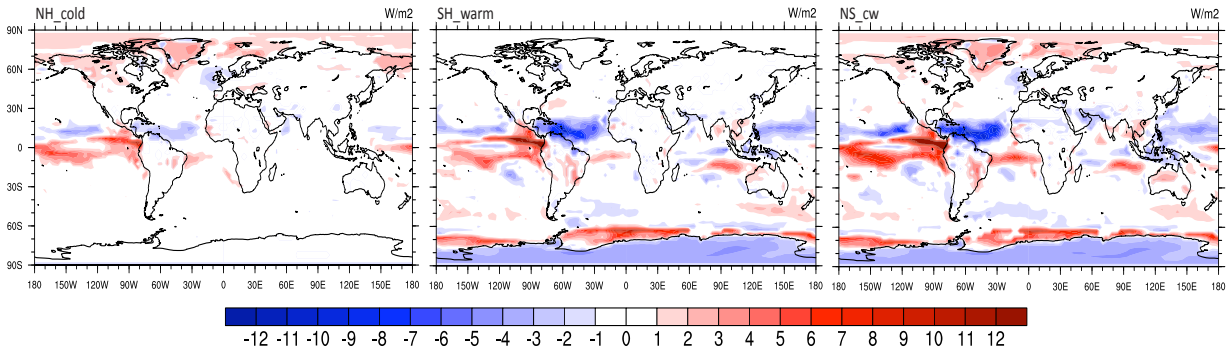

Figure 4.3: TOA net anomalies (positive downward) in NH_cold, SH_warm and NS_cw experiments. Anomalies are statistically significant at the 95% level.

In the NH_cold experiment (Figure 4.3, left panel) tropical TOA anomalies are mainly positive, with the exception being the tropical north Atlantic where small negative values are found. The global average TOA flux anomaly is thus positive and the main compensation for the northern extratropical surface energy loss is provided over the east tropical Pacific. In the SH_warm, positive TOA anomalies over the east tropical Pacific are still present, reinforcing the imposed positive surface forcing. The sink for this additional energy is chiefly over the tropical north Atlantic, where large negative TOA flux anomalies prevail. Thus, in the SH_warm, the overall TOA flux changes are negative. TOA budget anomalies observed in the NH_cold and SH_warm cases are even more pronounced in the NS_cw, where increased energy gain (and loss) over the east tropical Pacific (and north tropical Atlantic and Pacific) further enhance the difference in interhemispheric energy budgets, increasing the requirement for northward atmospheric heat transport.

Tropical energy sinks and sources are connected with the convection reorganizations due to the southward ITCZ shifts. Cloud anomalies (not shown) reveal an increase in low cloud cover in the northern tropics, especially over the north tropical Atlantic and a decrease over the southern tropics and equatorial Pacific. High and medium cloud cover increases over the southern tropics and equatorial Pacific with maximum over the Pacific cold tongue area and decreases over the northern tropics. Therefore, maximum positive (negative) tropical TOA flux anomalies coincide with areas of the increased (decreased) high and medium cloud cover that reduces the outgoing longwave radiation by emitting from higher and colder levels in the atmosphere.

This indicates that in our model simulations, the shortwave cloud radiative forcing (CRF) anomalies (due to the low cloud cover changes) are less important for the overall cloud forcing, as the total CRF mainly follows the sign of the longwave component (Figure 4.7*c*). If the shortwave effect due to cloud reorganization was stronger than the longwave effect, the overall CRF would have been positive in the northern and negative in the southern tropics. Our findings are in agreement with those of Cvijanovic and Chiang (2012) and further show that dominance of longwave CRF is not related to the geometry of the imposed forcing; cloud radiative forcing changes are additionally addressed in Sections 4.3.2 and 4.3.3.

Given the sign of the TOA and surface flux anomalies, the largest atmospheric cross equatorial heat transports are expected in NS_cw and SH_warm cases, as both the energy surplus from the imposed surface forcing and the east tropical Pacific TOA energy gain have to be transported north.

In the NH_cold, on the other hand, the only available energy for the transport comes from the TOA energy surplus in the southern tropics. Figure 4.4, showing northward atmospheric heat transport anomalies, illustrates this. In NH_cold, energy is gained over the area 20°S-10°N (due to TOA flux changes) and lost in the northern extratropics (around 60°N) due to the imposed surface cooling. In SH_warm, however, the energy surplus comes from the southern extratropics (where the surface forcing is imposed) and from the area 20°S-10°N (due to TOA energy flux gain) and it is lost in the northern tropics due to the TOA energy loss. Finally, in NS_cw, the atmospheric transport change is almost the sum of the previous two and the energy is gained in the southern extratropics and the area 20°S-10°N and lost in the northern tropics and extratropics.

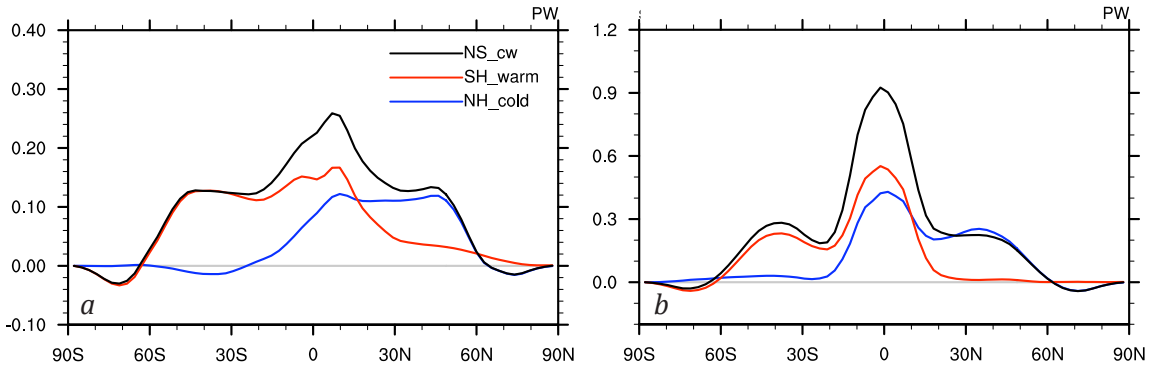

Figure 4.4: Atmospheric northward heat transport anomalies in slab ocean (a) and aquaplanet slab ocean (b) experiments. Blue, red and black lines represent the NH_cold, SH_warm and NS_cw cases, respectively.

The larger tropical convection reorganization (stronger ITCZ shift) and atmospheric heat transport (AHT) response in the NS_cw simulation compared to the other two cases could be seen as a response to the more substantial alteration of the interhemispheric thermal gradient (Chiang and Friedman 2012). The difference between the annual average surface temperatures over the northern (0°-30°N) and southern (0°-30°S) tropics, for example, equals 0.9 K in the control run and 0.3 K in the NS_cw simulation, while the NH_cold and SH_warm cases fall in between. The same conclusion is found when considering hemispheric surface temperature averages. Different interhemispheric thermal gradients in NH_cold and SH_warm are consistent with a larger Hadley cell anomaly (Figure 4.5) and tropical AHT response (Figure 4.4) in SH_warm than in NH_cold.

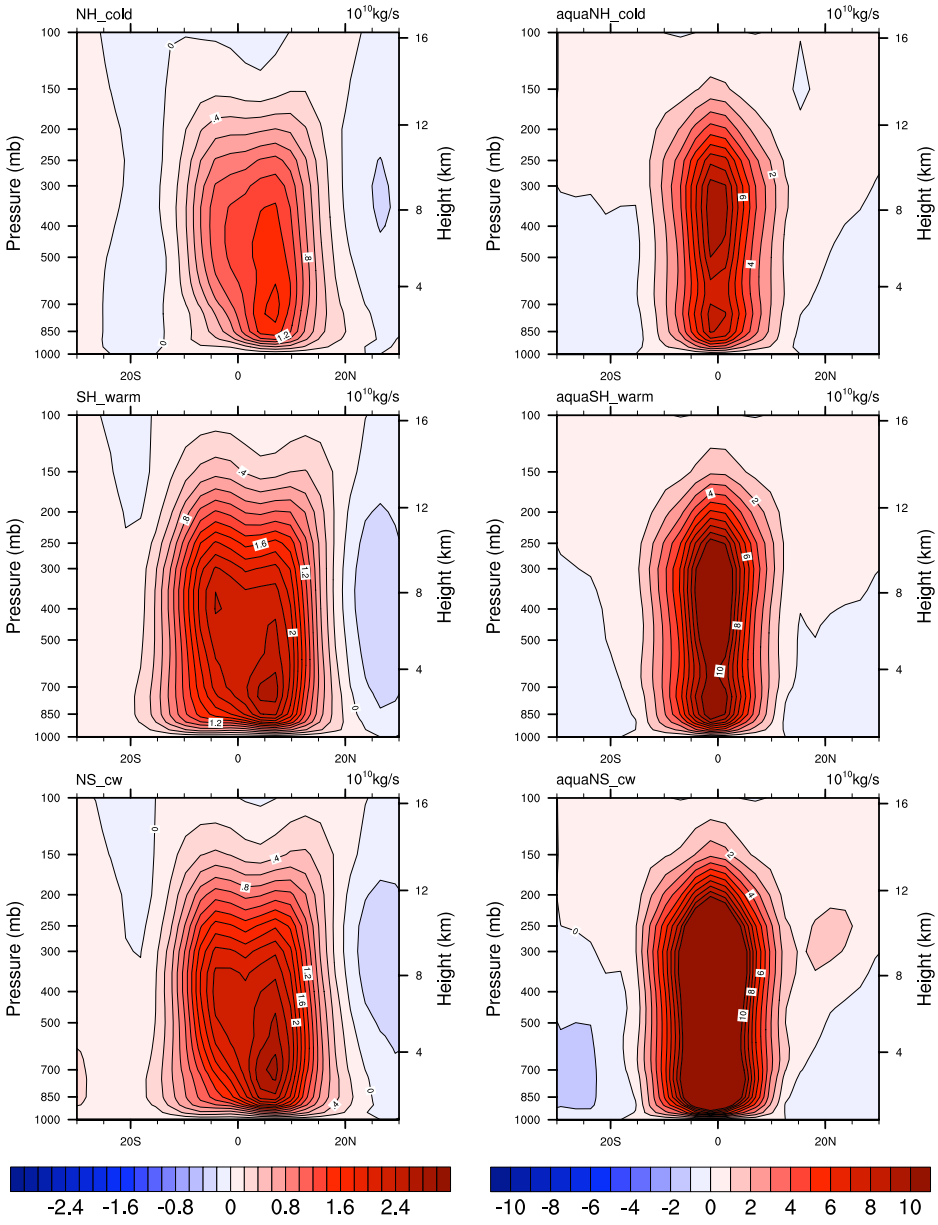

Figure 4.5: Meridional stream function anomalies in standard slab ocean (left plots) and aquaplanet (right plots) experiments

From this analysis it is difficult to discern whether the different interhemispheric thermal gradients and atmospheric responses are caused by the differences in the initial imposed forcing (due to land-ocean geometry), by the sea ice effects, or whether they are a consequence of nonlinear atmospheric processes like for example the water vapor response to temperature changes through the Clausius-Clapeyron relation. The aquaplanet experiments with disabled sea ice can provide an answer to this.

An additional reason for considering the aquaplanet simulations are the different features of the atmospheric transport anomaly in NS_cw, compared to the ones found by Kang et al. (2008) and (2009) in their aquaplanet experiments (K08 and K09 hereinafter). The differences are especially pronounced around the equator. In K09 and K08, tropical cloud radiative forcing acts as a negative feedback on the imposed forcing by inducing negative CRF anomalies in the southern tropics and positive in the northern tropics. In the next section, we thus also address the sign of tropical CRF anomalies in relation to different AHT responses.

4.3.2 Tropical atmospheric response in aquaplanet slab ocean experiments

The strength and geometries of the imposed NH cooling and SH warming in the aquaplanet experiments are equal (although opposite in sign) as illustrated in Figure 4.1*b*. Atmospheric heat transport anomalies in these simulations are plotted in Figure 4.4*b*. Similarly to what was found in the experiments that included land and sea ice, the AHT anomaly is larger in the southern warming aquaSH_warm simulation (red line) than in the northern cooling aquaNH_cold experiment (blue line), while the aquaNS_cw atmospheric heat transport anomaly resembles their sum (black line). This is also in accordance with the corresponding Hadley cell responses that are weakest in aqua_NHcold (Figure 4.5).

Cross-equatorial atmospheric heat transport anomalies are plotted against the anomalous interhemispheric tropical surface temperature gradients (IHTG) in Figure 4.6, revealing a linear relationship between the two. To additionally test this we have performed three new experiments with the same forcing geometries but increased forcing strengths, named aquaNH_cold_is, aquaSH_warm_is and aquaNS_cw_is. The maximum imposed Q-flux anomalies in these experiments are about 10 W/m^2. A linear fit through all aquaplanet experiment points yields an r^2 value of 99% (Figure 4.6). This not only illustrates a one-to-one relation between the interhemispheric surface temperature gradients and the AHT response but also confirms that the SH_warm and NH_cold experiments have different IHTGs and AHT anomalies that are not caused by discrepancies in the imposed forcing or sea ice effects.

We propose that this is related to the nonlinear water vapor response that acts as a positive feedback on the imposed forcing. Extratropical temperature changes due to the applied Q-flux anomalies will cause an increase in the specific humidity, which will in turn cause TOA energy budget changes. This effect will not be same in the warming and cooling experiments because of the non-linear relation between the temperature and water vapor. Consequently, the cooling experiment is less affected by the positive water vapor feedback effect than the warming experiment. Extratropical cloud responses to the initial cooling or warming may additionally complicate this picture.

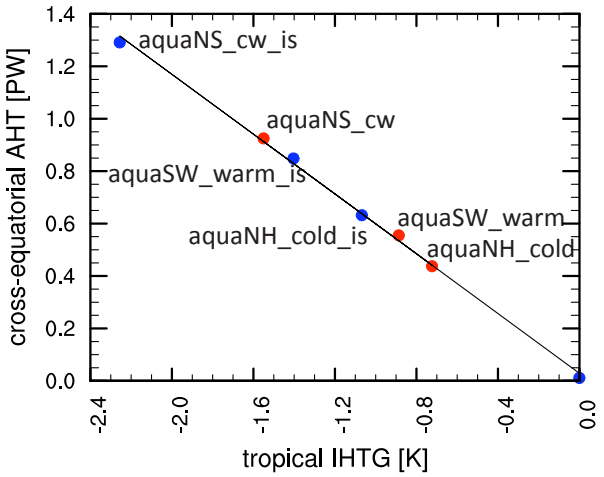

Figure 4.6: Cross equatorial atmospheric heat transport (PW) plotted against the tropical interhemispheric temperature gradient (K) for the aquaplanet experiments. White circles: aquaNH_cold, aquaSH_warm and aquaNS_cw simulations, black circles: corresponding experiments with increased forcing strength.

The initial difference in interhemispheric temperature gradients between the northern cooling and southern warming experiments will in turn cause different Hadley cell responses. However, there is also a dynamical factor to be considered. Development of the anomalous Hadley circulation and the corresponding AHT response leads to stronger northward dry static energy and southward latent heat transports. As a result, the water vapor content increases in the southern tropics and decreases in the northern tropics (Chiang and Bitz 2005). The different Hadley cell anomalies will therefore yield different amounts of latent heat transported in the two experiments that, in turn, additionally increase the difference in strengths of the tropical water vapor anomalies in aquaSH_warm compared to aquaNH_cold. The larger the difference in strengths of the water vapor anomalies, the larger difference in water vapor feedback effects that will further increase the interhemispheric thermal gradient.

Alternatively, larger Hadley cell response in aquaSH_warm compared to the aquaNH_cold could also be related to the initially wetter northern tropics in aquaSH_warm due to the weaker cooling. Under the less dry conditions (larger lapse rate) in aquaSH_warm, Hadley cell will become more vigorous due to the larger upper hemispheric pressure gradients between the equator and subtropics (Webster 2004).

Our experimental design did not allow deciphering which of the proposed mechanisms plays a major role. However, vertical integrals of specific humidity anomalies in the aquaSH_warm and aquaNH_cold simulations

given in Figure 4.7*a*, confirm stronger (by absolute value) aquaSH_warm water vapor response (red line) in the southern tropics compared to aquaNH_cold water vapor response in the northern tropics (blue line). Over the southern tropics, the aquaSH_warm water vapor response is larger than the aquaNH_cold response, both owing to the stronger southern tropical warming and stronger Hadley cell anomaly (Figure 4.5) in aquaSH_warm. In contrast, over the northern tropics, water vapor responses are almost the same due to the fact that the stronger Hadley cell transport in aquaSH_warm compensates for the less northern tropical cooling compared to the aquaNH_cold.

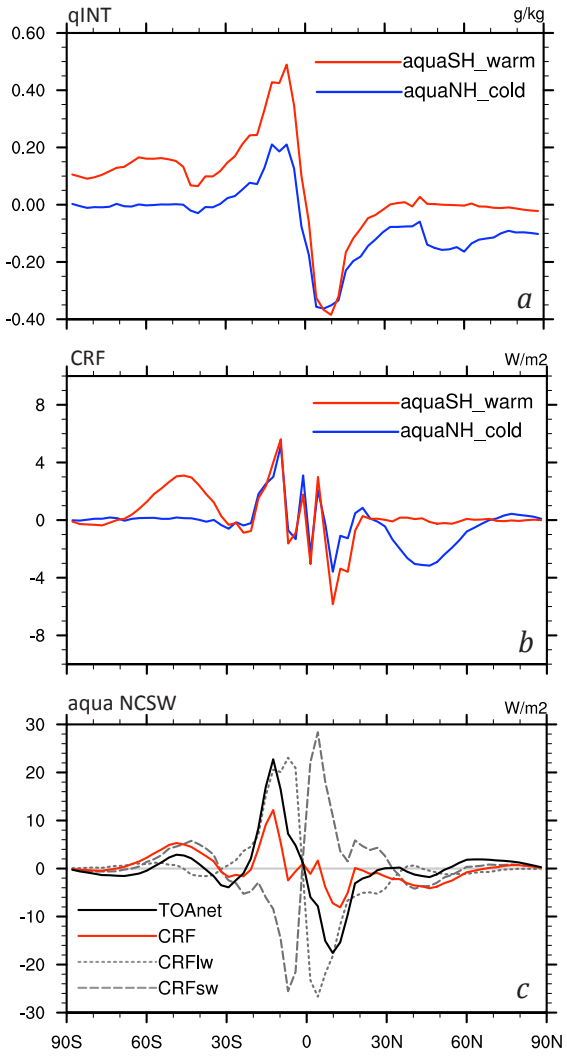

Figure 4.7: (*a*) Pressure weighted column mean specific humidity anomalies and (*b*) cloud radiative forcing anomalies (normalized by the cosine of latitude) in aquaNH_cold and aquaSH_warm experiments. (*c*) TOA net energy budget anomaly (black line), cloud radiative forcing (CRF) anomaly (red line) and its longwave (CRF lw) and shortwave (CRF sw) components (grey dashed lines) in the aquaNS_cw simulation (normalized by the cosine of latitude).

Cloud radiative forcing also affects the difference between the two responses (Figure 4.7*b*). In the northern tropics, the aquaSH_warm CRF response (red line) is more negative than that in aquaNH_cold (blue line). Mid-latitude CRF anomalies in the two experiments are of similar strengths and therefore do not contribute to different responses.

Overall, TOA flux changes are positive in the southern and negative in the northern tropics, enhancing the interhemispheric differences due to the imposed surface forcing. This enhancement is larger when the ITCZ shift southward due to southern warming compared to the northern coolingIn terms of geometry of the applied forcing and the aquaplanet slab ocean setup, our bipolar seesaw forcing experiment (aquaNS_cw) is very similar to the K08 and K09 experiments. However, the AHT response in our simulations is different, peaking at the equator and being symmetric around it. As already discussed, this increase in cross-equatorial AHT is related to the tropical TOA flux changes that are negative in the northern and positive in the southern tropics. The tropical TOA energy budget anomalies following the ITCZ shifts result from the temperature, water vapor and cloud feedback effects as shown by Cvijanovic and Chiang (2012). We focus here on cloud radiative forcing anomalies, as cloud responses are known to dominate inter-model differences (Cess et al. 1996). This is illustrated in Figure 4.7*c* showing TOA flux (black solid line) and CRF (red solid line) anomalies as well as the longwave and shortwave CRF components (grey dashed lines) for the aquaNS_cw experiment. Figure 4.7*c* confirms that the overall cloud radiative forcing anomalies follow the sign of the longwave CRF anomalies. On the contrary, CRF changes in K08 study are dominated by the shortwave component (Figure 8 and 13*a* in K08) and thus have the opposite sign in the tropics compared to our aquaNS_cw experiment. The CRF response in K08 is related to the response in low clouds, while in our experiments medium and high cloud anomalies dominate the tropical response (not shown).

A sensitivity of the magnitude of tropical precipitation responses to the convection scheme parameters has been documented by K09 study. Our results, however, point to large inter-model differences in low and high cloud cover responses. This further causes different signs in CRF and TOA flux anomalies and affects the cross-equatorial atmospheric heat transport. Compared to the imposed cross-equatorial ocean heat flux anomalies (implicit in the Q-flux forcing), the cross-equatorial AHT response in the aquaNS_cw experiment is about three times larger. In comparison, K09 find the tropical compensation of the imposed ocean heat transport by the AHT to vary between 47% and 115% depending on convection scheme.

4.3.3 Temperature, water vapor and cloud radiative feedback response to southward ITCZ shifts

In this section, we further investigate the anatomy of the global energy budget response following the three southward ITCZ shifts, by addressing the role of radiative feedbacks. As described in Cvijanovic and Chiang 2012, we apply the radiative kernel technique by Soden et al. (2006), adapted for CAM3 by Shell et al. (2008). The agreement between the overall TOA flux anomalies from the model output and from the kernel method is lower in the high latitudes due to the non-linearity of the surface albedo feedback (SAF). Since we are mainly interested in the tropical response, we limit our focus to temperature, water vapor and cloud feedback effects to the imposed forcing. However, one should be aware that the extratropical shortwave cloud feedback effect may be affected by discrepancies in the SAF calculation (more details can be found in Shell et al. 2008).

TOA flux anomalies and the main feedback effects are calculated over four areas, roughly representing the tropics and extratropics of the two hemispheres (Figure 4.8). The first panel in Figure 4.8 shows the TOA flux changes in the NH_cold experiment. The main energy gain comes from the southern tropics due to cloud and water vapor feedbacks while the remainder of the energy is obtained in the northern extratropics due to the temperature longwave feedback. Some energy is lost in the northern tropics as a consequence of negative water vapor and cloud feedback effects following the ITCZ shifts. This is because northern tropics become drier as the ITCZ shifts southward. As discussed before, the negative cloud feedback effect in the northern tropics arises from reduced medium and high cloud cover.

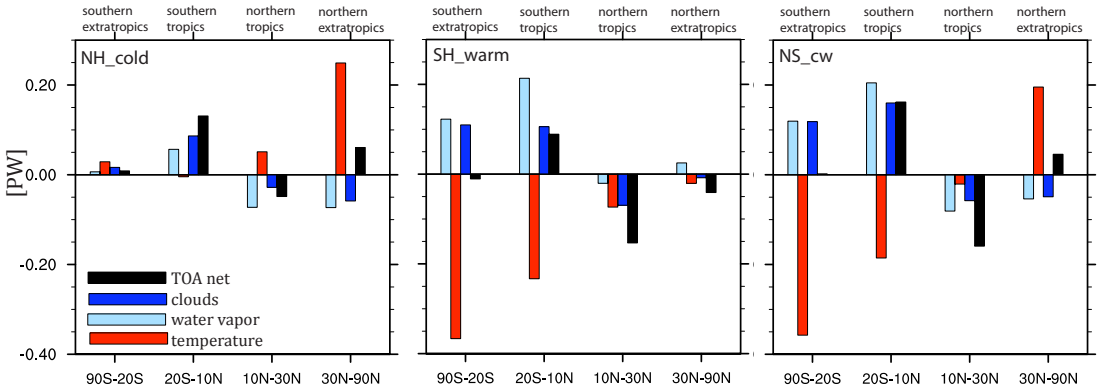

Figure 4.8: TOA energy budget anomalies and temperature, water vapor and cloud feedback effects summed over the extratropical and tropical regions in NH_cold, SH_warm and NS_cw experiments (sign convention is positive downward, i.e., a heating of the system).

The TOA energy budget changes in SH_warm and their separation into individual radiative feedback effects are shown in the middle panel of Figure 4.8. The main energy loss comes from the northern tropics, due to temperature, cloud and water vapor feedback effects. Although positive surface temperature anomalies did not progress deep into the northern tropics, the atmospheric temperature anomalies did (Figure 4.9*a*) and hence they induce a negative effect on the overall TOA flux anomalies. The negative cloud feedback effect is due to the southward precipitation shift as in the NH_cold experiment, although it is somewhat larger. The negative water vapor feedback effect is a consequence of the decreased humidity in the northern tropics (Figure 4.9*b*). Although the air temperatures increases in the northern tropics, this did not cause a specific humidity increase, as the dynamic processes related to Hadley cell changes are more important. The decrease in northern tropical water vapor content is thus related to the southward ITCZ shift and strengthened northern Hadley cell that causes an increased latent heat transport into the warmer (southern) hemisphere.

The remainder of energy in SH_warm is lost in the northern extratropics through temperature feedback effects associated with warm anomalies in the northern extratropics (Figure 4.9*a*). Despite a tropospheric cooling aloft in high northern latitudes, positive temperature anomalies at lower levels and latitudes have stronger feedback effects leading to a net cooling. The midlatitude warming is followed by an increase in specific humidity (Figure 4.9*b*) leading to a positive water vapor feedback effect in the extratropics that acts to counteract the temperature feedback effects (Figure 4.8, middle panel).

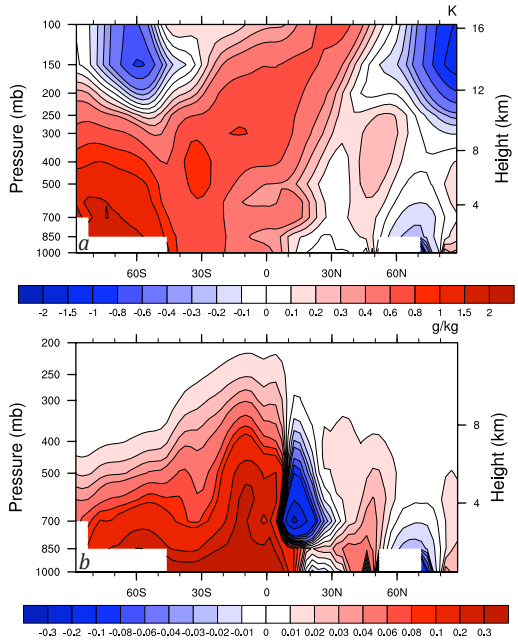

Figure 4.9: Vertical profiles of (*a*) zonal average temperature and (*b*) specific humidity anomalies in the SH_warm experiment.

Across the southern hemisphere, a negative temperature feedback effect acts to counter the warming imposed in the SH_warm experiment, but due to the opposing effects by water vapor and clouds, TOA flux changes over the southern hemisphere (predominantly due to the southern tropics) are positive.

The TOA energy flux changes in the NS_cw case are shown in the right panel of Figure 4.8. As in NH_cold and SH_warm, northern tropical feedback effects lead to overall negative TOA flux changes and the opposite is seen in the southern tropics. Tropical energy flux changes in the NS_cw experiment are larger (in absolute value) than the corresponding changes in NH_cold and SH_warm experiments. In general, the changes in NS_cw correspond roughly to the sum of those in NH_cold and SH_warm.

In summary, whether the total TOA flux changes will be positive or negative is a question of delicate balance between the temperature, water vapor and cloud responses and while their relation in the extratropics is more thermodynamically determined, in the tropics it is chiefly governed by the changes in Hadley cell dynamics.

4.4 Atmospheric teleconnection from the Southern Ocean to North Atlantic

Our considerations of surface temperature anomalies (Figure 4.2, bottom plots) revealed that the Southern Ocean warming causes temperature changes over the North Atlantic with cooling in the northern tropical Atlantic, warming off the east coast of America and cooling south of Greenland and over northern North America. These surface temperature anomalies are statistically significant at the 95% level (using the Student's *t*-test).

The question is how such a teleconnection comes about. As the tropics must mediate the communication between the two hemispheres, we turn once more to the comparison of the tropical responses. As noted previously, Hadley cell anomalies are positive, meaning that the northern cell is enhanced and southern weakened, in accord with the southward ITCZ shifts (not shown). The strengths of Hadley cell anomalies increase from NH_cold to SH_warm and NS_cw in agreement with the increasing AHT anomalies. Thus, the stronger Hadley circulation response in SH_warm compared to NH_cold should more strongly affect the subtropical jet (Hou and Lindzen 1992). In turn, the change in subtropical jet will affect the eddy-driven polar jet (Lee and Kim 2003). Following these arguments, jet changes can be predicted from the Hadley cell anomalies: a strengthened Hadley cell leads to an increase in the subtropical jet and this in turn causes a decrease in the polar jet and vice versa (Lee et al. 2011). This is indeed the case in our aquaplanet experiments (not shown) but in the presence of land, orography and sea ice, we find that the response becomes more complex.

Figure 4.10 reveals very similar geometries of the anomalies in 200 hPa wind strengths and surface wind stress in NH_cold and SH_warm. In both experiments, there is an increase in annual mean 200 hPa winds (left panels) in the North Atlantic area south of Greenland, the tropical North Atlantic and northern tropical east Pacific. Weakened high-level winds are found over the midlatitude North Atlantic and southern tropical east Pacific. As hypothesized, wind strength changes are more pronounced in SH_warm experiment (compared to NH_cold) in agreement with a stronger Hadley cell response. In the southern hemisphere, there is decrease in the annual mean wind strengths poleward of 45^{o}S and an increase between 30^{o}S and 45^{o}S.

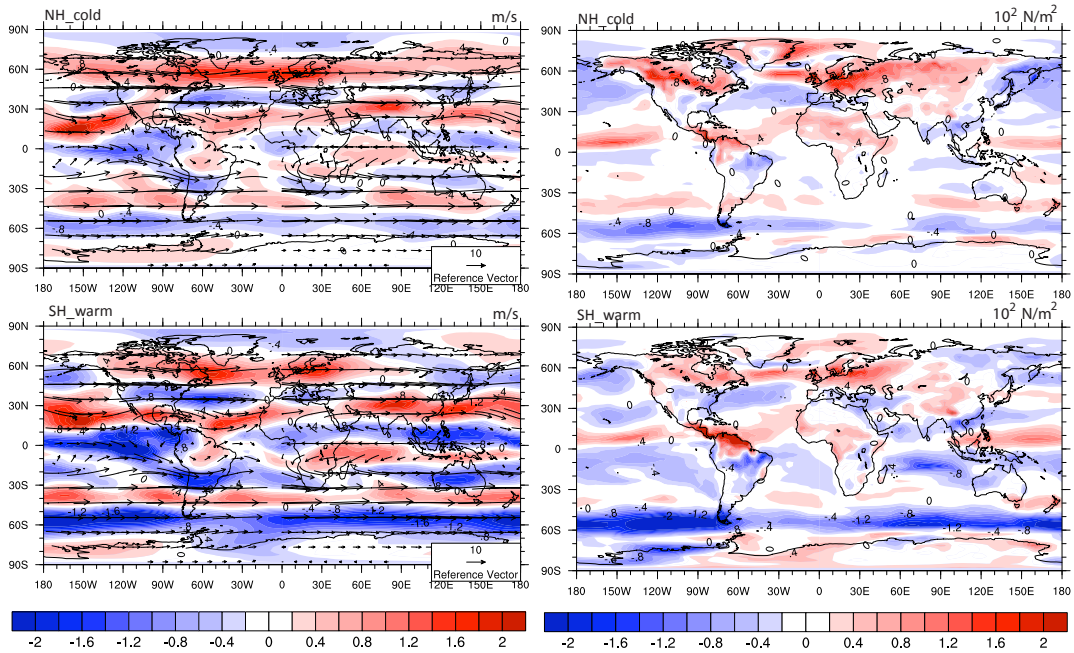

Figure 4.10: left panels – 200 hPa annual mean wind strength anomalies (colors) and wind vectors (arrows), right panels – surface wind stress anomalies. Upper and lower panels correspond to NH_cold and SH_warm experiments, respectively.

The surface wind changes, however, appear to also be affected by the presence (or absence) of the northern high latitude surface cooling. As a consequence, the northern circulation changes are larger in NH_cold than in SH_warm as seen from the right panels in Figure 4.10. Analogously to the 200 hPa wind strength anomalies, surface wind changes appear to be very similar over the North Atlantic and tropical Pacific with areas of decreased (increased) wind stress coinciding with areas of surface warming (cooling) in the SH_warm experiment. We have tested the robustness of the high latitude North Atlantic response by applying weaker and stronger warming over the Southern Ocean in our slab ocean simulations and arrived to the same conclusion (not shown).

Development of mid- and high latitude North Atlantic warming and cooling patterns in response to tropical Atlantic forcing has been previously investigated by Okumura et al. (2001). Their study included simulations with prescribed tropical SSTs and extratropical slab ocean, in which the response to an interhemispheric tropical Atlantic surface temperature dipole was examined. In response to the cold north/warm south tropics temperature gradient, they found positive SST anomalies developing off the eastern North America due to weakened winds and negative SST anomalies south of Greenland coincident with increased winds. The extratropical response is

found to project onto NAO through barotropic teleconnection. Their study also points out a striking resemblance to observational data during periods with strong cold-north warm-south tropical Atlantic SST gradient.

Terray and Cassou (2002), similarly in AGCM simulations, investigate the influence of tropical North Atlantic SSTs on the extratropical North Atlantic and demonstrate that the tropical SST anomalies can lead to changes that tend to reinforce the geopotential structure of the simulated NAO. According to their study, the mechanism includes changes in tropical convection, Hadley circulation and interaction between planetary waves and the subtropical wind variability induced by the tropical circulation anomalies. The relation they describe between wind and temperature anomalies is very similar to our findings.

Further work is required to test the sensitivity of the atmospheric teleconnection found in our experiments – the *atmospheric* bipolar seesaw, which can act on top of the slower oceanic bipolar seesaw. The novelty of this study is that the proposed interhemispheric communication merges two physically plausible mechanisms: the southward ITCZ shift due to Southern Hemisphere warming and the consequent tropical dipole forcing onto the high and mid-latitude North Atlantic circulation. The mechanism could have compelling implications for paleo-data interpretations as will be discussed in the next section.

4.5 Conclusions and paleo-data implications

This study provides a quantitative analysis of the global energy flux changes due to three different triggers of a southward ITCZ shift, namely Northern Hemisphere cooling, Southern Hemisphere warming and a combination of both referred to as a bipolar seesaw experiment. In addition to the energy flux changes we also tackle the dynamics of the shifts by comparing the atmospheric response to an oceanic bipolar seesaw-type of forcing with north-forcing-south and south-forcing-north simulations only. In particular, we are interested in teleconnections through which a Southern Ocean warming can affect the mid- and high-latitude North Atlantic and the strengths of the high-to-low-latitude teleconnections.

In NH cooling experiments (north-forcing-south), additional energy is required in high northern latitudes and we show that this is accomplished by increased northward energy transport from the tropics, with the dominant energy source being the east tropical Pacific. In SH warming experiments (south-forcing-north), the energy surplus due to the imposed forcing needs to be transported away from the southern latitudes and the sink for this energy is found to be in the northern tropics, mainly over the northern tropical Atlantic. Finally, in the bipolar seesaw experiment, an energy deficit and surplus are imposed in the northern and southern high latitudes, respectively. The locations of increased energy gain (equatorial east Pacific) and increased energy loss (tropical North Atlantic) due to the TOA flux changes, provide a positive feedback onto the imposed interhemispheric forcing by cooling the northern and warming the southern tropics.

The tropical TOA flux changes result from cloud, water vapor and temperature feedback interactions. The sign of cloud feedback response is of particular importance for the tropical TOA flux anomalies and cross-equatorial AHT response. A related study by Kang et al. (2008) showed somewhat different AHT anomalies at the equator. This is a consequence of dominant shortwave (over the longwave) tropical cloud radiative forcing and low cloud cover response that induces positive TOA anomalies in the northern and negative in the southern tropics. In contrast, our simulations show that longwave tropical CRF is dominant over the shortwave. Medium and high cloud changes are more pronounced, with the high cloud cover increasing in the southern and decreasing in the northern tropics. This provides further positive TOA flux changes in the southern and negative in the northern tropics, increasing the cross-equatorial AHT.

Atmospheric heat transport changes and Hadley cell anomalies are largest in the NS_cw experiment, followed by the SH_warm and NH_cold simulations in accord with the corresponding interhemispheric tropical temperature gradients (IHTG). The larger IHTG and AHT response in SH_warm compared to NH_cold simulation was proposed to be a consequence of the nonlinear water vapor response. Possible mechanisms through which the nonlinearities in the water vapor response could have affected the tropical response are suggested, but deciphering between their individual importance was not possible with our experimental setup and is beyond the scope of the current study.

Two important points arise from these experiments: firstly, a proposed teleconnection between the high southern and northern latitudes and secondly, high-to-low-latitude teleconnections. According to the first, that has been named the atmospheric bipolar seesaw, the high latitude North Atlantic cools in response to Southern Ocean warming. This is a two step interaction in which the SH warming causes a southward ITCZ shift while the associated tropical Atlantic SST gradient and circulation changes cause an extratropical North Atlantic response.

If also robust under LGM conditions, an atmospheric teleconnection from the Southern Ocean to the North Atlantic could have interesting paleo-climate implications. For example, NGRIP ice core data by Steffensen et al. (2008) suggest that changes in the dust record started before changes in the $\delta^{18}O$ and deuterium excess records during the Bølling-Allerød warming. As the dust in Greenland originates mainly from low-latitude Asian deserts (Svensson et al. 2000), this lead the authors to propose that tropical circulation changes occurred before the high northern latitude warming, and that the trigger was the tropical reorganization. This interpretation, however, requires that the ITCZ shifts to the colder hemisphere, which does not seem physically plausible (Chiang and Cuffey 2008).

However, if a Southern Ocean cooling was the trigger of the Bølling-Allerød warming instead of the tropical reorganization, as suggested by Weaver et al. (2003) for example, this could have caused the tropical circulation reorganization through an atmospheric teleconnection. Following this line of thought, the high latitude North Atlantic temperatures would be affected first due to the atmospheric and then the oceanic circulation changes. Such a scenario would support the conclusion of Steffensen et al. (2008) that tropical circulation changes came first. In that respect, the Steffensen et al. (2008) Bølling-Allerød dust and temperature change timing could be alternatively explained by the atmospheric teleconnection due to the Southern Ocean cooling that is mediated by the tropics.

Another compelling implication is related to the study by Montoya and Levermann (2008) which demonstrated the existence of a surface wind threshold affecting the AMOC strength under glacial conditions. Thus, if the atmospheric teleconnection described in our study persists under glacial conditions, it could have a much larger effect than anticipated from the slab ocean simulations. In particular, if AMOC strength would be also affected by the wind stress changes described in our study, this would mean a much larger high northern latitude impact. The North Atlantic response to Southern Ocean temperature changes under glacial conditions will be addressed in future work.

The second paleo-implication arising from this study concerns high-to-low-latitude teleconnections, as our results indicate that the southern high-latitude forcing is as important for tropical precipitation shifts as the northern forcing. According to the oceanic bipolar seesaw mechanism (Stocker and Johnsen, 2003), North Atlantic cooling (due to AMOC slowdown) yields a gradual Southern Ocean warming which, in turn, causes an additional ITCZ shift. The impact of this secondary shift will depend on both the magnitude and timing of the Southern Ocean temperature change.

A simple scheme of such consecutive ITCZ shifts is given in Figure 4.11. We only consider two possible states for the North Atlantic and Southern Ocean: 1. strong AMOC (warm North Atlantic) or 2. weak AMOC (cold North Atlantic) and 1. warm Southern Ocean or 2. cold Southern Ocean. More elaborate considerations would include neutral states of the North Atlantic and Southern Ocean as well as differences in the magnitudes, but this simple scheme is sufficient to illustrate our points.

Combination strong AMOC (warm North Atlantic) and cold Southern Ocean in this simple framework corresponds to our control simulation (Scenario 1 in Figure 4.11). In this case, the Northern Hemisphere is warmer than the Southern and the ITCZ has a more northerly position. Scenario 2 assumes an AMOC slowdown with the North Atlantic being cold but without the Southern Ocean having had time to warm significantly. In response to this North Atlantic cooling, the ITCZ shifts south. According to the transient simulations by Chiang and Bitz (2005), Mahajan et al. (2011) and Cvijanovic and Chiang (2012), it takes less than a decade for the precipitation to shift to its southward location due to atmosphere-surface ocean teleconnections. This scenario is illustrated in our NH_cold simulation and the corresponding precipitation change is shown in panel (a) of Figure 4.11 with the solid blue line.

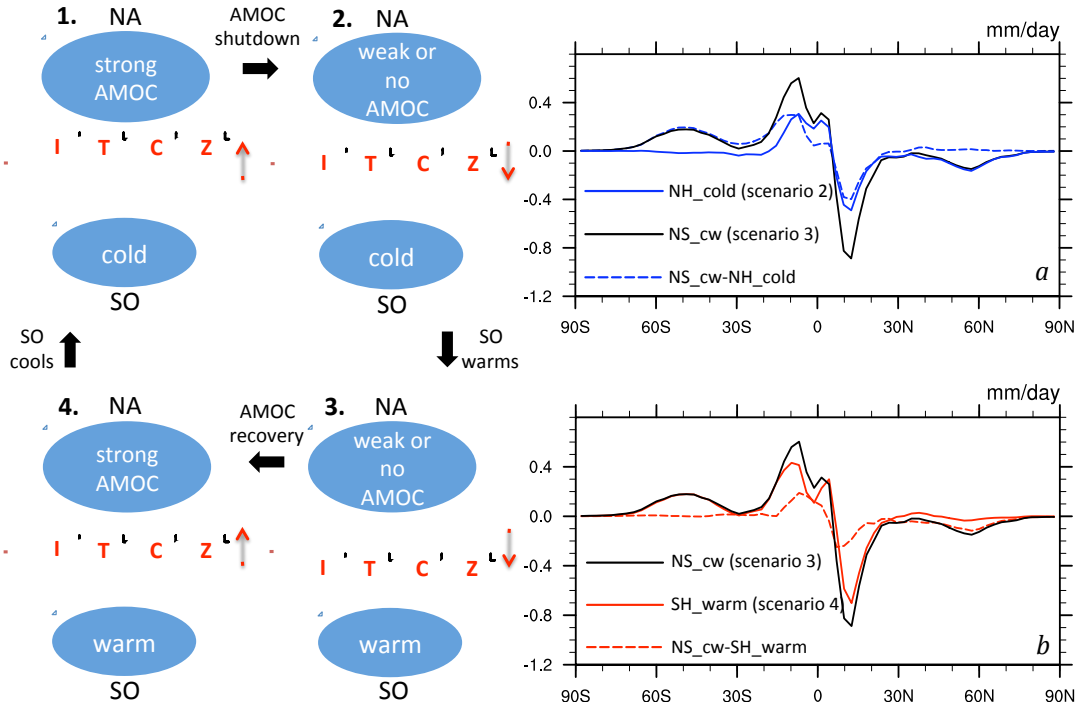

Figure 4.11: Scheme illustrating the possible atmospheric teleconnections leading to ITCZ shifts: 1 – base case (control run), 2 – NH_cold simulation, 3 – NS_cw simulation and 4 – SH_warm simulation. Panels: Annual and zonal mean precipitation anomalies - (a) NH_cold (blue solid) and NS_cw (black solid) simulations and their difference (blue dashed line); (b) SH_warm (red solid) and NS_cw (black solid) simulations and their difference (red dashed line). NA – North Atlantic, SO – Southern Ocean.

In scenario 3, enough time has passed for the Southern Ocean to become warmer due to ocean circulation changes. Maximum Southern Ocean response develops in about a century after the AMOC slowdown (Stouffer et al. 2007, Otto-Bliesner and Brady 2010). The warming of the Southern Ocean additionally alters the interhemispheric temperature gradient and causes stronger ITCZ shifts south towards the warmer hemisphere. This is again caused by atmosphere-surface ocean teleconnection only. Scenario 3 corresponds to our bipolar seesaw experiment NS_cw and is shown in panels (a) and (b) of Figure 4.11 (solid black line). The blue dashed line in panel (a) shows the difference in precipitation anomalies between Scenario 2 (NH_cold case) and Scenario 3 (NS_cw) indicating that the precipitation increase (decrease) at 10° S (10° N) has doubled after the second shift.

Scenario 4 corresponds to the situation just after an AMOC recovery when the North Atlantic is warm but the Southern Ocean did not cool yet. Due to the NH warming, the precipitation shifts northward compared to the scenario 3. As the strong AMOC - cold Southern Ocean is our control state, then the strong AMOC - warm Southern Ocean corresponds to our SH_warm simulation. Panel (b) in Figure 4.11 compares the tropical precipitation shifts in the SH_warm and NS_cw experiments showing significant absolute decrease in precipitation anomalies in SH_warm. The northward shift occurs here because of the direction chosen in the scheme: we follow the change going from NS_cw to SH_warm experiment. Finally, as the Southern Ocean cools, the ITCZ will return to the state we started from.

This simple scheme illustrates that past tropical precipitation changes result from the complex interactions lead by high latitude changes in both hemispheres. Consequently, there may rarely be just one southward or northward ITCZ shift, but at least a two-step shift: the first one being abrupt, due to the atmospheric teleconnection from the location where the change was triggered (e.g, the North Atlantic) and the second more gradual, in response to the atmospheric teleconnection from the location to where the change was transmitted through ocean circulation changes. In our slab ocean configuration, however, we were unable to consider the fast oceanic changes, or any tropical SST changes originating directly from the ocean dynamics. These processes are likely to further complicate the understanding of the observed precipitation signal.

Despite the fact that our analysis does not consider the full complexity of high-to-low-latitude communication, it does point out the necessity of considering the ITCZ shifts in a wider framework than traditionally done. As inferred from our results, the atmospheric teleconnection due to Southern Ocean warming is as important for tropical precipitation shifts as the one due to North Atlantic cooling. The coupled model study by Stouffer et al. (2007) supports our conclusion – in response to freshwater forcing in the North Atlantic and Southern Ocean, they find noticeable symmetry in the atmospheric responses and suggest that the shutdown of deep water formation in any hemisphere can produce a seesaw effect in the opposite one. However, their study addresses the oceanic seesaw, while ours implies the existence of an atmospheric seesaw. Additional work is required to test the considered atmospheric scenario under less idealized configurations.

Chapter 5

Conclusions and the future outlook

In this thesis, global atmospheric teleconnections to high latitude forcing have been investigated with special emphasis on possible paleoclimate implications. One of the major goals of the presented work is understanding the atmospheric reorganization following the Atlantic Meridional Overturning Circulation shutdown that leads to tropical precipitation and atmospheric heat transport changes.

This was first investigated in an atmospheric general circulation model with prescribed sea surface temperatures as described in Chapter 2. The focus of the study was on the sensitivity of the atmospheric heat transport response under present day and Last Glacial Maximum (LGM) conditions. The results revealed larger present day mid-latitude atmospheric heat transport sensitivity compared to glacial conditions. This was linked to the greater transient eddy heat flux response in the present day climate. In comparison, stationary eddy heat flux response was found to be stronger in glacial climate. However, as the transient eddy heat flux anomalies dominate the mid-latitude eddy driven transport over the stationary eddy heat flux anomalies, this effect had more impact in present day than in LGM simulations.

In terms of paleoclimate implications, these results imply that the present day climate is more efficient in damping the high latitude oceanic forcing due to the strong mid-latitude response (there is a much larger negative feedback on the imposed temperature gradients as a consequence of the enhanced atmospheric transport response). Decreased glacial energy transport feedback is likely related to larger sea ice extent in LGM simulations and to the LGM orography that forces a different partitioning of the transient and stationary components between the two climates.

The analysis of the atmosphere only response presented in this study did not allow for the surface ocean feedbacks and the prescribed sea surface temperature setup may have had large influence on the results obtained. With this motivation, in the further work an attempt is made to better understand the role of sea surface temperatures in atmospheric response to high latitude forcing. This problem was addressed in Chapter 3. In a set of idealized simulations, with fixed tropical SSTs and slab ocean

boundary condition in the extratropics, the role of SST anomalies in the tropical ITCZ response was examined. These results have suggested direct tropical SST control of the ITCZ response, with the SST anomalies propagating into the tropics being both necessary and sufficient for the ITCZ shift. Only as the surface temperature anomalies reach the tropics, the convection reorganizes and this leads to TOA energy flux changes resulting from cloud, water vapor and temperature feedbacks.

In addition to the idealized experiments, detailed study of the global energy budget changes to high latitude North Atlantic cooling and the southward ITCZ shift has been performed in an atmospheric general circulation model coupled to a slab ocean. Energy budget changes in extratropics, northern and southern tropics were quantified and then decomposed into the individual feedbacks using a radiative kernel technique. About 35% of the initial high latitude surface forcing was found to be compensated locally in the northern extratropics, by TOA changes due to the longwave temperature feedback. The remainder of the energy was provided from the southern tropics, mainly due to the longwave cloud and water vapor feedbacks. The northern tropics did not significantly contribute to the net energy fluxes.

In the final part of this work, described in Chapter 4, we have expanded our consideration with different scenarios of southward ITCZ shifts, including the Northern Hemisphere cooling, Southern Hemisphere warming and a bipolar seesaw forcing (that combines both). Besides the energetics of the shifts, the strength of high-to-low-latitude teleconnections and the influence of the Southern Ocean warming on the northern high latitudes were also investigated. Southward precipitation shifts found in these three experiments were shown to vary in strength and geometry while the Southern Ocean warming experiment was shown to affect the mid- and high- latitude North Atlantic surface temperatures and wind fields. The proposed atmosphere-surface ocean teleconnection, involving the southward ITCZ shift to the warmer hemisphere and the consequent tropical Atlantic surface temperature dipole forcing the extratropical North Atlantic circulation changes, was named an atmospheric bipolar seesaw mechanism.

It was found that the locations of maximal energy gain and loss in all experiments are consistently located in the east tropical Pacific and tropical North Atlantic, respectively. The tropical TOA flux changes were decomposed into cloud, water vapor and temperature feedback effects and it was found that the sign of cloud radiative forcing is of particular importance for the cross-equatorial atmospheric heat transport response.

This was related to the pronounced medium and high cloud changes, that are positive over the southern and negative over the northern tropics leading to a positive (negative) TOA flux changes in the southern (northern) tropics. As a consequence, tropical TOA changes act as a positive feedback to the imposed high latitude forcing increasing the cross-equatorial atmospheric heat transport. Atmospheric heat transport changes and Hadley cell anomalies were found to be largest in the bipolar seesaw forcing experiment, followed by the southern warming and northern cooling simulations and such response was attributed to changes in interhemispheric tropical temperature gradient and nonlinear water vapor response.

Experiments described in Chapter 4 could have compelling paleoclimate implications, especially if the proposed atmospheric seesaw mechanism proves to be robust also under the LGM conditions. Of particular interest would be the analogous Southern Ocean *cooling* experiment that would investigate whether there is a similar atmospheric reorganization that could lead to the North Atlantic warming. If such atmospheric teleconnection does exist, it could act as a positive feedback on the underlying ocean circulation changes (Southern Ocean cooling and North Atlantic warming) and this could help resolve the question of B/A warming overshoot.

This is particularly important given that the freshwater hosing experiments with coupled climate models are not able to simulate the warming of D/O type under realistic fresh water forcing (Valdes et al. 2011). More specifically, an attempt by Liu et al. (2009) to simulate the B/A event required thousands of years longer fresh water forcing than implied from the geological evidence. Besides this, coupled models also have difficulties in simulating the correct magnitude of oceanic response during the abrupt cooling events. Fresh water forcing during the Heinrich events is estimated to be 0.1-0.2 Sv (Hemming 2004) while the simulations using such realistic fresh water flux result in a much weaker response than suggested by the ice cores (Kageyama et al. 2010). Consequently, validation of the proposed atmospheric teleconnection would imply that the B/A temperature overshoot that the coupled models have not been able to produce so far under the realistic forcing, may also be an expression of the atmospheric teleconnection from the Southern Ocean that acts to further enhance the North Atlantic warming.

Another paleo-implication arising from this work suggests that the past tropical precipitation changes are a result of the complex interactions due to the high latitude changes in both hemispheres. In that sense, once that

high resolution tropical data becomes available it is very likely that the precipitation changes will reveal at least a two phase change, starting abruptly (due to the atmospheric teleconnection from the location where the oceanic change had occurred) and continuing gradually (due to the atmospheric teleconnection from the location to where the change was transmitted through ocean circulation changes).

Regarding the future outlook, there are still plenty of "known unknowns" in comprehending the global atmospheric teleconnections, promising an exciting path to the ones who decide to pursue it. Some of the outstanding questions remain to be the exact magnitude and location of the tropical response to high latitude northern cooling, the role of atmosphere in D/O type of events (in particular the Bølling-Allerød northern hemisphere warming) and the robustness of atmospheric teleconnection between the Southern Ocean and the high northern latitudes.

Given the difficulties that the current coupled models are having in reproducing the observed abrupt climate events with the realistic forcing, using the atmospheric models coupled to the mixed layer ocean simplifies the problem by enabling to constrain first the strength and magnitude of the atmospheric response. An important next step is to provide a proper estimate of cooling and warming ocean anomalies to be used as forcing for the atmospheric models. This would involve thorough integration of the ocean proxy and model data into the forcing data sets.

Using the advanced atmospheric general circulation models of the latest generations could significantly decrease the widespread uncertainties. The specific relevance of the later point is highlighted by the fact that the current atmospheric simulations of abrupt past climate change are hampered by the large discrepancies that exist amongst them (as shown in this study). This points to an inherent lack of understanding of the underlying mechanisms involved and suggests the need for comprehensive data-model integration in the field of atmospheric teleconnections.

At present, the scientific efforts of the paleoclimate community have branched into two main directions. The first has focused on the retrieval of paleo-proxy records from the around the world while the second have worked towards the development of increasingly complex Earth system models. Although the overall understanding of global atmosphere-ocean interactions has improved tremendously over the recent years, it still lags behind the advances made in the individual fields. The cause for this is an insufficient integration of findings from the modeling and data oriented

research areas. While pioneering research in these two fields is still mandate, it is also an imperative to integrate and verify the understanding of the atmospheric teleconnections from both the modeling and data perspectives. Major step in this direction arises from the efforts of the Paleoclimate Modeling Intercomparison Projects (Braconnot et al. 2004 and Braconnot et al. 2007). Similarly, defining the protocol for testing the tropical atmospheric response to high latitude cooling would provide a valuable contribution to understanding of abrupt climate change. In comparison to other possible scientific objectives this one is remarkably *inexpensive* and yet it provides an essential envelope for all the further actions. As such, this objective would provide the foundation and directions for the future research.

Epilogue

It has been more than two decades since the United Nations Framework Convention on Climate Change reached an agreement in Kyoto acknowledging the need for the global response in treating the problem of climate change. Since that time, remarkable scientific efforts have been invested towards reducing the uncertainties related to the topic of climate change. The awareness of the general public about our changing world has also increased. Despite this, the continuation and implementation of such global climate treaty remains unresolved till present, in spite of the thorough scientific input provided to the decision makers.

Finding the ways to communicate the state-of-the-art knowledge thus remains a long lasting challenge and a duty of climate scientists. In that sense, being able to provide simple, but objective, overview is essential in raising the awareness about the problems the society needs to address today. Hence, one of the crucial tools for future sustainable societal development is the *education*. Impressive endeavors have been undertaken in the last years in attempt to inform a broad range of audiences about the future challenges, from the IPCC reports to educational films by Sir David Attenborough, Richard Alley and many others. Despite the fact that we do not see the immediate results in terms of the decision making or political agreements, these efforts may still not be in vain, as the changes may need to wait for the future generations. And within them, lies an amazing eagerness for learning (as illustrated in Figure 5.1) that should keep one hopeful.*

* unless ones home is located on a small flat tropical island in which case moving is recommended.

Figure 5.1: Planet Earth, continents (green) and oceans (blue) with imposed high northern latitude cooling (dark blue circles) and southward ITCZ shift (red and blue lines). By Sophia, 5 years old, Berkeley, 2011.

Appendix 1

The angular momentum M of unit parcel in the rotating atmosphere can be expressed as follows (Peixoto and Oort, 1992):

$$M = (\Omega a \cos\phi + u) a \cos\phi \tag{A1}$$

Where a is the mean radius of the Earth, Ω represents the mean angular velocity of the planetary rotation, φ is latitude and u zonal wind component. Assuming the angular momentum conservation, then for a particle initially at the equator the following expression must hold:

$$M \leq \Omega a^2 \tag{A2}$$

Combining (A1) and upper limit of (A2), provides an upper limit for angular momentum conserving zonal winds:

$$u_M = \Omega a \sin^2\phi / \cos\phi \tag{A3}$$

The expression (A3) is known as Hide's theorem (Hide 1969, Schneider 2006) and states that in steady axisymmetric circulations, zonal wind cannot exceed angular momentum–conserving zonal wind.

In the upper branch of Hadley cell close to the equator, in the absence of the friction, one can assume that angular momentum conservation is a valid approximation, conditional on the fact that the horizontal eddy divergence is small. As shown by Held and Hou (1980), this angular momentum conservation provides an upper limit to the possible temperature gradients in the tropics. Using the small angle approximation $\varphi << 1$, one can transform A3 into:

$$u_M = \Omega a \varphi^2 \tag{A4}$$

Assuming the thermal wind approximation, zonal mean flow u_M becomes:

$$u_M = -\frac{1}{fa}\frac{\partial \Phi}{\partial \varphi} \tag{A5}$$

with Φ representing the geopotential.

Combining the equations A4 and A5 and integrating the new expression from the equator, we arrive to the following dependence:

$$\frac{\partial \Phi}{\partial \varphi} = 2\Omega^2 a^2 \varphi^3 \tag{A6}$$

$$\Phi(\varphi) = \Phi(0) - \frac{\Omega^2 a^2}{2}\varphi^4 \tag{A7}$$

where $\Phi(0)$ is the geopotential value at the equator.

The derived expressions illustrate that there cannot be large geopotential distribution changes in the deep tropics. This, in turn, keeps the upper tropospheric winds from increasing faster than allowed by angular momentum conservation. In reality, zonal winds in the tropics are much weaker than this angular momentum conserving limit (Schneider 2006). As the geopotential is proportional to the vertical temperature average within the pressure layer, this means that large gradients in vertically averaged temperatures cannot be sustained in the deep tropics.

Due to the fact that the large horizontal geopotential/temperature gradients cannot be preserved in the tropical upper troposphere, asymmetric tropical heating about the equator results in a shift of the rising branch of the Hadley circulation to the warmer hemisphere (Lindzen and Hou, 1988).

However, it is important to note that the Held-Hou model of the Hadley circulation is an approximation and amongst other things, it does not account for horizontal eddy flux divergence. It has been shown that the midlatitude eddy propagation can have a strong effect on Hadley circulation (Becker et al. 1997, Kim and Lee, 2001) and that the Held and Hou inviscid axisymmetric regime does not apply well to the summer Hadley cell (Walker and Schneider 2006, Caballero 2007).

Bibliography

Alley, R., Clark, P. U., Keigwin, L. D. and Webb, R. S.: Making sense of millennial-scale climate change. In: Clark, P. U, Webb, R. S. and Keigwin, L. D. (ed.): Mechanisms of Global Climate Change at Millennial Time Scales, Geophys. Monogr. Ser., vol. 112, , pp. 385–394, AGU, Washington, D. C. 1999.

Banakar, V. K., Mahesh, B.S., Burr, G., and Chodankar, A.R.: Climatology of the Eastern Arabian Sea during the last glacial cycle reconstructed from paired measurement of foraminiferal d18O and Mg/Ca, Quat. Res. 73/3, 535-540, doi: 10.1016/j.yqres.2010.02.002, 2010.

Becker, E., Schmitz, G. and Geprags, R.: The feedback of midlatitude waves onto the

Hadley cell in a simple general circulation model. Tellus. 49A:182–99, 1997.

Blunier, T., et al.: Asynchrony of Antarctic and Greenland climate change during the last glacial period, Nature, 394, 739–743, doi:10.1038/29447, 1998.

Bonan, Gordon B., 1998: The land surface climatology of the ncar land surface model coupled to the ncar community climate model*. J. Climate, 11, 1307–1326.doi:
http://dx.doi.org/10.1175/15200442(1998)011<1307:TLSCOT>2.0.CO;2

Bonan, G. B., Oleson, K. W., Vertenstein, M., Levis, S., Zeng, X., Dai, Y., Dickinson, R. E. and Yang, Z. L.: The land surface climatology of the Community Land Model coupled to the NCAR Community Climate Model. J. Clim. 15, 3123–3149, 2002.

Bond, G., Broecker, W., Johnsen, S., McManus, J., Labeyrie, L., Jouzel, J. and Bonani, G.: Correlations between climate records from North Atlantic sediments and Greenland ice, Nature, 365, 143–147, doi:10.1038/365143a0, 1993.

Braconnot, P., Harrison, S. P., Joussaume, S., Hewitt, C. D., Kitoh, A., Kutzbach, J. E., Liu, Z., Otto-Bliesner, B., Syktus, J. and Weber, N.: Evaluation of PMIP coupled ocean-atmosphere simulations of the mid-Holocene. In (ed.) Batterbee, R. W. et al.: Past Climate Variability Through Europe and Africa, pp. 515-533, Springer, New York, 2004.

Braconnot P., Otto-Bliesner, B. L., Harrison, S. P., Joussaume, S., Peterchmitt, J.-Y., Abe-Ouchi, A., Crucifix, M., Fichefet, T., Hewitt, C. D., Kageyama, M., Kitoh, A., Loutre, M. F., Marti, O., Merkel, U., Ramstein, G., Valdes, P. J., Weber, S. L., Yu, Y., Zhao, Y. : Results of PMIP2 coupled simulations of the mid-holocene and last glacial maximum—part 1: experiments and large-scale features. Clim Past 3:261–277, 2007.

Broccoli, A. J., Dahl, K. A., and Stouffer, R. J.: Response of the ITCZ to

Northern Hemisphere cooling, Geophys. Res. Lett., 33, L01702, doi:10.1029/2005GL024546, 2006.

Broecker, W. S.: Massive iceberg discharges as triggers for global climate change, Nature, 372, 421–424, 1994.

Broecker, W. S.: Paleocean circulation during the last deglaciation: A bipolar seesaw?, Paleoceanography, 13(2), 119–121, doi:10.1029/97PA03707, 1998.

Caballero, R., and Langen, P. L.: The dynamic range of poleward energy transport in an atmospheric general circulation model, Geophys. Res. Lett., 32, L02705, doi:10.1029/2004GL021581, 2005.

Caballero, R.: Role of eddies in the interannual variability of Hadley cell strength, Geophys. Res. Lett. 34, L22705. doi:10.1029/2007GL030971, 2007.

Caballero, R. and Anderson, B. T.: Impact of midlatitude stationary waves on regional Hadley cells and ENSO. Geophys. Res. Lett. 36, L17704. doi: 10.1029/2009GL039668, 2009.

Cess, R. D. et al.: Cloud feedback in atmospheric general circulation models: An update. J. Geophys. Res., 101, 12791-12794,1996.

Cessi, P., Bryan, K. and Zhang, R.: Global seiching of thermocline waters between the Atlantic and the Indian-Pacific Ocean basins, Geophys. Res. Lett., 31, L04302, doi:10.1029/2003GL019091, 2004.

Chang, P., Saravanan, R., Ji, L., Hegerl, G.C.: The effect of local sea surface temperatures on the atmospheric circulation over the tropical Atlantic sector. J. Clim 13, 2195–2216, 2000.

Cheng, W., Bitz, C. M. and Chiang, J. C. H.: Adjustment of the global climate to an abrupt slowdown of the Atlantic meridional overturning circulation, in: Schmittner, A.: Ocean Circulation: Mechanisms and Impacts, Geophys. Monogr. Ser., 173, 2006.

Chiang, J. C. H., Kushnir, Y., Giannini, A.: Deconstructing Atlantic Intertropical Convergence Zone variability: Influence of the local cross-equatorial sea surface temperature gradient and remote forcing from the eastern equatorial Pacific. J. Geophys. Res. Atmos. 17, 4004. doi:10.1029/2000JD000307, 2002.

Chiang, J. C. H., and Bitz, C. M.: Influence of high latitude ice cover on the marine Intertropical Convergence Zone, Clim. Dyn., 25, 477– 496, 2005.

Chiang, and S. R. Hemming, pp. 295– 313, AGU, Washington, D. C., 2007.

Chiang, J. C. H, Cheng, W., and Bitz, C. M.: Fast teleconnections to the tropical Atlantic sector from Atlantic thermohaline adjustment, Geophys. Res. Lett., 35, L07704, doi:10.1029/2008GL033292, 2008.

Chiang, J. C. H. and Cuffey, K. M.: A simpler interpretation for high-resolution Greenland Ice Core Data. E-letter comment on Steffensen et al. (2008) to Science, 25, 2008.

Chiang, J.C.H., and Friedman, A. R.: Extratropical Cooling, Interhemispheric Thermal Gradients, and Tropical Climate Change, Annual Review of Earth and

Planetary Sciences 40, 383–412, doi: 10.1146/annurev-earth-042711-105545, 2012.

CLIMAP: CLIMAP 18K Database, IGBP PAGES/World Data Center for Paleoclimatology Data Contribution Series 94-001, Technical report NOAA/NGDC Paleoclimatology Program, Boulder CO, USA, 1994.

Collins, W. D. et al.: Description of the NCAR Community Atmosphere Model (CAM3). Tech. Note NCAR/TN - 464+STR, Natl. Cent. for Atmos. Res., Boulder, Colorado, 2004.

Collins, W. D. et al.: The formulation and atmospheric simulation of the Community Atmosphere Model version 3 (CAM3). J. Clim. 19 (11), 2144-2161, 10.1175/2007JCLI2146.1, 2006.

Cook, K. H. and Held, I. M.: Stationary waves of the ice age climate, J. Clim. 1: 807-819, 1988.

Cvijanovic, I., Langen, P. L. and Kaas, E.: Weakened atmospheric energy transport feedback in cold glacial climates, Clim. Past, 7, 1061-1073, doi:10.5194/cp-7-1061-2011, 2011.

Dahl, K. A., Broccoli, A. J., and Stouffer, R. J.: Assessing the role of North Atlantic freshwater forcing in millennial scale climate variability: A tropical Atlantic perspective, Clim. Dyn., 24, 325– 346, 2005.

Dansgaard, W. et al.: North Atlantic climatic oscillations revealed by deep Greenland ice cores. In: Hansen, J. E. and Takahashi, T. (ed) : Climate Processes and Climate Sensitivity, Geophys. Monogr. Ser., vol. 29, pp. 288–298, AGU, Washington, D. C. 1984.

deMenocal, P.B.: Cultural responses to climate change during the late Holocene, Science, 292, 667-673, 2001.

Dong, B.-W., and Sutton R. T.: Adjustment of the coupled ocean–atmosphere system to a sudden change in the thermohaline circulation, Geophys. Res. Lett., 29(15), 1728, doi:10.1029/ 2002GL015229, 2002.

Donohoe, A. and Battisti, D. S.: Causes of reduced North Atlantic storm activity in a CAM3 simulation of the Last Glacial Maximum. J. Climate, 22, 4793-4808, 2009.

Dubois, N., M. Kienast, S. S. Kienast, C. Normandeau, S. E. Calvert, T. D. Herbert, and Mix, A.C.: Millennial - scale variations in hydrography and biogeochemistry in the eastern equatorial Pacific over the last 100 kyr, Quat. Sci. Rev., 30, 210–223, 2011.

EPICA Community Members: One-to-one coupling of glacial climate variability in Greenland and Antarctica, Nature 444, 195–198, 2006.

Fleitmann, D. et al.: Holocene forcing of the Indian monsoon recorded in a stalagmite from southern Oman, Science, 300, 1737–1739, doi:10.1126/science.1083130, 2003.

Grootes, P. M., E. J. Steig, M. Stuiver, E. D. ,Waddington, and. Morse, D. L.: The Taylor Dome Antarctic ^{18}O record and globally synchronous changes in

climate, Quat. Int., 56, 289– 298, 2001.

Goosse., H., and Fichefet, T.: Importance of ice-ocean interactions for the global ocean circulation: A model study, J. Geophys. Res. 104, 1999, 23337-23355, 1999.

Hastenrath, S., and Greischar L.: Circulation mechanisms related to northeast Brazil rainfall anomalies, J. Geophys. Res., 98(D3), 5093-5102, 1993.

Haug, G. H., Hughen, K. A., Sigman, D. M., Peterson, L. C. and Rohl, U.: Southward migration of the Intertropical Convergence Zone through the Holocene, Science, 293, 1304–1308, doi:10.1126/science.1059725, 2001.

Haug, G. H., Gunther, D., Peterson, L. C.: Climate and the collapse of Maya civilisation. Science 299:1731–1735, 2003.

Held, I. M. and Hou, A.Y.: Nonlinear axially symmetric circulations in a nearly inviscid atmosphere. J. Atmos. Sci. 37:515–33, 1980.

Hemming, S. R.: Heinrich events: Massive late Pleistocene detritus layers of the North Atlantic and their global climate imprint. Rev. Geophys. 42, 2004.

Hide R.: Dynamics of the atmospheres of the major planets with an appendix on the viscous boundary layer at the rigid bounding surface of an electricallyconducting rotating fluid in the presence of a magnetic field. J. Atmos. Sci. 26:841–53, 1969.

Holden, P. B., et al.: Interhemispheric coupling, the West Antarctic Ice Sheet and warm Antarctic interglacials, Clim. Past, 6, 431–443, 2010.

Hou, A. Y., and Lindzen R. S.: The influence of concentrated heating on the Hadley circulation, J. Atmos. Sci., 49(14), 1233–1241, doi:10.1175/1520-0469(1992)049<1233:TIOCHO>2.0.CO;2, 1992.

Huang, R. X., Cane, M. A., Naik, N. and Goodman, P.: Global adjustment of the thermocline in response to deepwater formation, Geophys. Res. Lett., 27, 759 – 762, doi:10.1029/1999GL002365, 2000.

Hurrell, J. W., Hack, J. J., Boville, B. A., Williamson, D. L. and Kiehl, J. T.: The Dynamical Simulation of the NCAR Community Climate Model Version 3 (CCM3)*, J. Climate, 11, 1207–1236. doi: 10.1175/1520 0442, 1998.

Hwang Y.T and Frierson, D. M. W.: Increasing atmospheric poleward energy transport with global warming, Geophys. Res. Lett., 37, L24807, doi:10.1029/2010GL045440, 2010.

Jouzel, J., C. Lorius, J. R. Petit, C. Genthon, N. I. Barkov, V. M. Kotlyakov, and Petrov, V. M.: Vostok ice core: A continuous isotope temperature record over the last climatic cycle (160,000 years), Nature, 329, 403 – 408, 1987.

Jouzel, J. et al.: Orbital and millennial antarctic climate variability over the past 800,000 years, Science, 317, 793–796, DOI: 10.1126/science.1141038, 2007.

Kageyama, M., Paul, A., Roche, D. M., and C. J. Van Meerbeeck (2010), Modelling glacial climatic millennial-scale variability related to changes in the Atlantic meridional overturning circulation: a review, Quaternary Science Reviews 29, 2931-2956.

Kang S. M., Held, I. M., Frierson, D. M. W. and Zhao M.: The response of the ITCZ to extratropical thermal forcing: Idealized slab-ocean experiments with a GCM. J. Clim. 21, 3521-32. doi:10.1175/2007JCLI2146.1, 2008.

Kang, S. M., Frierson, D. M. W., and Held, I. M.: The tropical response to extratropical thermal forcing in an idealized GCM: The importance of radiative feedbacks and convective parameterization. J. Atmos. Sci. 66, 2812–2827, doi:10.1175/2009JAS2924.1, 2009.

Kang, S. M. and Held, I. M.: Tropical precipitation, SSTs and the surface energy budget: A zonally symmetric perspective. Clim. Dyn. doi:10.1007/s00382-011-1048-7, 2011.

Kanner, L. C. et al.: High-Latitude Forcing of the South American Summer Monsoon, Science 335, 570, DOI: 10.1126/science.1213397, 2012

Keigwin, L. D., Curry, W. B., Lehman, S. J., and Johnsen, S.: The role of the deep ocean in North Atlantic climate change between 70 and 130 kyr ago. Nature 371, 323-326, 1994.

Kiehl J. T., Hack, J. J., Bonan, G. B., Boville, B. A., Williamson, D. L., and Rasch, P. J.: The National Center for Atmospheric Research Community Climate Model: CCM3. J. Clim., 11:1131–1149, 1998.

Kienast, M., Steinke, S., Stattegger, K., Calvert, S.E.: Synchronous tropical South China Sea SST Change and Greenland warming during deglaciation. Science 291, 2132–2134, 2001.

Kienast, M., Kienast, S.S., Calvert, S.E., Eglinton, T.I., Mollenhauer, G., Francois, R., and A. C. Mix: Eastern Pacific cooling and Atlantic overturning circulation during the last deglaciation. Nature 443, 846-849, 2006.

Keigwin, L. D., and Boyle E. A. : Surface and deep ocean variability in the northern Sargasso Sea during marine isotope stage 3, Paleoceanography, 14(2), 164 – 170, doi:10.1029/1998PA900026, 1999.

Kelly, M. J., Edwards, R. L., Cheng, H., Yuan, D., Cai, Y., Zhang, M. , Lin, Y. and Zhisheng A.: High resolution characterization of the Asian monsoon between 146000 and 99000 years B. P. from Dongge Cave, China and global correlation of events surrounding Termination II, Palaeogeogr. Palaeoclimatol. Palaeoecol., 236, 20–38, doi:10.1016/j.palaeo.2005.11.042, 2006.

Kim, H. K. and Lee, S.: Hadley cell dynamics in a primitive equation model. Part II: Nonaxisymmetric flow. J. Atmos. Sci. 58, 2859-71, 2001.

Knorr, G., and Lohmann, G.:Southern Ocean origin for the resumption of Atlantic thermohaline circulation during deglaciation, Nature 424, 532-536, 2003.

Koutavas, A., and Sachs, J. P.: Northern timing of deglaciation in the eastern equatorial Pacific from alkenone paleothermometry, Paleoceanography, 23, PA4205, doi:10.1029/2008PA001593, 2008.

Landais A., Jouzel J., Masson-Delmotte V. and Caillon N.: Large temperature variations over rapid climatic events in Greenland: a method based on air isotopic measurements. C. R. Geosci. 337(10–11), 947–956, 2005.

Lang, C., M. Leuenberger, J. Schwander, and Johnsen, S: 16ºC rapid temperature variation in central Greenland 70,000 years ago, Science, 286, 934– 937, 1999.

Langen, P. L., Graversen, R. G. and Mauritsen, T.: Separation of contributions from radiative feedbacks to polar amplification on an aquaplanet, American Meteorological Society, doi: 10.1175/JCLI-D-11-00246.1, 2012.

Lea, D. W., Pak, D. K., Peterson, L. C., and Hughen, K. A.: Synchronicity of tropical and high-latitude Atlantic temperatures over the last glacial termination, Science, 301, 1361–1364, 2003.

Lea, D.W., Pak, D.K., Belanger, C.L., Spero, H.J., Hall, M.A. and N. J. Shackleton: Paleoclimate history of Galapagos surface waters over the last 135,000 yr. Quaternary Science Reviews 25, 1152-1167, 2006

Lee, S., and Kim, H. K.: The dynamical relationship between subtropical and eddy driven jets, J. Atmos. Sci., 60(12), 1490–1503, doi:10.1175/1520-0469(2003)060<1490:TDRBSA>2.0.CO;2, 2003.

Lee, S.-Y., Chiang, J. C. H., Matsumoto, K. and Tokos, K. S.: Southern Ocean wind response to North Atlantic cooling and the rise in atmospheric CO2: Modeling perspective and paleoceanographic implications, Paleoceanography, 26, PA1214, 2011.

Levitus, S.: Climatological atlas of the world ocean. NOAA Professional Paper 13, U.S. Government Printing Office, Rockville, Md., 1982.

Li, C., and Battisti, D. S.: Reduced Atlantic Storminess during Last Glacial Maximum: Evidence from a Coupled Climate Model, J. Clim., 21,14, 3561-3579, 2008.

Lindzen, R. S. and Nigam, S.: On the role of sea-surface temperature gradients in forcing low level winds and convergence in the tropics. J. Atmos. Sci. 44, 2440-58, 1987.

Lindzen, R. S. and Hou, A.Y.: Hadley Circulations for Zonally Averaged Heating Centered Off the Equator. J. Atmos. Sci. 45, 2416-27, 1988.

Liu, Z., et al.: Transient simulation of last deglaciation with a new mechanism for Bølling-Allerød warming. Science, 325, 310–314, 2009.

Magnusdottir, G. and Saravanan, R.: The response of atmospheric heat transport to zonally averaged SST trends. Tellus A, 51: 815–832. doi: 10.1034/j.1600-0870.1999.00019.x, 1999.

Mahajan, S., Saravanan, R. and Chang, P.: The Role of the Wind-Evaporation-Sea Surface Temperature (WES) Feedback as a Thermodynamic Pathway for the Equatorward Propagation of High-Latitude Sea Ice-Induced Cold Anomalies. J. Clim. 24, 1350-61. doi: 10.1175/2010JCLI3455.1, 2011.

Manabe, S., and Stouffer R. J.: Two stable equilibria of a coupled ocean-atmosphere model, J. Clim.,1, 841–866, doi:10.1175/1520-0442(1988)001<0841:TSEOAC>2.0.CO;2, 1988.

Mashiotta, T.A., Lea, D.W. and Spero, H.J.: Glacial–interglacial changes in Subantarctic sea surface temperature and δ18O-water using foraminiferal Mg,

Earth and Planetary Science Letters 170, 417-432,1999.

McManus, J. F., Anderson, R. F., Broecker, W. S., Fleisher, M. Q. and Higgins S. M.: Radiometrically determined fluxes in the sub-polar North Atlantic during the last 140,000 years. Earth Planet. Sci. Lett. 135, 29–43, 1998.

McManus, J.F., Francois, R., Gherardi, J.M., Keigwin, L.D. and Brown-Leger, S.: Collapse and rapid resumption of Atlantic meridional circulation linked to deglacial climate changes. Nature 428, 834–837, 2004.

Montoya M. and Levermann A.: Surface wind-stress threshold for glacial atlantic overturning, Geophys Res Lett 35, doi: 10.1029/2007GL032,560, 2008.

Murakami, S., Ohgaito, R., Abe-Ouchi, A., Crucifix, M., and Otto-Bliesner, B. L.: Global-Scale Energy and Freshwater Balance in Glacial Climate: A Comparison of Three PMIP2 LGM Simulations, J. Clim., 21,19, 5008-5033, 2008.

NGRIP members: High-resolution record of Northern Hemisphere climate extending into the last interglacial period, Nature 432,147–151, 2004.

Neelin, J. D. and Held, I. M.: Modeling tropical convergence based on the moist static energy budget. Mon. Weather Rev. 115, 3–12, 1987.

Okumura, Y., Xie, S.-P., Numaguti, A. and Tanimoto Y.: Tropical Atlantic airsea interaction and its influence on the NAO. Geophys. Res. Lett., 28, 1507-1510, 2001.

Oleson, K. W. et al.: Technical description of the Community Land Model (CLM). Tech. Note NCAR/TN - 461+STR, Natl. Cent. for Atmos. Res., Boulder, Colorado, 2004.

Opsteegh J. D., Haarsma, R. J., Selten, F. M., and Kattenberg, A.: ECBILT: a dynamic alternative to mixed boundary conditions in ocean models, Tellus 50A, 348-367, 1998.

Otto-Bliesner, B. L. and Brady, E. C.: The sensitivity of the climate response to the magnitude and location of freshwater forcing: last glacial maximum experiments, Quaternary Science Reviews 29, 56-73, 2010.

Peixoto, J. P. and Oort, A. H.: "Physics of climate", New York, USA: American Institute of Physics, 1992. 520 pp. ISBN 0 88318 712 4.

Peltier, W. R.: Global glacial isostasy and the surface of the ice age Earth: The ICE-5G (VM2) model and GRACE, Ann Rev Earth Planet Sci 32,111–149, 2004.

Peterson, L. C., Haug, G. H., Hughen, K. A., and Rohl U.: Rapid changes in the hydrologic cycle of the tropical Atlantic during the last glacial, Science 290, 1947– 1951, doi: 10.1126/science.290.5498.1947, 2000.

Peterson, L. C., and Haug G. H.: Variability in the mean latitude of the Atlantic Intertropical Convergence Zone as recorded by riverine input of sediments to the Cariaco Basin (Venezuela), Palaeogeogr. Palaeoclimatol. Palaeoecol., 234, 97–113, doi:10.1016/j.palaeo.2005.10.021, 2006.

Rahmstorf, S.: Timing of abrupt climate change: A precise clock, Geophys.

Res. Lett., 30(10), 1510, doi:10.1029/2003GL017115, 2003.

Renssen H., Goose, H., and Fichefet, T.: Modeling the effect of freshwater pulses on the early Holocene climate: The influence of high-frequency climate variability, Paleoceanography 17(2), 1020, 10.1029/2001PA000649, 2002.

Sachs, J. P., and Lehman S. J.: Subtropical North Atlantic temperatures 60,000 to 30,000 years ago, Science, 286, 756–759, doi:10.1126/science.286.5440.756, 1999.

Severinghaus, J.P. and Brook, E.J: Abrupt Climate Change at the End of the Last Glacial Period Inferred from Trapped Air in Polar Ice,Science 286, 930, 1999.

Shea, D. J., Trenberth, K. E., and Reynolds, R. W.: A global monthly sea surface temperature climatology, J. Clim., 5, 987–1001, 1992.

Schneider, T.: The General Circulation of the Atmosphere, Annu. Rev. Earth Planet. Sci. 34:655–88, doi: 10.1146/annurev.earth.34.031405.125144, 2006.

Shell, K. M., Kiehl, J. T., Shields, C. A.: Using the Radiative Kernel Technique to Calculate Climate Feedbacks in NCAR's Community Atmospheric Model. J. Clim. 21, 2269-2282, doi:10.1175/2007JCLI2044.1, 2008.

Shemesh, A., Hodell, D., Crosta, X., Kanfoush, S., Charles, C., Guilderson, T.: Sequence of events during the last deglaciation in Southern Ocean sediments and Antarctic ice cores. Paleoceanography 17 (4), 1056, 2002.

Soden, B. J., Held, I. M., Colman, R., Shell, K. M., Kiehl, J. T. and Shields, C. A.: Quantifying climate feedbacks using radiative kernels. J. Clim. 21, 3504–3520. doi: 10.1175/2007JCLI2110.1, 2008.

Soden, B. J. and Held, I. M.: An assessment of climate feedbacks in coupled ocean-atmosphere models. J. Clim. 19, 3354–3360, 2006.

Steffensen, J. P., et al.: High-resolution Greenland ice core data show abrupt climate change happens in a few years, Science 321, 680–684, 2008.

Stocker, T. F., The seesaw effect, Science, 282, 61–62, 1998.

Stocker, T. F. and Johnsen, S. J.: A minimum thermodynamic model for the bipolar seesaw. Paleoceangraphy, 18, 1087, doi:10.1029/2003PA000920, 2003.

Stouffer, R., Yin, J., Gregory, J. M, Dixon, K.W., Spelman, M. J., Hurlin, W., Weaver, A. J., Eby, M., Flato, G.M., Hasumi, H., Hu, A., Jungclaus, J. H., Kamenkovich, I.V., Levermann, A., Montoya, M., Murakami, S., Nawrath, S., Oka, A., Peltier, W.R., Robitaille, D.Y., Sokolov, A.P., Vettoretti, and Weber, G. N.: Investigating the causes of the response of the thermohaline circulation to past and future climate changes. J. Clim., 19, 1365–1387, 2006.

Stouffer, R. J., D. Seidov, and Haupt B. J.: Climate response to external sources of freshwater: North Atlantic versus the Southern Ocean, J. Cim., 20, 436– 448, 2007

Svensson, A., Biscaye, P. E. and Grousset, F. E.: Characterization of late glacial continental dust in the Greenland Ice Core Project ice core, Journal of Geophysical Research 105: 4637–56, 2000.

Su, H. and Neelin, J. D.: Teleconnection mechanisms for tropical Pacific descent anomalies during El Nino, J. Atmos. Sci. 59, 2682– 2700, 2002.

Terray, L., and Cassou, C.: Tropical Atlantic sea surface temperature forcing of quasi-decadal climate variability over the North Atlantic-European region, J. Climate, 15, 3170-3187, 2002.

Timmermann, A., Krebs, U., Justino, F., Goosse, H. and Ivanochko, T.: Mechanisms for millennial-scale global synchronization during the last glacial period, Paleoceanography, 20, PA4008, doi:10.1029/2004PA001090, 2005.

Timmermann, A., et al.: The influence of a collapse of the meridional circulation of the Atlantic on ENSO, J. Clim., 20, 4899–4919, doi:10.1175/JCLI4283.1, 2007.

Timmermann, A., Menviel, L., Okumura, Y., Schilla, A., Merkel, U., Timm, O., Hu, A., Otto-Bliesner, B. and Schulz, M: Towards a quantitative understanding of millennial-scale Antarctic warming events, Quaternary Science Reviews 29, 74-85, 2010.

Trenberth, K. E., and Caron, J. M.: Estimates of meridional atmosphere and ocean heat transports. J. Clim.,14, 3433–3443, 2001.

Trenberth K.E., Caron J.M., and Stepaniak D.P.: The atmospheric energy budget and implications for surface fluxes and ocean heat transports, Clim. Dyn, 17, 259-276, 2000.

Trenberth, K. E., and Stepaniak, D. P.: Covariability of components of poleward atmospheric energy transports on seasonal and interannual timescales, J. Clim., 16, 3691–3705, 2003.

UNEP: Keeping Track of Our Changing Environment: From Rio to Rio+20 (1992-2012), Division of Early Warning and Assessment (DEWA), United Nations Environment Programme, Nairobi, 2011.

Valdes, P. J.: Built for stability Nature Geoscience 4, 414–416, 2011.

Vellinga, M., and Wood, R. A.: Global climatic impacts of a collapse of the Atlantic thermohaline circulation, Clim. Change, 54, 251–267, doi:10.1023/A:1016168827653, 2002.

Walker, C. C., Schneider, T.: Eddy influences on Hadley circulations: Simulations with an idealized GCM. J. Atmos. Sci. 63, 3333-3350. doi: 10.1175/JAS3821.1, 2006.

Wang, Y. J., Cheng, H., Edwards, R. L., An, Z. S., Wu, J. Y., Shen, C.C., and Dorale, J. A.: A High-Resolution Absolute-Dated Late Pleistocene Monsoon Record from Hulu Cave, China, Science, 294, 2345 - 2348, doi: 10.1126/science.1064618, 2001.

Wang, Y. J. et al., Millennial- and orbital-scale changes in the East Asian monsoon over the past 224,000 years, Nature 451, 1090, 2008.

Wang, P.: Seasonality over Greenland during the Holocene and possible explanations of the 8.2 kyr event - A study based on the circulation model ECBilt-CLIO, Msc Thesis, NBI, University of Copenhagen, Denmark, 2009.

Webster, P. J.: The Elementary Hadley Circulation. In: Diaz, H. F. and Bradley, R. S. (ed): The Hadley Circulation: Present, Past, and Future, Springer Netherlands. Isbn: 978-1-4020-2944-8, volume: 21, doi: 10.1007/978-1-4020-2944-8_1, 2004.

Weaver, A. J., Saenko, O. A., Clark, P. U. and Mitrovica, J. X,: Meltwater pulse 1a from Antarctica as a trigger for the Bølling-Allerød warm interval. Science 209, 1709–1713, 2003.

Wong, T., Stackhouse, Jr. P. W., Kratz, D. P. and Wilber, A. C.: Earth radiation budget at top-of-atmosphere. In: State of the Climate in 2008, Bull. Amer. Meteor. Soc., 90 (8), S1–S196, 2009.

Wunsch, C.: The total meridional heat flux and its oceanic and atmospheric partition, J. Clim., 18, 4374–4380, 2005.

Xie, S.-P.: A dynamic ocean-atmosphere model of the tropical Atlantic decadal variability, J. Clim., 12, 64–70, 1999.

Xie, S.-P. and Carton, J. A.: Tropical Atlantic variability: patterns, mechanisms, and impacts. In: Wang C., Xie S.-P. and Carton J. A. (ed): Earth Climate: The Ocean-Atmosphere Interaction, Geophysical Monograph, AGU, Washington D.C., 2004.

Yoshimori M. and Broccoli A. J.: On the link between Hadley circulation changes and radiative feedback processes, Geophys. Res. Lett., 36, L20703, doi:10.1029/2009GL040488, 2009.

Yuan, D., et al.: Timing, duration, and transitions of the last interglacial Asian monsoon, Science, 304, 575 – 578, doi:10.1126/science.1091220, 2004.

Zelinka, M. and Hartmann, D. L.: Climate Feedbacks and their Implications for Poleward Energy Flux Changes in a Warming Climate. J. Clim. in press, doi: 10.1175/JCLI-D-11-00096.1, 2011.

Zhang, R. and Delworth, T. L.: Simulated tropical response to a substantial weakening of the Atlantic thermohaline circulation, J. Clim., 18, 1853–1860, 2005.

List of tables:

List of Figures:

5.1 Illustration of high northern latitude cooling and southward ITCZ shift